



INTEGRATION OF A STAR TRACKER AND INERTIAL SENSORS USING AN
ATTITUDE UPDATE

THESIS
SEPTEMBER 2014

Humood Alkhaldi, Captain, RSAF

AFIT-ENG-T-14-S-16

DEPARTMENT OF THE AIR FORCE
AIR UNIVERSITY

AIR FORCE INSTITUTE OF TECHNOLOGY

Wright-Patterson Air Force Base, Ohio

DISTRIBUTION STATEMENT A.
APPROVED FOR PUBLIC RELEASE; DISTRIBUTION UNLIMITED.

The views expressed in this thesis are those of the author and do not reflect the official policy or position of the United States Air Force, Department of Defense, or the United States Government. This material is declared a work of the U.S. Government and is not subject to copyright protection in the United States.

AFIT-ENG-T-14-S-16

INTEGRATION OF A STAR TRACKER AND INERTIAL SENSORS USING AN
ATTITUDE UPDATE

THESIS

Presented to the Faculty

Department of Electrical and Computer Engineering

Graduate School of Engineering and Management

Air Force Institute of Technology

Air University

Air Education and Training Command

In Partial Fulfillment of the Requirements for the
Degree of Master of Science in Electrical Engineering

Humood Alkhaldi, BS

Captain, RSAF

September 2014

DISTRIBUTION STATEMENT A.
APPROVED FOR PUBLIC RELEASE; DISTRIBUTION UNLIMITED.

AFIT-ENG-T-14-S-16

INTEGRATION OF A STAR TRACKER AND INERTIAL SENSORS USING AN
ATTITUDE UPDATE

Humood Alkhaldi, BS

Captain, RSAF

Approved:

//signed//
John F. Raquet, PhD (Chairman)

19 Aug, 2014
Date

//signed//
Meir Pachter, PhD (Member)

19 Aug, 2014
Date

//signed//
Kyle Kauffman, PhD (Member)

19 Aug, 2014
Date

Abstract

The Global Positioning System (GPS) is widely used in most of the military and civilian applications because of its precision navigation capability. Unfortunately, GPS is not available in all environments (e.g., indoors, under sea, underground, or jamming environment). The motivation of this research is to address the limitations of GPS by using star trackers as an attitude update to an inertial navigation system (INS). Commercial, tactical, and navigation grade INS are modeled and simulated with measurements from GPS, star tracker, and barometer. GPS measurements are used to update the INS position and velocity for a small duration in the beginning of the vehicle's flight time. Star tracker and barometer measurements are used to update the INS attitude and altitude, respectively. This research uses a Linear Kalman Filter as a recursive estimation system, to estimate the INS errors (i.e. position, velocity, tilts, accelerometer bias, gyroscope bias, and barometer bias) using the three types of measurement updates. The simulation results show that the star tracker was able to improve the performance of the commercial and tactical grades INS, for any duration of the vehicle's flight time. Also, the improvement in the performance of the navigation grade INS was not significant until the vehicle's flight time was more than approximately 1000 seconds. Also, the research shows the performance impact on the three INS grades when using different star tracker accuracies.

Acknowledgments

I would like to thank my parents and my brothers for their priers and support throughout my thesis. Also, I would like to thank my advisor Dr. John Raquet for all the guidance and knowledge I got from him. In addition, I thank my thesis committee members, Dr. Meir Pachter and Dr. Kyle Kauffman for their teachings throughout my courses and thesis. Finally, I thank my friend, 1Lt. Muflih Alqahtani for his support and friendship through my thesis time.

Humood Alkhaldi

Table of Contents

	Page
Abstract.....	iv
Acknowledgments.....	v
List of Figures.....	ix
List of Tables.....	xii
I. Introduction.....	1
1.1 Problem Definition.....	2
1.2 Research Contributions.....	3
1.3 Thesis Outline.....	3
II. Mathematical Background.....	5
2.1 Inertial Navigation System.....	5
2.2 Direction Cosine Matrix.....	6
2.3 Reference Frames.....	7
2.3.1 Earth-Centered Inertial Frame.....	8
2.3.2 Earth-Centered Earth-Fixed Frame.....	8
2.3.3 Navigation Frame.....	8
2.3.4 Body Frame.....	9
2.3.5 Sensor Frame.....	10
2.4 The WGS-84 Coordinate System.....	11
2.5 Star Trackers.....	12

	Page
2.6 Kalman filter	14
2.6.1 Linear Kalman Filter	15
2.6.2 Unscented Kalman Filter.....	17
2.7 Previous Work	18
2.7.1 Correction Technique for Velocity and Position Errors of Inertial Navigation System by Celestial Observations	18
2.7.2 Alternate of GPS for Ballistic Vehicle Navigation	20
2.7.3 Compass Star Tracker for GPS-Like Applications	21
2.8 Chapter Summary.....	25
III. Methodology	26
3.1 System Block Diagram	26
3.2 Truth Model	27
3.3 Dynamic Model.....	29
3.3.1 Inertial Navigation System Error Model	29
3.4 Measurement Model.....	32
3.4.1 Global Positioning System Model.....	33
3.4.2 Barometer Model.....	34
3.4.2 Star Tracker Model.....	35
3.5 Kalman Filter Implementation	37
3.6 Chapter Summary.....	37
IV. Simulation Results.....	38

	Page
4.1 Simulation Scenarios	39
4.2 Filter Validation	40
4.3 Star Tracker Performance Improvement on INS Grades	51
4.4 Impact of Star Tracker Accuracy and INS Quality	60
4.5 Chapter Summary	62
V. Conclusion	66
5.1 Conclusions	66
5.2 Future Work Recommendations	68
Appendix A	70
Bibliography	100

List of Figures

Figure	Page
2.1. Strapdown Inertial Navigation System (SINS) Diagram	6
2.2. Illustration of Earth-centered Inertial, Earth-centered Earth-fixed and Navigation Frames	9
2.3. Illustration of The Body Frame	10
2.4. Illustration of The Sensor Frame.....	11
2.5. Reference Frame for Earth and Optical Axis	22
3.1. The System Block Diagram	27
4.1. Position Ensemble Standard Deviation and Mean Versus Filter Computed Standard Deviation for Commercial Grade INS	41
4.2. Position Ensemble Standard Deviation and Mean Versus Filter Computed Standard Deviation for Tactical Grade INS	42
4.3. Position Ensemble Standard Deviation and Mean Versus Filter Computed Standard Deviation for Navigation Grade INS	43
4.4. Position Error for 1000 Monte Carlo Runs of The First Scenario for a Navigation Grade INS	44
4.5. Velocity Error for 1000 Monte Carlo Runs of The First Scenario for a Navigation grade INS	45
4.6. Tilt Error for 1000 Monte Carlo Runs of The First Scenario for a Navigation Grade INS	46

Figure		Page
4.7.	Accelerometer Error for 1000 Monte Carlo Runs of The First Scenario for a Navigation Grade INS	47
4.8.	Gyroscope Error for 1000 Monte Carlo Runs of The First Scenario for a Navigation Grade INS	48
4.9.	Barometer Error for 1000 Monte Carlo Runs of The First Scenario for a Navigation Grade INS	49
4.10.	Position Error for 1000 Monte Carlo Runs of The First Scenario for a Commercial Grade INS	50
4.11.	Position Error for 1000 Monte Carlo Runs of The First Scenario for a Navigation Grade INS	51
4.12.	Estimated Position Error Covariance for The Two Scenarios for Commercial Grade INS	53
4.13.	Tilt Covariance for Both Scenarios for Commercial Grade INS	54
4.14.	Estimated Position Error Covariance for The Two Scenarios for Tactical Grade INS	55
4.15.	Estimated Tilt Covariance for Both Scenarios for Tactical Grade INS	56
4.16.	Estimated Position Error Covariance for The Two Scenarios for Navigation Grade INS	57
4.17.	Estimated Tilt Covariance for Both Scenarios for Navigation Grade INS ..	58
4.18.	Estimated Position Error Covariance for The Two Scenarios for Navigation Grade INS	59

Figure	Page
4.19. Estimated Tilt Covariance for Both Scenarios for Navigation Grade INS..	60
4.20. Star Tracker Accuracy Effect After GPS Outage for Both Scenarios for Navigation Grade INS.....	62
4.21. Star Tracker Accuracy Effect After GPS Outage for Scenario One for Tactical Grade INS.	64
4.22. Star Tracker Accuracy Effect After GPS Outage for Scenario One for Commercial Grade INS.....	65

List of Tables

Table		Page
2.1.	Key WGS-84 Parameters	21
2.2.	Comparison of Attitude Sensors	22
2.3.	LIST and FAR-MST Specifications	23
2.4.	Performance Parameters of the SUNSAT Star Tracker	23
2.5.	Error Statistics	30
4.1.	Parameters Used in Simulation for Different INS Grades	46
4.2.	Star Tracker Parameter	48
4.3.	Simulation Parameters for Navigation Filter	48
4.4.	Results Summary for the Three INS Grades for Both Scenarios.....	60
4.5.	Performance Improvement in DRMS Values	61

INTEGRATION OF A STAR TRACKER AND INERTIAL SENSORS USING AN ATTITUDE UPDATE

I. Introduction

This thesis outlines a research effort to integrate star trackers with inertial sensors for self-contained, robust, autonomous navigation. This research is motivated by the requirement for self-contained navigation in environments where the Global Positioning System is unavailable.

Navigation precision is the cornerstone of combat operations success in modern wars. The Global Positioning System (GPS) was developed in 1973 for more accurate and precise navigation capabilities than the old navigation systems. In the Gulf War, GPS was used for the first time for precision navigation in combat [15]. The precision of the Guided-GPS missiles and the precise aircraft navigation used in the war, made a huge rule in controlling the war and furthermore successes for the coalition forces. Thus, precision of navigation is an important factor in all military operations and especially the Air Force, and it cannot be achieved in areas where GPS signals are not available (e.g., underwater, under trees, beside mountains or in jamming environments).

The motivation of this research is to address the limitations of the current navigation methods by using star trackers and inertial systems. This concept is inspired from the Noble Qur'an. Allah said *"And it is He who placed for you the stars that you may be guided by them through the darknesses of the land and sea. We have detailed the signs for a people who know"* [16]. Stars were explained in the Noble Qur'an to be used to guide people, and it is been used from the beginning of human until the modern

century. With the new technology and the development of electronics, star trackers can be advanced and enhanced with new navigation methods to be used with the inertial sensors for precise navigation.

The following sections will explain the problem definition of the research, the contributions to the research area, and the outline of the research chapters.

1.1 Problem Definition

Considering the unreliability of GPS, as it can be denied through external interference, it is important to consider different navigation systems. An inertial navigation system (INS) combined with a Celestial Navigation System (CNS) can enhance the accuracy of navigating, by using star trackers mounted on the aircraft to correct the accumulated errors in the INS.

Celestial navigation system primary consists of a star tracker mounted on a navigating vehicle (e.g. aircraft, spacecraft, ship, and missile) that capture stars available in the field of view of the star tracker camera and then compare it with a star catalogue saved in the vehicle computer. From this process, the vehicle's attitude can be estimated and then used to aid the INS as an attitude update.

This research will simulate the star trackers when integrated with different qualities of INS, and show the impact and improvement to the navigating vehicle.

1.2 Research Contributions

As mentioned in the previous section, the objective of this research is to simulate and show the advantage of star trackers when used to aid different grades of the INS.

There are three primary contributions in the research. The first contribution is to model the different grades of the INS (i.e. commercial, tactical, and navigation), and that is described in Chapter III, Section 3.2.

The second contribution is to model different aiding measurements, which will be the star tracker model, GPS, and barometer. The GPS model will be shown and explained in Chapter III, Section 3.4.1. The barometer model will be explained in Chapter III, Section 3.4.2. Finally, the star tracker model will be explained in Chapter III, Section 3.4.3.

The third contribution is to simulate the previous models in MATLAB, using Kalman filter as an estimator, to show the performance development to the different grades of INS.

1.3 Thesis Outline

This research is organized as follows. Chapter II will provides a mathematical background for reference frames, transformation between reference frames, star tracker concepts and specifications, linear and nonlinear Kalman filter estimators, and previous work in the field of celestial navigation. Chapter III will presents the methodology used in the research and the models developed. Chapter IV will show the simulation results of the developed methodology and the impact of star tracker accuracy on the different

grades of INS. Finally, Chapter V will conclude the research results and provide recommendations for future work related to the research.

II. Mathematical Background

This chapter reviews the mathematical background materials that are required to understand the methodology used to aid the inertial navigation system using celestial observations. The chapter begins with introduction to the inertial navigation system. Next, the reference frames used in navigation are defined and the transformation of coordinates between reference frames is explained. Then, the WGS-84 coordinate system is reviewed. Next, star trackers are introduced along with their specifications. In addition, a discussion of the Kalman filter is presented as a widely used recursive estimation system. Finally, previous work related to this research is discussed.

2.1 Inertial Navigation System

The Inertial Navigation System (INS) is a navigation system that uses two types of sensors and a processing computer to calculate the position, velocity and attitude of a vehicle. There are two types of sensors used, accelerometers and gyroscopes [2]. An accelerometer is a motion sensor that measures the specific force of a vehicle, and the gyroscope is a rotation sensor that measures the angular velocity of a vehicle [2].

There are two types of INS, gimbaled and strapdown, and the Strapdown Inertial Navigation System (SINS) will be used in the research. In the strapdown inertial navigation system, the accelerometers and gyroscopes are directly mounted on the vehicle body [2]. A diagram that explains the mechanism of the SINS is shown in Fig. 2.1.

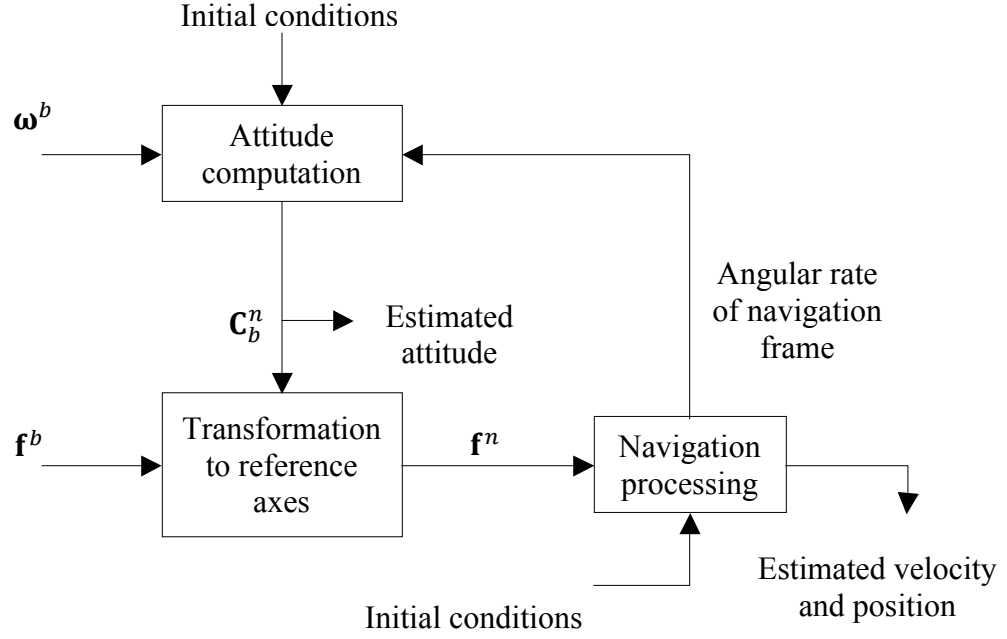


Figure 2.1: Strapdown Inertial Navigation System (SINS) diagram [10]

In Fig. 2.1, the measurements of the body angular rate (ω^b) and specific force (f^b) are the main inputs to the SINS, and they are calculated by using gyroscopes and accelerometers respectively. Also, the C_b^n is called the Direction Cosine Matrix (DCM) and it will be explained in the following section.

2.2 Direction Cosine Matrix

The direction cosine matrix is a 3×3 matrix, used to transform a vector or a matrix from one reference frame to another coordinate frame using cosine of the angles between the two frames [2].

A transformation from body frame to navigation frame is denoted by \mathbf{C}_b^n , which can be calculated by three rotations about different axes as expressed in the following equation

$$\mathbf{C}_b^n = \begin{bmatrix} \cos \theta \cos \psi & -\cos \phi \sin \psi & \sin \phi \sin \psi \\ \cos \theta \sin \psi & +\sin \phi \sin \theta \cos \psi & +\cos \phi \sin \theta \cos \psi \\ -\sin \theta & \sin \phi \cos \theta & \cos \phi \cos \theta \end{bmatrix} \quad (2.1)$$

where ψ (yaw) is the rotation angle about z -axis, θ (pitch) is the rotation angle about y -axis and ϕ (roll) is the rotation angle about x -axis [2].

Also the DCM to transform from navigation frame to body frame is simply the transpose of the previous equation, i.e., $\mathbf{C}_n^b = (\mathbf{C}_b^n)^T$.

2.3 Reference Frames

For navigating on the earth, it is important to define a number of reference frames to represent the inertial measurements in the cardinal directions of the earth. Each one of the reference frames is a right handed, orthogonal co-ordinate frame [2]. A list of the most used reference frames is shown below:

- The Earth-centered inertial frame (*i-frame*)
- The Earth-centered Earth-fixed frame (*e-frame*)
- The navigation frame (*n-frame*)
- The body frame (*b-frame*)

- The sensor frame (*s-frame*)

Each of the frames is described in the following subsections.

2.3.1 Earth-Centered Inertial Frame (*i-frame*)

The Earth-centered inertial frame has its origin at the center of the earth and its axes (x^i, y^i and z^i) are non-rotating with respect to the fixed stars [2], see Fig. 2.2 for axes illustration.

2.3.2 Earth-Centered Earth-Fixed Frame (*e-frame*)

The Earth-centered Earth-fixed frame has its origin at the center of the earth and its axes are fixed with respect to the earth. Its axes are defined by x^e, y^e and z^e . The x^e axis lies along the intersection of the plane of the Greenwich meridian and the earth's equatorial plane, the z^e axis is aligned with the North Pole and the y^e axis is perpendicular to x^e and z^e with a direction that follows the right hand rule. The Earth-centered Earth-fixed frame rotates with respect to the inertial frame, at a rate of ω_{ie} about the z^e axis [2]. See Fig. 2.2 which includes an illustration of the e-frame axes.

2.3.3 Navigation Frame (*n-frame*)

The navigation frame is denoted by n and has its origin at the location of the navigation system. Its axes are aligned with the directions of north, east, and local vertical (down), defined by x^t, y^t and z^t respectively in Fig. 2.2. The turn rate of the

navigation frame in relation to the earth fixed frame is determined by the motion of the frame's origin with respect to the earth [2], see Fig. 2.2.

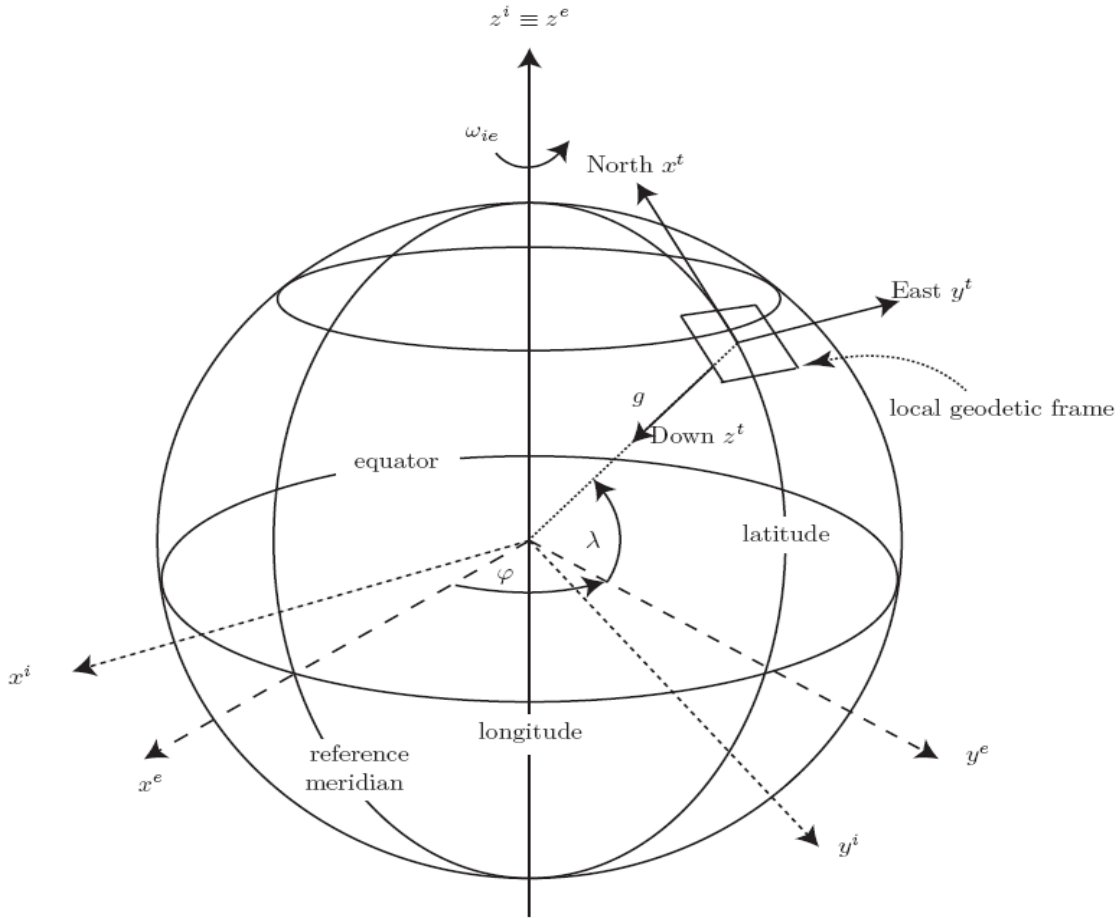


Figure 2.2: Illustration of Earth-centered inertial, Earth-centered Earth-fixed and Navigation frames [1]

2.3.4 Body Frame (*b-frame*)

The body frame has its origin at the center of the vehicle's body. The orthogonal axes of the body frame are aligned with the roll, pitch and yaw axes of the vehicle in

which the navigation system is installed, defined as x^b, y^b and z^b , respectively [2]. Fig. 2.3 shows the axes of the body frame with their corresponding rotations.

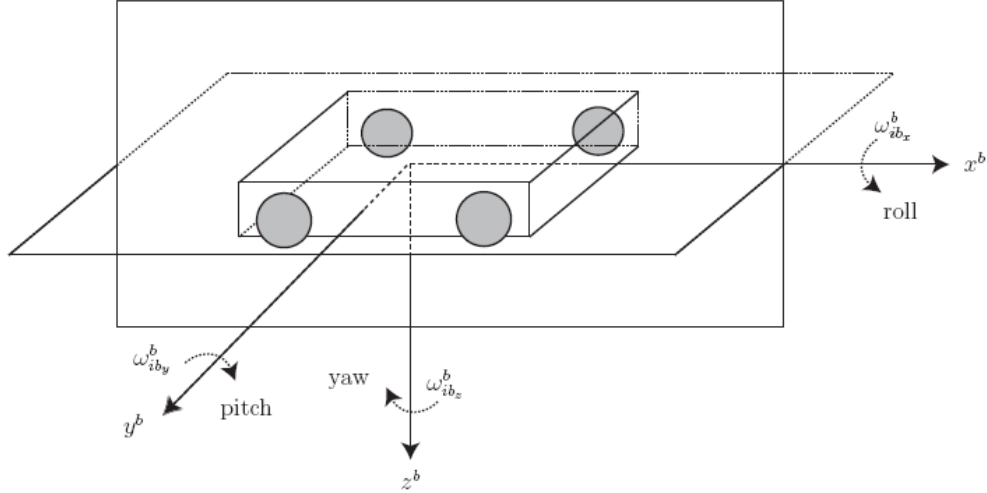


Figure 2.3: Illustration of the body frame [1]

2.3.5 Sensor Frame (*s-frame*)

The sensor frame can be designed in any way the sensor's designer likes, by determining the axes and origin. Its axes should be right handed and orthogonal and in order for the sensor frame to be useful, the relationship between the sensor and body frames must be known. Fig. 2.4 demonstrates a sensor frame with axes denoted by x^s, y^s and z^s .

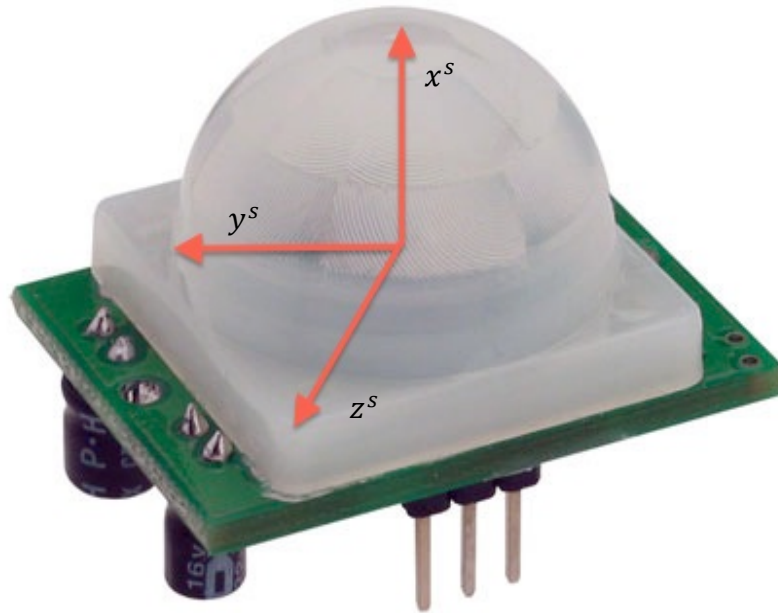


Figure 2.4: Illustration of the sensor frame

2.4 The WGS-84 Coordinate System

The World Geodetic System (WGS) is a system used to refer to all terrestrial locations in a convenient manner. The system mainly helps in navigation, geodesy and cartography [2]. It is important to note that the WGS-84 coordinate system is right handed, and major parameters used in WGS-84 are shown in Table 2.1

Table 2.1: Key WGS-84 parameters [2]

Parameter (Sample)	Value (Units)
Semi-major axis (a)	6378137 m
Flattening of the ellipsoid (f)	1/298.257223563
Angular velocity (ω)	$7.292115 \times 10^{-5} \text{ rad/s}$
Geocentric gravitational constant (GM)	$398600.5 \text{ km}^3/\text{s}^2$

2.5 Star Trackers

Star trackers use star catalogs to measure the attitude information of a vehicle in the vehicle coordinate frame by comparing the angles of the captured star with the star catalog that it has [9].

Star trackers are extremely accurate sensors for attitude sensing and there are different types of star trackers:

- Star scanners
- Gimbaled star trackers
- Fixed head star trackers

Star scanners provide the searching and sensing function using the vehicle rotation [9]. Gimbaled star trackers use mechanical action to search out and acquire stars and the fixed head star trackers use an electronic searching and tracking capabilities over a limited field of view to track stars [9]. A comparison of attitude sensors is shown in Table 2.2.

Table 2.2: Comparison of attitude sensors [9]

Sensor	Num. Axes	Operating Angular Range	Orbits	Size/Mass/Power/Cost	Accuracy/Angular Rate
Earth Sensor	2	Narrow: Nadir $\pm \sim 10^\circ$	Circ., small alt. range	Medium	Medium/High
Sun Sensor	2	Narrow: Sun $\pm \sim 30^\circ$ None in eclipse	Any	Low	Low/High
Magnetometer	2	Full sphere, but need magnetic clean sat.	LEO only	Low	Low/High
Available GPS Attitude Receivers	3	Medium: Zenith $\pm \sim 90^\circ$	Alt < 10k km No GEO	Medium	Medium/High
Available Star Trackers	3	Wide: All except Earth/Sun	Any	High	High/Low
New Opportunity Star Tracker	3	Wide: All except Earth/Sun	Any	Low	Medium/High

Star trackers vary by weight, accuracy, and cost and there are many developments in modern days to develop a star tracker that can meet all the requirements of accurate attitude determination along with low cost and weight. AeroAstro, Inc. and the Massachusetts Institute of Technology Space Systems Laboratory did develop the Lightweight Inexpensive Star Tracker (LIST) and the Fast Angular Rate Miniature Star Tracker (FAR-MST) with the specifications shown in Table 2.3. [9]

Nowadays, star trackers are been more developed with much better accuracy and lightweight. The accuracy varies from 0.1 arcsecond to less than 100 arcsecond for attitude determination [17]. One of the good star trackers is called SUNSAT, and its performance parameters are shown in Table 2.4. This star tracker specifications are used in the simulation results in Chapter IV.

Table 2.3: LIST and FAR-MST specifications [9]

Parameter (Units)	LIST	FAR-MST
Dimensions (cm^3)	$5.1 \times 7.6 \times 7.6$	$15 \times 8 \times 8$
Mass (kg)	0.3	0.9
Power consumption ($Watt$)	<1	3
Number of stars in FOV	< 4	> 2
Pitch/Yaw accuracy ($arcsecond$)	70	100
Roll accuracy ($arcsecond$)	1080	$\cong 1080$
Field of view (deg)	30	25 to 45

Table 2.4: Performance parameters of the SUNSAT star tracker [13]

Parameter	Units
Size	425 cm^3
Mass	0.5 kg
Power consumption	1.27 Watt
Number of stars in FOV	>3
Accuracy	12 arcsecond
Update rate for tracking stars	every 1 second
Field of view	$8.33 \times 11.17\text{ deg}$

2.6 Kalman Filter

Kalman filter is a recursive, optimal data processing algorithm that is used to predict the mean and covariance of specified states [11]. There are different types of Kalman filters which can be used, depending on the system dynamics and behavior,

including linear and nonlinear Kalman filters. For the nonlinear Kalman filter, there are two famous systems used for nonlinear systems, the Unscented Kalman Filter (UKF) and the Extended Kalman Filter (EKF). This research will focus on the linear Kalman filter and could use aspects of the unscented Kalman filter.

2.6.1 Linear Kalman Filter

The linear Kalman filter is used when the dynamic and measurement models are linear. The dynamic model of the continuous linear Kalman filter is

$$\dot{\mathbf{x}}(t) = \mathbf{F} \mathbf{x}(t) + \mathbf{B} \mathbf{u}(t) + \mathbf{G} \mathbf{w}(t) \quad (2.2)$$

$$\mathbf{z}(t_k) = \mathbf{H} \mathbf{x}(t_k) + \mathbf{v}(t_k) \quad (2.3)$$

where $\mathbf{x}(t)$ is the state vector, \mathbf{F} is the dynamics matrix, \mathbf{B} is the control input matrix, \mathbf{u} is the control input vector, $\mathbf{z}(t_k)$ is the measurement vector, \mathbf{H} is the measurement matrix, and where the dynamic noise $\mathbf{w}(t)$ and the measurement noise $\mathbf{v}(t_k)$ are uncorrelated white Gaussian noises with zero mean and covariances defined as [11]

$$E[\mathbf{w}(t)\mathbf{w}^T(t + \tau)] = \mathbf{Q} \delta(\tau) \quad (2.4)$$

$$E[\mathbf{v}(t_k)\mathbf{v}^T(t_j)] = \mathbf{R} \delta(k - j) \quad (2.5)$$

where $\delta(\tau)$ is the Dirac delta function, and $\delta(k - j)$ is the Kronecker delta function.

Since this model will be implemented in a discrete system, we are interested in transforming the above continuous model into a discrete model. The discrete model of a linear Kalman filter is defined by

$$\mathbf{x}(t_k) = \boldsymbol{\Phi}(t_k, t_{k-1}) \mathbf{x}(t_{k-1}) + \mathbf{B}_d \mathbf{u}(t_{k-1}) + \mathbf{G}_d \mathbf{w}_d \quad (2.6)$$

where the above matrices are calculated as

$$\boldsymbol{\Phi}(t_k, t_{k-1}) = e^{\mathbf{F}(t_k - t_{k-1})} \quad (2.7)$$

$$\mathbf{B}_d = \mathbf{F}^{-1}(\boldsymbol{\Phi}(t_k, t_{k-1}) - \mathbf{I})\mathbf{B} \quad (2.8)$$

$$\mathbf{G}_d = \mathbf{I} \quad (2.9)$$

And \mathbf{w}_d is a zero mean white Gaussian noise with covariance defined by

$$\mathbf{Q}_d = \mathbb{E}[\mathbf{w}_d \mathbf{w}_d^T] \quad (2.10)$$

where \mathbf{Q}_d can be found by using the Van Loan Method to convert from continuous to discrete noise [11].

Kalman filtering consists of two steps, time propagation and measurement updates. The quantities that we are interested in are the mean and covariance of the states, which will be given the symbols \mathbf{x}_k and \mathbf{P}_k , respectively.

2.6.1.1 Propagation

Propagation consists of estimating the current mean and covariance using the previous mean and covariance [11], we define propagation as

$$\mathbf{x}_{t_k}^- = \boldsymbol{\Phi}(t_k, t_{k-1}) \mathbf{x}_{t_{k-1}}^+ + \mathbf{B}_d \mathbf{u}_{t_{k-1}} \quad (2.11)$$

$$\mathbf{P}_{t_k}^- = \boldsymbol{\Phi}(t_k, t_{k-1}) \mathbf{P}_{t_{k-1}}^+ \boldsymbol{\Phi}^T(t_k, t_{k-1}) + \mathbf{Q}_d \quad (2.12)$$

where "-" denotes the previous value before the measurement update and "+" denotes the value after the measurement update.

2.6.1.2 Measurement Update

When a measurement \mathbf{z}_k is available at time k , the states are updated in the following manner

$$\mathbf{x}_{t_k}^+ = \mathbf{x}_{t_k}^- + \mathbf{K}_{t_k} (\mathbf{z}_{t_k} - \mathbf{H}_{t_k} \mathbf{x}_{t_k}^-) \quad (2.13)$$

where \mathbf{K}_k is the kalman filter gain, and it is given by the following equation

$$\mathbf{K}_{t_k} = (\mathbf{H}_{t_k} \mathbf{P}_{t_k}^-)^T [\mathbf{H}_{t_k} \mathbf{P}_{t_k}^- \mathbf{H}_{t_k}^T + \mathbf{R}_{t_k}]^{-1} \quad (2.14)$$

And \mathbf{H}_k is the measurement matrix. Using the gain and measurement matrix, the covariance after an update can be calculated by

$$\mathbf{P}_{t_k}^+ = (\mathbf{I} - \mathbf{K}_{t_k} \mathbf{H}_{t_k}) \mathbf{P}_{t_k}^- \quad (2.15)$$

2.6.2 Unscented Kalman Filter

The Unscented Kalman Filter (UKF) is used for nonlinear systems and it is based on the principle of using a set of appropriately chosen weighted points to parameterize the means and covariances of probability distributions [6]. The UKF is based on the unscented transformation, which is the transformation of a set of so-called sigma points, using a nonlinear function [6]. The sigma points along with their weighting are chosen in a well-known algorithm, which is given by the following equations:

$$\chi_0 = \bar{x} \quad W_0 = \frac{k}{n+k} \quad (2.16)$$

$$\chi_i = \bar{x} + (\sqrt{(n+k)P_{xx}})_i \quad W_i = \frac{1}{2(n+k)} \quad (2.17)$$

$$\chi_{i+n} = \bar{x} - (\sqrt{(n+k)P_{xx}})_i \quad W_{i+n} = \frac{1}{2(n+k)} \quad (2.18)$$

where χ denotes the sigma points, and W is the associated weight of the sigma points. These sigma points are passed through a nonlinear mapping function to result in transformed sigma points [6]. The transformed sigma points with their mean and covariance are shown by the following equations:

The transformed sigma points are

$$\mathcal{Y}_i = f[\chi_i] \quad (2.19)$$

The weighted mean of the transformed sigma points is

$$\bar{y} = \sum_{i=0}^{2n} W_i y_i \quad (2.20)$$

The weighted covariance of the transformed sigma points is

$$P_{yy} = \sum_{i=0}^{2n} W_i \{y_i - \bar{y}\} \{y_i - \bar{y}\}^T \quad (2.21)$$

The UKF performs exactly like the Second Order Gauss Filter but without the need to calculate Jacobians of the nonlinear functions in the system [6]. The ease of implementation and the high estimation accuracy of the unscented transformation (UKF), sometimes make it better filtering/estimation algorithm than the Extended Kalman Filter (EKF) for nonlinear systems [6].

2.7 Previous Work

In this section, previous work related to my thesis will be presented and discussed. It will include researches in the celestial navigation field.

2.7.1 *Correction Technique for Velocity and Position Errors of Inertial Navigation System by Celestial Observations [3]*

Gul and Jiancheng [3] presented a technique to correct some of the accumulated errors in the inertial navigation system (INS) of a space vehicle using stars observations.

The accumulated errors that were considered in their research are:

- Accelerometer bias.
- Gyro drift (ε).
- Initial misalignment error (φ_0).

In their research, a ballistic missile is simulated to demonstrate the validity of the method. The flight path of the missile is divided into three phases. The first phase is from

the launch point until the missile crosses the atmosphere, the second phase is from the point where the missile crosses the atmosphere to the point of burnout (the point where the engine of the missile is disconnected), and the third phase is after the burnout point to the point of impact of the missile with the ground target.

The misalignment error (φ_{tm}) is calculated by observing a star at time tm after the missile crosses the atmosphere, using a star tracker mounted on the missile, then a few seconds later another star observation is made which results in a second misalignment error ($\varphi_{tm+\tau}$) at time $tm + \tau$. Using the two calculated observations, the gyro drift (ε) can be calculated as follows:

$$\varphi_{tm+\tau} - \varphi_{tm} = \int_{tm}^{tm+\tau} \mathbf{C}_b^i dt \varepsilon = \mathbf{P} \varepsilon \quad (2.22)$$

$$\varepsilon = \mathbf{P}^{-1}(\varphi_{tm+\tau} - \varphi_{tm}) \quad (2.23)$$

where \mathbf{C}_b^i is the DCM to transform from the body frame to the inertial frame.

Using the gyro drift in (2.23), the initial misalignment error (φ_0) is calculated by

$$\varphi_0 = \varphi_{tm} - tm \varepsilon \quad (2.24)$$

By using the gyro drift and the initial misalignment error, the position and velocity of the missile is corrected at this time. After the burnout point, the missile takes in a free flight motion until it hits the ground target, so the output of the accelerometer of the missile's INS after the burnout point is used as the accelerometer bias. Then, the position and velocity errors due to the accelerometer bias can be calculated to correct the position and velocity of the missile.

The celestial navigation method used in the research [3] is simulated for 200 seconds flight time for a ballistic missile, providing a tremendous enhancement for the

INS of the missile. The technique presented in the research is valid for small misalignment angles and gyro drift. The technique could be enhanced to result in more accurate results by using Kalman filters to reduce the propagated errors in the INS. However, their technique does not apply for aircraft trajectories, because there is not a free-fall portion of the trajectory.

2.7.2 Alternate of GPS for Ballistic Vehicle Navigation [4]

This research [4] is a continuation of the previous discussed approach of Gul and Jiancheng [3]. In this research, they enhanced the accuracy of the technique by implementing an Unscented Kalman Filter (UKF) to reduce the accumulated errors in the INS. In this research, the sigma points (UKF technique) were propagated through the inertial navigation equations, mechanized in launch inertial frame. A simulation of 158 seconds of data for the powered phase of a ballistic missile is simulated. The error mean and covariance at time instant 160 seconds from the beginning of navigation were computed from the transformed sigma points. The previous process was repeated with velocity and position error correction by incorporating the detected initial misalignment, gyro drift and accelerometer bias. The mean and standard deviation of the errors in velocity and position obtained from INS, with and without incorporation of the correction technique, are listed in Table 2.5.

Table 2.5: Error statistics at time instant 160 seconds from launch time [4]

Parameter (Units)	Without correction		With correction	
	Mean	1-sigma	Mean	1-sigma
V_x (m/s)	-0.019	8.494	0.004	0.013
V_y (m/s)	-0.009	6.932	0	0.014
V_z (m/s)	0	10.910	0.006	0.012
r_x (m)	-1.51	739.60	0.01	1.23
r_y (m)	-0.91	476.70	0.62	1.98
r_z (m)	0	878.15	0.17	0.79

In Table 2.5, V_x , V_y , V_z , r_x , r_y and r_z are the missile velocity and position in three axes, respectively. From table 1, the results show that the velocity errors (1-sigma) are reduced from (7 to 11) m/s to less than 0.015 m/s along each axis. Also, position errors (1-sigma) are reduced from (470 to 870) meters to less than 2 meters along each axis.

The results found by using the UKF gives a motivation for further analysis by implementing different types of Kalman filters.

2.7.3 Compass Star Tracker for GPS-like Applications [7]

Samaan, Mortari and Juan in their article [7] have made an in depth description and analysis of the Compass Star Tracker, which is believed to be a new technological innovation with regards to estimating of attitude and location of spacecrafts. The article outlines the alignment of camera optical axis in relation to the gravitational direction and time as the basic concept behind this system. Although the system employees the use of a

number of significant concepts of Global Positioning System (GPS), it cannot be used as its substitute due to the fact that it suffers from the night-only limitation in addition to the need for calm and clear weather conditions [7].

The Compass Star Tracker (CST) application can be applied when navigating in non-GPS environments such as the Moon and planets or as backup system when GPS fails, with its accuracy depending on aspects such as CCD resolution, time precision and centroiding accuracy [7]. In this article, they described the estimation of latitude and longitude positions in space using the Monte-Carlo stimulated image and the night sky test through a gravity pendulum [7]. Their description embraces the use of the earth centered inertial frame and camera body frame (axes x, y, z) as shown in Fig. 2.5.

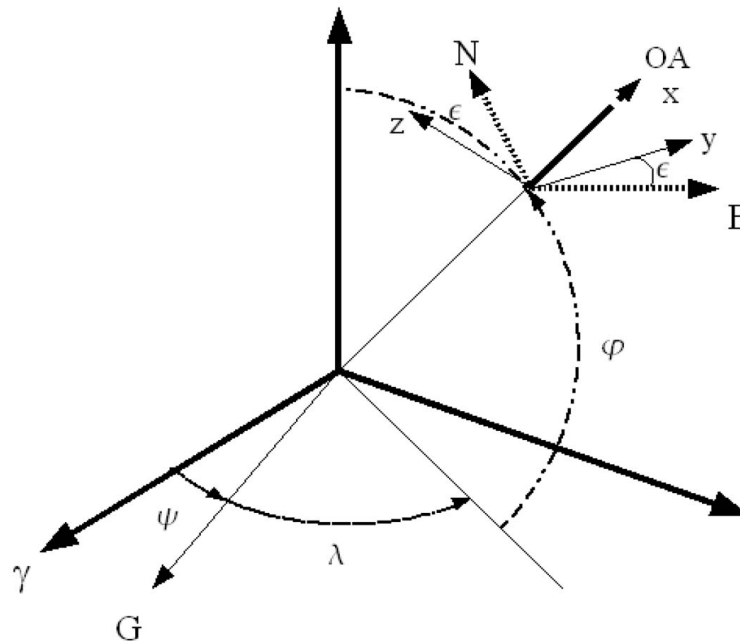


Figure 2.5: Reference frame for Earth and optical axis [7]

In Fig. 2.5, the x-axis is the camera optical axis, aligned to the local vertical. There are number of parameters in the figure, defined as, λ being the longitude, φ the latitude, ψ the angle between the vernal equinox (γ) and the Greenwich Meridian (G), and ε is the angle between the camera's y-axis and the local East (E). Samaan, Mortari and Juan identified these as the unknown parameters that to be calculated.

In the following equations, there are reference frames that to be explained. The subscript B is used for the body frame of the camera, G as the Greenwich frame, I as the inertial frame and L as the local frame [7].

Assume $A^{B/I}$ is the attitude matrix for the camera body frame with respect to the inertial frame and assume that $A^{B/L}$ is the attitude matrix for the camera body frame with respect to the local frame [7], then

$$A^{B/L} \equiv R_3(\varepsilon) = \begin{bmatrix} \cos \varepsilon & \sin \varepsilon & 0 \\ -\sin \varepsilon & \cos \varepsilon & 0 \\ 0 & 0 & 1 \end{bmatrix} \quad (2.25)$$

Also, assume that $A^{L/G}$ is the attitude matrix for the local reference frame with respect to the Greenwich frame [7], then

$$A^{L/G} \equiv R_2(-\varphi) R_3(\lambda) \quad (2.26)$$

$$A^{L/G} = \begin{bmatrix} \cos \varphi & 0 & \sin \varphi \\ 0 & 1 & 0 \\ -\sin \varphi & 0 & \cos \varphi \end{bmatrix} \begin{bmatrix} \cos \lambda & \sin \lambda & 0 \\ -\sin \lambda & \cos \lambda & 0 \\ 0 & 0 & 1 \end{bmatrix} \quad (2.27)$$

These equations relate through the equation $A^{B/G} = A^{B/I} A^{I/G} = A^{B/L} A^{L/G} = A^{B/G}$, that can be used to solve the unknown parameters using the following equations

The latitude φ is computed by

$$C_\varphi = A^{B/G}(3,3) \quad (2.28)$$

The longitude λ is computed by

$$\tan \lambda = \frac{-A^{B/G} (3,2)}{-A^{B/G} (3,1)} \quad (2.29)$$

The East direction ε is computed by

$$\tan \varepsilon = \frac{-A^{B/G} (2,3)}{A^{B/G} (1,3)} \quad (2.30)$$

Using the night sky test that employed the use of a star image captured by a Star1000 camera, Samaan, Mortari and Juan carried out a centroiding algorithm to find the star centers, while star identification was done using the Pyramid Star-ID technique. This led to estimating the attitude matrix $A^{B/I}$ using the ESOQ-2 algorithm. Having been able to find the time of the measured image, the $A^{G/I}$ matrix was evaluated [7].

Consequently, the equation matrixes, led to identifying the longitude and latitude, with 0.008^0 and 0.02^0 errors, respectively, as compared to the actual longitude and latitude values of a GPS receiver [7]. The Monte-Carlo simulation was also applied through the use of a camera with its optical axis pointing at the zenith. They selected the longitude to be at -104.9658^0 and the latitude at 39.7546^0 with a compass angle ε of 10^0 . After obtaining the initial and observed directions of the star, an optimal estimate of attitude matrix is done using the ESOQ-2 estimator, and the estimated values of the longitude was found to be -104.9704^0 , latitude of 39.7528^0 and local east angle of 10.0393^0 [7].

For Samaan, Mortari and Juan, these results provided optimism in the CST approach through which standard algorithm can be used in processing the images of stars

and location of the stars using a camera [7]. Although this method seems applicable, it has limitations of accuracy in the system, which necessitates more research and studies through which WGS-84 model would be quantified. Samaan, Mortari and Juan have evidently brought into light the possibility of using star trackers in estimating position together with attitude [7].

2.8 Chapter Summary

In this chapter, mathematical background related to the research was discussed and explained. In the next chapter, the methodology that will be used in the research will be explained in details.

III. Methodology

This chapter will explain the mathematical approach for simulating the inertial navigation system aided by a star tracker, global positioning system, and barometer. The chapter is organized as follows. First, a block diagram that describes the system structure is shown. Second, a truth model that represents the true trajectory of the aircraft will be presented. Next, a dynamic model for the inertial navigation system error model is explained in detail. Finally, measurements models for different measurements sources are discussed and explained.

3.1 System Block Diagram

The system block diagram is important to understand the functions and rule of the different components in the system. Fig. 3.1 shows the interrelationships between the system's components in a functional block diagram.

In the system block diagram, we first start to generate the system parameters that will have all the parameters of the navigating vehicle. Then, we generate a truth trajectory using Trajectory Generator block, which will be explained in the next Section. Next, we use the INS simulator to generate the system dynamics, and it will be explained in Section 3.3. The GPS, barometer, and star tracker measurements are generated by using the truth trajectory plus additional sensors biases, the measurement models will be shown and explained in Section 3.4. Then, a Kalman filter is used to estimate the navigation errors. Finally, we use the estimated errors to correct the INS navigation parameters.

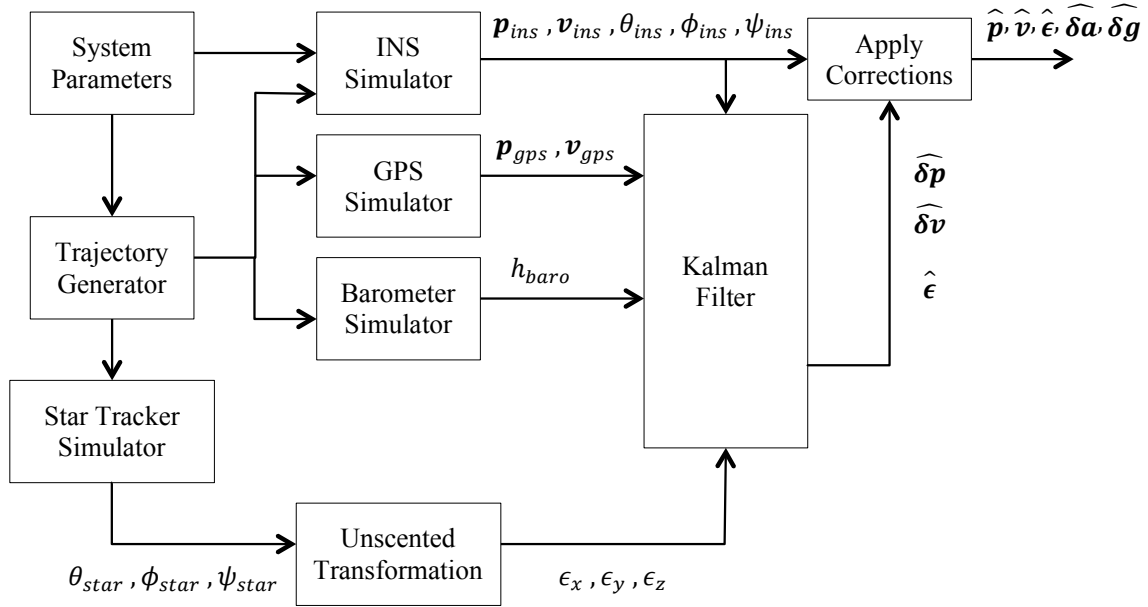


Figure 3.1: The system block diagram

3.2 Truth Model

There are different truth models that can be used to represent the aircraft trajectory. For this research the First Order Gauss Markov Acceleration (FOGMA) model was selected for its wide range of use in aircraft simulation applications. The general form of a dynamic model is given by

$$\dot{\mathbf{x}}(t) = \mathbf{F} \mathbf{x}(t) + \mathbf{G} \mathbf{w}_x(t) \quad (3.1)$$

The dynamics of a FOGMA model are described in terms of velocity \mathbf{v} , position \mathbf{p} and acceleration \mathbf{a} , by

$$\dot{\mathbf{p}} = \mathbf{v} \quad (3.2)$$

$$\dot{\mathbf{v}} = \mathbf{a} \quad (3.3)$$

$$\dot{\mathbf{a}} = -\frac{1}{\tau} \mathbf{a} + \mathbf{w}_x \quad (3.4)$$

where τ is the time constant. The matrices and vectors in Equation (3.1) are defined as

$$\mathbf{x} = \begin{bmatrix} p_x \\ p_y \\ p_z \\ v_x \\ v_y \\ v_z \\ a_x \\ a_y \\ a_z \end{bmatrix}_{9 \times 1} \quad (3.5)$$

$$\mathbf{F} = \begin{bmatrix} 0 & 0 & 0 & 1 & 0 & 0 & 0 & 0 & 0 \\ 0 & 0 & 0 & 0 & 1 & 0 & 0 & 0 & 0 \\ 0 & 0 & 0 & 0 & 0 & 1 & 0 & 0 & 0 \\ 0 & 0 & 0 & 0 & 0 & 0 & 1 & 0 & 0 \\ 0 & 0 & 0 & 0 & 0 & 0 & 0 & 1 & 0 \\ 0 & 0 & 0 & 0 & 0 & 0 & 0 & 0 & 1 \\ 0 & 0 & 0 & 0 & 0 & 0 & -1/\tau & 0 & 0 \\ 0 & 0 & 0 & 0 & 0 & 0 & 0 & -1/\tau & 0 \\ 0 & 0 & 0 & 0 & 0 & 0 & 0 & 0 & -1/\tau \end{bmatrix}_{9 \times 9} \quad (3.6)$$

$$\mathbf{G} = \begin{bmatrix} 0 & 0 & 0 \\ 0 & 0 & 0 \\ 0 & 0 & 0 \\ 0 & 0 & 0 \\ 0 & 0 & 0 \\ 0 & 0 & 0 \\ 0 & 0 & 0 \\ 1 & 0 & 0 \\ 0 & 1 & 0 \\ 0 & 0 & 1 \end{bmatrix}_{9 \times 3} \quad (3.7)$$

And $\mathbf{w}_x(t)$ is an additive white Gaussian noise process sampled at time t , with covariance defined as

$$\mathbf{E} [\mathbf{w}_x(t) \mathbf{w}_x^T(t + \tau)] = \mathbf{Q} \delta(\tau) \quad (3.8)$$

$$\mathbf{Q} = \begin{bmatrix} \frac{2\sigma^2}{\tau} & 0 & 0 \\ 0 & \frac{2\sigma^2}{\tau} & 0 \\ 0 & 0 & \frac{2\sigma^2}{\tau} \end{bmatrix} \quad (3.9)$$

where σ^2 is the desired variance of the components of acceleration vector a_x , a_y , and a_z , and $\delta(\tau)$ is the Dirac delta function.

3.3 Dynamic Model

3.3.1 Inertial Navigation System Error Model

There are several models that can be used to represent the INS errors. For this research the 16 states error model expressed in the navigation frame (NED) will be used, based on the model given in [12]. As before, the system dynamics are given by

$$\dot{\mathbf{x}}(t) = \mathbf{F} \mathbf{x}(t) + \mathbf{G} \mathbf{w}(t) \quad (3.10)$$

where \mathbf{F} is the system continuous-time dynamics matrix and $\mathbf{w}(t)$ is the system noise vector [14].

The system states are represented by the system state vector $\mathbf{x}(t)$, which contains the INS position error $\delta\mathbf{P}$, velocity error $\delta\mathbf{v}$, tilt error $\delta\boldsymbol{\epsilon}$, accelerometer bias $\delta\mathbf{b}_a$ and gyroscope bias $\delta\mathbf{b}_g$. Each of the previous states are in three axis dimensions (i.e., x , y and z), and the last state is the scalar barometer bias, $\delta\text{baro}(t)$. The system state vector is described as

$$\mathbf{x}(t) = \begin{bmatrix} \delta\mathbf{P}(t) \\ \delta\mathbf{v}(t) \\ \delta\boldsymbol{\epsilon}(t) \\ \delta\mathbf{b}_a(t) \\ \delta\mathbf{b}_g(t) \\ \delta\text{baro}(t) \end{bmatrix}_{16 \times 1} \quad (3.11)$$

The system continues-time dynamics matrix \mathbf{F} is a 16×16 matrix that represents the INS navigation equations mechanized in the local geographic frame (navigation-frame, NED) [12], expressed as

$$\mathbf{F} = \begin{bmatrix} \mathbf{0}_{3 \times 3} & \mathbf{I}_{3 \times 3} & \mathbf{0}_{3 \times 3} & \mathbf{0}_{3 \times 3} & \mathbf{0}_{3 \times 3} & \mathbf{0}_{3 \times 1} \\ \mathbf{C}_e^n \mathbf{G} \mathbf{C}_n^e & -2\mathbf{C}_e^n \boldsymbol{\Omega}_{ie}^e \mathbf{C}_n^e & (\mathbf{f}^n \times) & \mathbf{C}_b^n & \mathbf{0}_{3 \times 3} & \mathbf{0}_{3 \times 1} \\ \mathbf{0}_{3 \times 3} & \mathbf{0}_{3 \times 3} & -(\mathbf{C}_e^n \boldsymbol{\omega}_{ie}^e) & \mathbf{0}_{3 \times 3} & -\mathbf{C}_b^n & \mathbf{0}_{3 \times 1} \\ \mathbf{0}_{3 \times 3} & \mathbf{0}_{3 \times 3} & \mathbf{0}_{3 \times 3} & -1/\tau_a \mathbf{I}_{3 \times 3} & \mathbf{0}_{3 \times 3} & \mathbf{0}_{3 \times 1} \\ \mathbf{0}_{3 \times 3} & \mathbf{0}_{3 \times 3} & \mathbf{0}_{3 \times 3} & \mathbf{0}_{3 \times 3} & -1/\tau_g \mathbf{I}_{3 \times 3} & \mathbf{0}_{3 \times 1} \\ \mathbf{0}_{1 \times 3} & \mathbf{0}_{1 \times 3} & \mathbf{0}_{1 \times 3} & \mathbf{0}_{1 \times 3} & \mathbf{0}_{1 \times 3} & -1/\tau_b \end{bmatrix}_{16 \times 16} \quad (3.12)$$

The components in the \mathbf{F} matrix are described as follows

- \mathbf{C}_e^n Is the DCM from ECEF-frame to navigation-frame, and it is computed as

$$\mathbf{C}_e^n = \begin{bmatrix} -\sin L \cos \lambda & -\sin L \sin \lambda & \cos L \\ -\sin \lambda & \cos \lambda & 0 \\ -\cos L \cos \lambda & -\cos L \sin \lambda & -\sin L \end{bmatrix} \quad \begin{array}{l} \lambda \text{ is Longitude} \\ L \text{ is the Latitude} \end{array} \quad (3.13)$$

- \mathbf{C}_n^e Is the DCM from navigation-frame to ECEF-frame, and it is the transpose of \mathbf{C}_e^n (i.e., $\mathbf{C}_n^e = \mathbf{C}_e^{nT}$)
- \mathbf{C}_b^n Is the DCM from the body-frame to the navigation-frame, and it is computed as

$$\mathbf{C}_b^n = \begin{bmatrix} \cos \theta \cos \psi & -\cos \phi \sin \psi & \sin \phi \sin \psi \\ \cos \theta \sin \psi & \cos \phi \cos \psi & -\sin \phi \cos \psi \\ -\sin \theta & \sin \phi \cos \theta & \cos \phi \cos \theta \end{bmatrix} \quad (3.14)$$

where ψ is the rotation angle around the z-axis (yaw), θ is the rotation angle around the y-axis (pitch), and ϕ is the rotation angle around the x-axis (roll) [12].

- \mathbf{G} is the gradient of the gravity vector [1], and it is computed as

$$\mathbf{G} = \frac{GM}{\|\mathbf{p}^e\|^3} [3\tilde{\mathbf{p}}^e(\tilde{\mathbf{p}}^e)^T - \mathbf{I}] - (\boldsymbol{\Omega}_{ie}^e)^2 \quad (3.15)$$

where \mathbf{p}^e is the ECEF position vector, $\tilde{\mathbf{p}}^e$ is the ECEF position unit vector, and $\boldsymbol{\Omega}_{ie}^e$ is the skew symmetric form of the Earth's angular rate ω_{ie}^e (7.292115×10^{-5} rad/s) [1].

- \mathbf{f}^n is the specific force expressed in the navigation-frame, and it is computed by

$$\mathbf{f}^n = \mathbf{C}_b^n \mathbf{f}^b \quad (3.16)$$

where \mathbf{f}^b is the specific force in the body-frame.

- $(\mathbf{f}^n \times)$ Is the skew symmetric form of the specific force expressed in the navigation frame.
- τ_a Is the accelerometer time constant
- τ_g Is the gyroscope time constant
- τ_b Is the barometer time constant
- $\mathbf{0}_{3 \times 3}$ Is 3×3 Zero matrix
- $\mathbf{I}_{3 \times 3}$ Is 3×3 Identity matrix

The system noise vector $\mathbf{w}(t)$ in Equation 3.10, is described as

$$\mathbf{w} = \begin{bmatrix} 0 \\ \mathbf{w}_a \\ \mathbf{w}_g \\ \mathbf{w}_{a,bias} \\ \mathbf{w}_{g,bias} \\ \mathbf{w}_{b,bias} \end{bmatrix} \quad (3.17)$$

where \mathbf{w}_a , \mathbf{w}_g , $\mathbf{w}_{a,bias}$, $\mathbf{w}_{g,bias}$, and $\mathbf{w}_{b,bias}$ are the accelerometer random walk, gyro random walk, accelerometer bias, gyro bias, and barometer bias random process, respectively [12]. The noise matrix \mathbf{G} is given by

$$\mathbf{G} = \begin{bmatrix} \mathbf{0}_{3 \times 3} & \mathbf{0}_{3 \times 3} & \mathbf{0}_{3 \times 3} & \mathbf{0}_{3 \times 3} & \mathbf{0}_{3 \times 1} \\ \mathbf{C}_b^n & \mathbf{0}_{3 \times 3} & \mathbf{0}_{3 \times 3} & \mathbf{0}_{3 \times 3} & \mathbf{0}_{3 \times 1} \\ \mathbf{0}_{3 \times 3} & -\mathbf{C}_b^n & \mathbf{0}_{3 \times 3} & \mathbf{0}_{3 \times 3} & \mathbf{0}_{3 \times 1} \\ \mathbf{0}_{3 \times 3} & \mathbf{0}_{3 \times 3} & \mathbf{I}_{3 \times 3} & \mathbf{0}_{3 \times 3} & \mathbf{0}_{3 \times 1} \\ \mathbf{0}_{3 \times 3} & \mathbf{0}_{3 \times 3} & \mathbf{0}_{3 \times 3} & \mathbf{I}_{3 \times 3} & \mathbf{0}_{3 \times 1} \\ \mathbf{0}_{1 \times 3} & \mathbf{0}_{1 \times 3} & \mathbf{0}_{1 \times 3} & \mathbf{0}_{1 \times 3} & 1 \end{bmatrix}_{16 \times 13} \quad (3.18)$$

3.4 Measurement Model

Three different sources of measurements will be used to update the Kalman filter to correct the INS states. The measurement sources that will be used are

- Global positioning system (GPS)
- Star tracker
- Barometer

The Global positioning system (GPS) is a space-based navigation system that provides time information and location of a vehicle (e.g., car, ship, aircraft) in all weather conditions. It is a well used navigation system in most of military and civilian systems because of its high accuracy of positioning and global coverage. However, GPS can be inadequate to use in some cases when its signals are not available due to obstacles or jamming techniques.

In the other hand, star trackers or what is called celestial navigation, is a robust system that is not susceptible to GPS interference and can be used for high accuracy

positioning and navigation. The last measurement source is the barometer, which is a device used to calculate the altitude of an aircraft using the atmosphere pressure.

In general the measurement models will be expressed in the following linear form

$$\mathbf{z}(t_k) = \mathbf{H} \mathbf{x}(t_k) + \mathbf{v}(t_k) \quad (3.19)$$

where $\mathbf{z}(t_k)$ is the measurement vector, \mathbf{H} is the measurement matrix and $\mathbf{v}(t_k)$ is a white Gaussian noise with zero mean and covariance defined as [11]

$$\mathbf{E}[\mathbf{v}(t_k)\mathbf{v}^T(t_j)] = \mathbf{R}\delta(k-j) \quad (3.20)$$

where $\delta(k-j)$ is the Kronecker delta function.

3.4.1 Global Positioning System Model

For the GPS measurement model, the measurement vector $\mathbf{z}_{gps}(t_k)$ is the difference between the GPS position and velocity in 3-axis and the INS position and velocity in 3-axis. The GPS position and velocity are assumed to be calculated from a GPS receiver on the aircraft, and it is equal to the true position and velocity plus an additional noises. The INS position and velocity are equal to the true position and velocity minus the INS position and velocity errors that are calculated from the dynamic model in Section 3.3. The measurement vector $\mathbf{z}_{gps}(t_k)$ is given by

$$\mathbf{z}_{gps}(t_k) = \begin{bmatrix} p_{x,gps} - p_{x,ins} \\ p_{y,gps} - p_{y,ins} \\ p_{z,gps} - p_{z,ins} \\ v_{x,gps} - v_{x,ins} \\ v_{y,gps} - v_{y,ins} \\ v_{z,gps} - v_{z,ins} \end{bmatrix}_{6 \times 1} \quad (3.21)$$

The measurement matrix \mathbf{H}_{gps} is 6×16 matrix and given by

$$\mathbf{H}_{gps} = \begin{bmatrix} 1 & 0 & 0 & 0 & 0 & 0 & 0 & 0 & 0 & 0 & 0 & 0 & 0 & 0 & 0 & 0 \\ 0 & 1 & 0 & 0 & 0 & 0 & 0 & 0 & 0 & 0 & 0 & 0 & 0 & 0 & 0 & 0 \\ 0 & 0 & 1 & 0 & 0 & 0 & 0 & 0 & 0 & 0 & 0 & 0 & 0 & 0 & 0 & 0 \\ 0 & 0 & 0 & 1 & 0 & 0 & 0 & 0 & 0 & 0 & 0 & 0 & 0 & 0 & 0 & 0 \\ 0 & 0 & 0 & 0 & 1 & 0 & 0 & 0 & 0 & 0 & 0 & 0 & 0 & 0 & 0 & 0 \\ 0 & 0 & 0 & 0 & 0 & 1 & 0 & 0 & 0 & 0 & 0 & 0 & 0 & 0 & 0 & 0 \end{bmatrix}_{6 \times 16} \quad (3.22)$$

The measurement noise covariance \mathbf{R}_{gps} is 6×6 matrix and given by

$$\mathbf{R}_{gps} = \begin{bmatrix} \sigma_{p,x,gps}^2 & 0 & 0 & 0 & 0 & 0 \\ 0 & \sigma_{p,y,gps}^2 & 0 & 0 & 0 & 0 \\ 0 & 0 & \sigma_{p,z,gps}^2 & 0 & 0 & 0 \\ 0 & 0 & 0 & \sigma_{v,x,gps}^2 & 0 & 0 \\ 0 & 0 & 0 & 0 & \sigma_{v,y,gps}^2 & 0 \\ 0 & 0 & 0 & 0 & 0 & \sigma_{v,z,gps}^2 \end{bmatrix}_{6 \times 6} \quad (3.23)$$

where $\sigma_{p,x,gps}^2$, $\sigma_{p,y,gps}^2$, and $\sigma_{p,z,gps}^2$ are the variances of the GPS position measurement noise in x , y , and z axis, respectively. Also, $\sigma_{v,x,gps}^2$, $\sigma_{v,y,gps}^2$, and $\sigma_{v,z,gps}^2$ are the variances of the GPS velocity measurement noise in x , y , and z axis, respectively.

3.4.2 Barometer Model

The barometer measurement vector is expressed by the following equation

$$\mathbf{z}_{baro}(t_k) = h_{baro} - p_z \quad (3.24)$$

where p_z is the true altitude, and h_{baro} is the barometer altitude which is given by

$$h_{baro} = b^b + w_b$$

where b^b is the barometer bias, and w_b is an additive white Gaussian noise process.

The barometer bias is modeled as first order Gauss-Markov process, which is expressed by the following differential equation

$$\dot{b}^b = -\frac{1}{\tau_b} b^b + w_{bias}^b \quad (3.25)$$

where τ_b is the barometer time constant and w_{bias}^b is a zero mean white Gaussian noise with a covariance $R_{b,bias}$

$$R_{b,bias} = \frac{2\sigma_{b,bias}^2}{\tau_b} \quad (3.26)$$

The measurement noise covariance R_{baro} is given by

$$R_{baro} = \sigma_b^2 \quad (3.27)$$

where σ_b^2 is the standard deviation of the barometer altitude. The measurement matrix \mathbf{H}_{baro} is given by

$$\mathbf{H}_{baro} = [0 \quad 0 \quad -1 \quad 0 \quad 0 \quad 0 \quad 0 \quad 0 \quad 0 \quad 0 \quad 0 \quad 0 \quad 0 \quad 0 \quad 0 \quad 1]_{1 \times 16} \quad (3.28)$$

3.4.2 Star Tracker Model

The star tracker calculates the attitude of the aircraft and the accuracy of attitude calculation depends on the specifications of the star tracker used and the surrounding environment.

In this research, an unscented transformation is used to transform the star tracker output (Euler angles) along with their uncertainties to get the tilts and their uncertainties. The star tracker output is given by

$$\mathbf{out}_{z_{star}}(t_k) = \begin{bmatrix} \theta_{star} \\ \phi_{star} \\ \psi_{star} \end{bmatrix} \quad (3.29)$$

where θ_{star} , ϕ_{star} , and ψ_{star} are the roll, pitch, and heading angles respectively, that are obtained from the star tracker. In this research, these angles are simulated by adding a white Gaussian noise to the true angles that are obtained from the truth model.

The star tracker output variances are given by

$$\mathbf{out}_{Rstar} = \begin{bmatrix} \sigma_{\theta}^2 & 0 & 0 \\ 0 & \sigma_{\phi}^2 & 0 \\ 0 & 0 & \sigma_{\psi}^2 \end{bmatrix} \quad (3.30)$$

where σ_{θ}^2 , σ_{ϕ}^2 , and σ_{ψ}^2 are the variances in the roll, pitch, and heading respectively. These variances are the accuracy of the star tracker used, and they are given by Table 2.4.

The star tracker and INS Euler angles are used to form a new DCM, which is given by

$$\mathbf{C}_n^n = \mathbf{C}_{bstar}^n \cdot \mathbf{C}_{nins}^b \quad (3.31)$$

where \mathbf{C}_n^b and \mathbf{C}_b^n are given by Equation (2.1).

Using the new DCM, a skew symmetric matrix of the tilts is obtained by taking the matrix natural logarithm

$$\mathbf{A} = \ln(\mathbf{C}_n^n) \quad (3.32)$$

Where the tilts in each axis are obtained as follows

$$\boldsymbol{\epsilon} = \begin{bmatrix} \epsilon_x \\ \epsilon_y \\ \epsilon_z \end{bmatrix} = \begin{bmatrix} \mathbf{A}(3,2) \\ -\mathbf{A}(3,1) \\ \mathbf{A}(2,1) \end{bmatrix} \quad (3.33)$$

Equations (3.31) through (3.33) describe a nonlinear function that maps measured and INS Euler angles to tilt vectors $\boldsymbol{\epsilon}$

$$\boldsymbol{\epsilon} = f(\theta_{star}, \phi_{star}, \psi_{star}, \theta_{INS}, \phi_{INS}, \psi_{INS}) \quad (3.34)$$

The variables θ_{INS} , ϕ_{INS} , and ψ_{INS} are considered to be known values in this equation.

We then use an unscented transformation [6] to calculate the expected values for $\boldsymbol{\epsilon}$ ($E[\boldsymbol{\epsilon}]$) and the covariance matrix of $\boldsymbol{\epsilon}$ ($\text{Cov}(\boldsymbol{\epsilon})$), these are then used directly as

measurements in the Kalman filter. Therefore, the star tracker measurement vector and covariance matrix are given by

$$\mathbf{z}_{star}(t_k) = \mathbf{E}[\boldsymbol{\epsilon}] \quad (3.35)$$

$$\mathbf{R}_{star} = \text{Cov}(\boldsymbol{\epsilon}) \quad (3.36)$$

The measurement matrix of the star tracker model is given by

$$\mathbf{H}_{star} = \begin{bmatrix} 0 & 0 & 0 & 0 & 0 & 0 & 1 & 0 & 0 & 0 & 0 & 0 & 0 & 0 & 0 \\ 0 & 0 & 0 & 0 & 0 & 0 & 0 & 1 & 0 & 0 & 0 & 0 & 0 & 0 & 0 \\ 0 & 0 & 0 & 0 & 0 & 0 & 0 & 0 & 1 & 0 & 0 & 0 & 0 & 0 & 0 \end{bmatrix}_{3 \times 16} \quad (3.37)$$

3.5 Kalman Filter Implementation

Based on the linear dynamic and measurement models of this system, a linear Kalman filter is a good choice for this system. The Kalman filter equations described in Section 2.6 are used in the simulation with the measurement models described in Section 3.4 to update the INS parameters.

3.6 Chapter Summary

This chapter explained and discussed the truth, dynamic, and measurement models that will be implemented in MATLAB to get simulation results for the system. Next chapter will show the simulation parameters used and the simulation results developed.

IV. Simulation Results

In this chapter, simulated performance results for the methodology discussed in the previous chapter will be shown and analyzed. We will start with explaining the different INS grades that will be used in the simulation along with their parameters. Next, simulation scenarios will be explained. Then, a Kalman filter validation step will be shown. Then in the following sections, results of different scenarios including GPS, star tracker and barometer aiding is presented and analyzed.

There are three different grades of INS; commercial, tactical and navigation. The commercial grade INS has low quality sensors (i.e. Accelerometers and Gyroscopes) and these sensors should be calibrated after installation in the Inertial Measurement Unit (IMU) to be used for short duration flights. In contrast, tactical grade INS is a medium quality grade that is used for medium flight durations of several minutes. Finally, the navigation grade INS is used for long flight durations and has good quality sensors. Key error parameters for the three INS grades are shown in Table 4.1.

Table 4.1: Parameters used in simulation for different INS grades. All INS grades have a time constant of $\tau_a = \tau_g = 3600$ seconds [14].

INS Grade	σ_g (rad/s)	σ_a (m/s ²)	σ_{grw} (rad/s ^{1/2})	σ_{arw} (m/s ^{3/2})
Commercial (Cloudcap Crista)	8.7e-3	1.96e-1	6.5e-4	4.3e-3
Tactical (HG1700)	4.8e-6	9.8e-3	8.7e-5	9.5e-3
Navigation (HG9900 – H764G)	7.2e-9	2.45e-4	5.8e-7	2.3e-4

In Table 4.1, the gyroscope time-correlated bias time constant is denoted by τ_g , the accelerometer time-correlated bias time constant is denoted by τ_a , the gyroscope time-correlated bias standard deviation is denoted by σ_g , and the accelerometer time-correlated bias standard deviation is denoted by σ_a . Also, the accelerometer and gyroscope random walk noise strength is denoted by $\sigma_{a_{rw}}$ and $\sigma_{g_{rw}}$, respectively [14].

The flight dynamics and duration limits the criteria of selecting the inertial grade needed for the application. In the research, the previous discussed INS grades will be simulated for different flight durations depending on the INS grade used and the result analysis. In addition, the flight dynamics is assumed to be a normally straight and level flight with no maneuvers and very little acceleration.

4.1 Simulation Scenarios

In the following sections of this chapter, there are two scenarios selected to compare between the different measurements models described in chapter III. The two scenarios are as follows

- Scenario one: *GPS initialization, Star tracker and Barometer.*
- Scenario two: *GPS initialization and Barometer.*

In the first scenario, GPS, star tracker, and barometer measurements will be used from the beginning of the flight but the GPS will be only for the first 200 seconds. The second scenario will be like the first scenario but without the star tracker. Table 4.2 describes the star tracker parameters used in the research, which were obtained from [13].

Table 4.2: Star Tracker Parameters

Star Tracker Name	SUNSAT Star Tracker
Roll Accuracy	12 arcseconds
Pitch Accuracy	12 arcseconds
Yaw Accuracy	12 arcseconds

4.2 Filter Validation

This section contains simulated navigation results using the INS model developed in Section 3.3 and the measurement models developed in Section 3.4. The simulations in this section use the INS parameters from Table 4.1, the star tracker parameters from Table 4.2, and the navigation parameters from Table 4.3.

Before developing the results, Kalman filter validation is an important step to verify that the filter is well designed and can estimate the states needed for this research. The filter validation is carried out through simulation of 1000 Monte Carlo runs for the three INS grades.

Figures 4.1, 4.2, and 4.3 show the Monte Carlo runs for the position error for the commercial grade INS, tactical grade INS, and navigation grade INS, respectively.

Table 4.3: Simulation Parameters for Navigation Filter

Kalman Filter Propagation Time	1 second
Initial Position	(0,0,0) m
Initial Velocity	(200,0,0) m/s
Initial Acceleration	(0,0,0) m/s ²

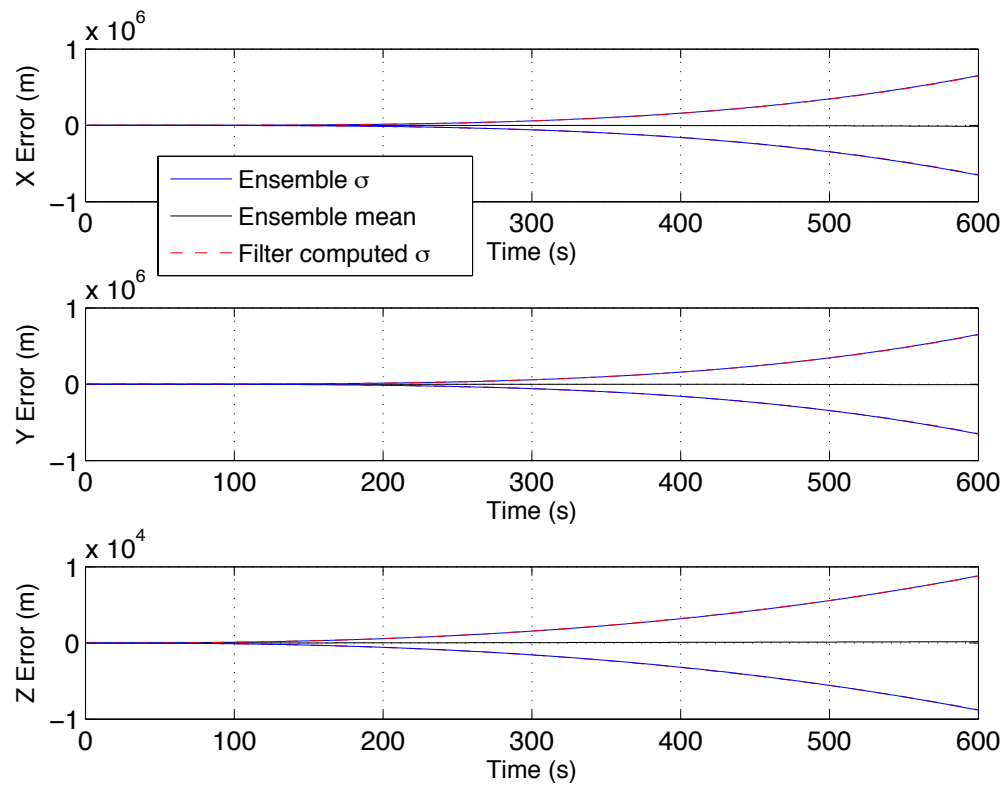


Figure 4.1: Position ensemble standard deviation and mean versus filter computed standard deviation for commercial grade INS.

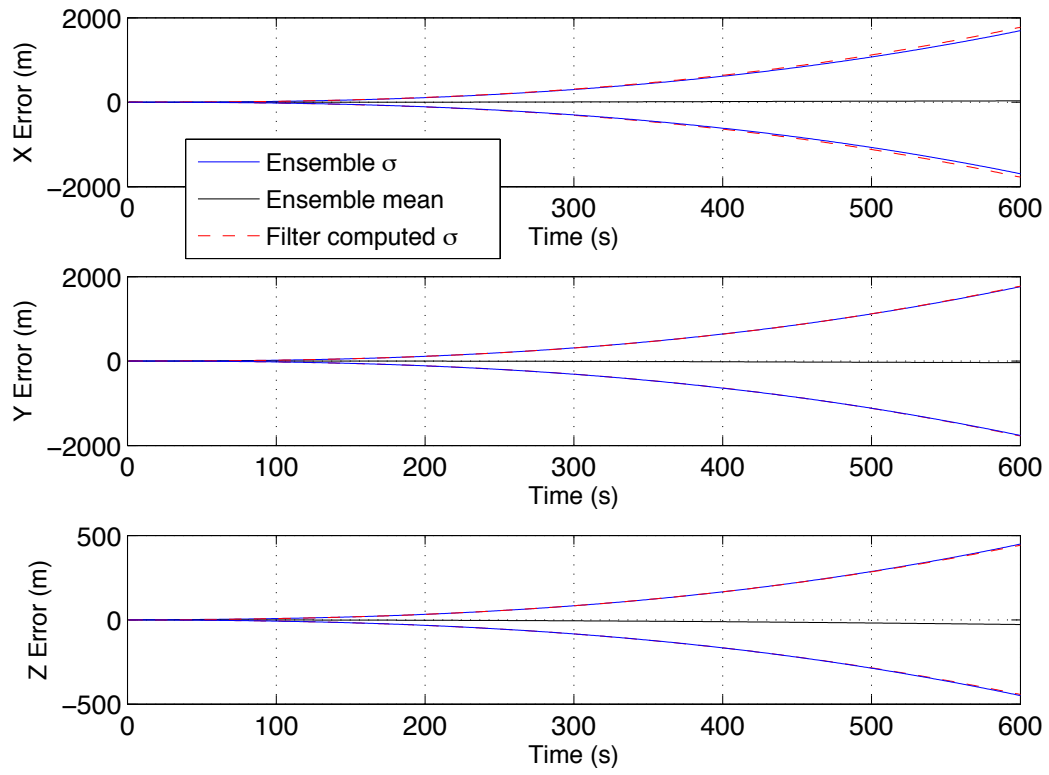


Figure 4.2: Position ensemble standard deviation and mean versus filter computed standard deviation for tactical grade INS.

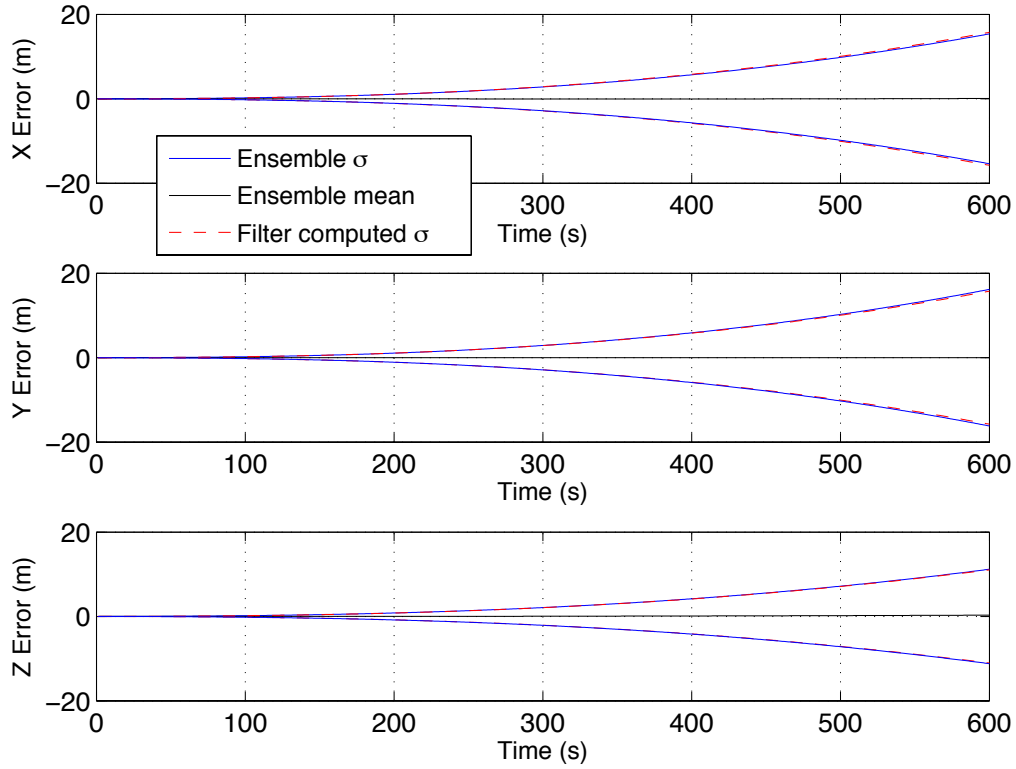


Figure 4.3: Position ensemble standard deviation and mean versus filter computed standard deviation for navigation grade INS.

The previous figures are simulation runs when INS only is used and they match the results developed in [14] and [12]. Also, we see that the filter computed standard deviation predicts the ensemble standard deviation, which would be expected for a properly functioning filter.

For further filter validation, the first scenario is simulated for 1000 Monte Carlo runs with a navigation grade INS, and the position error is shown in Fig. 4.4.

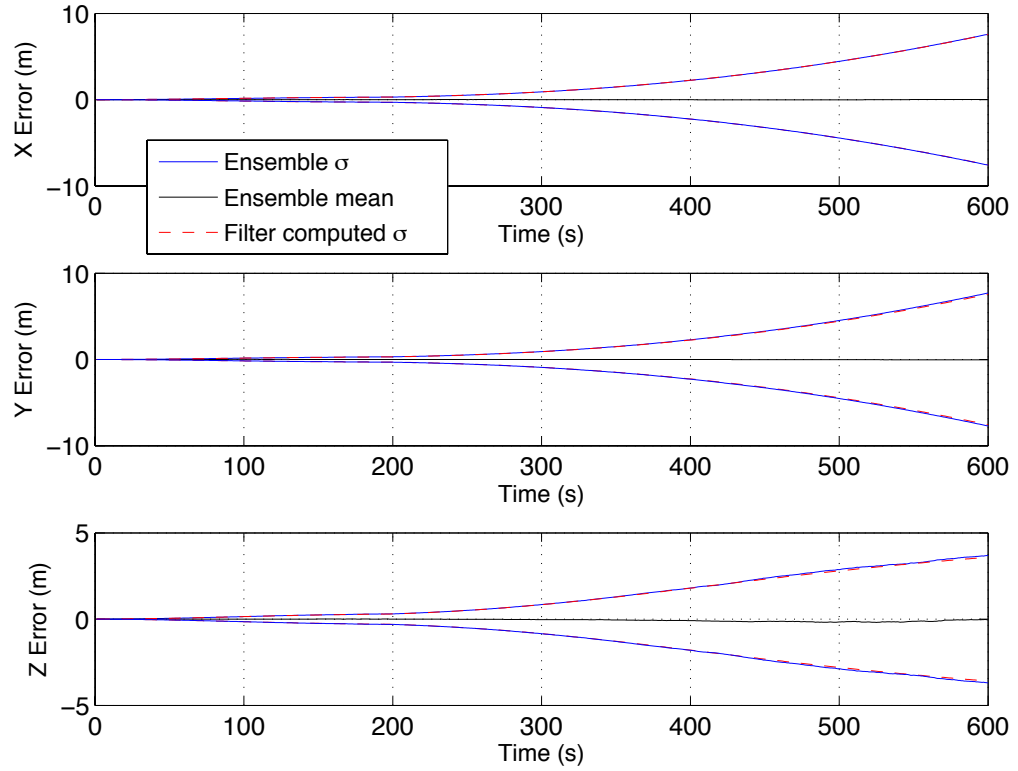


Figure 4.4: Position error for 1000 Monte Carlo runs of the first scenario for a navigation grade INS.

Fig. 4.4 proves that the results in Fig. 4.3 are not outliers, and that the 1000 Monte Carlo runs when measurements are used is on the same order as the filter computed standard deviation of the 1000 Monte Carlo runs in Fig. 4.3. In Fig. 4.4, we see that there is improvement in the filter computed standard deviation when using the star tracker and the barometer measurements. In addition, the errors in velocity, tilt, accelerometer, gyroscope, and barometer are shown in Fig. 4.5-4.9, respectively.

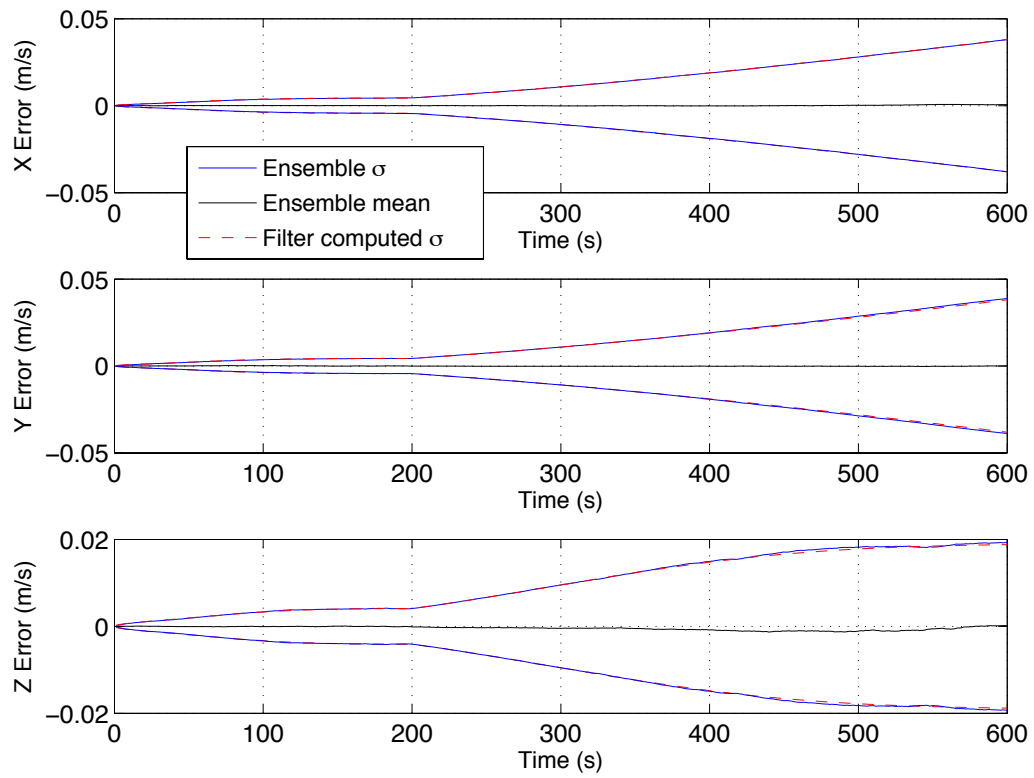


Figure 4.5: Velocity error for 1000 Monte Carlo runs of the first scenario (GPS outage at 200 sec.) for a navigation grade INS.

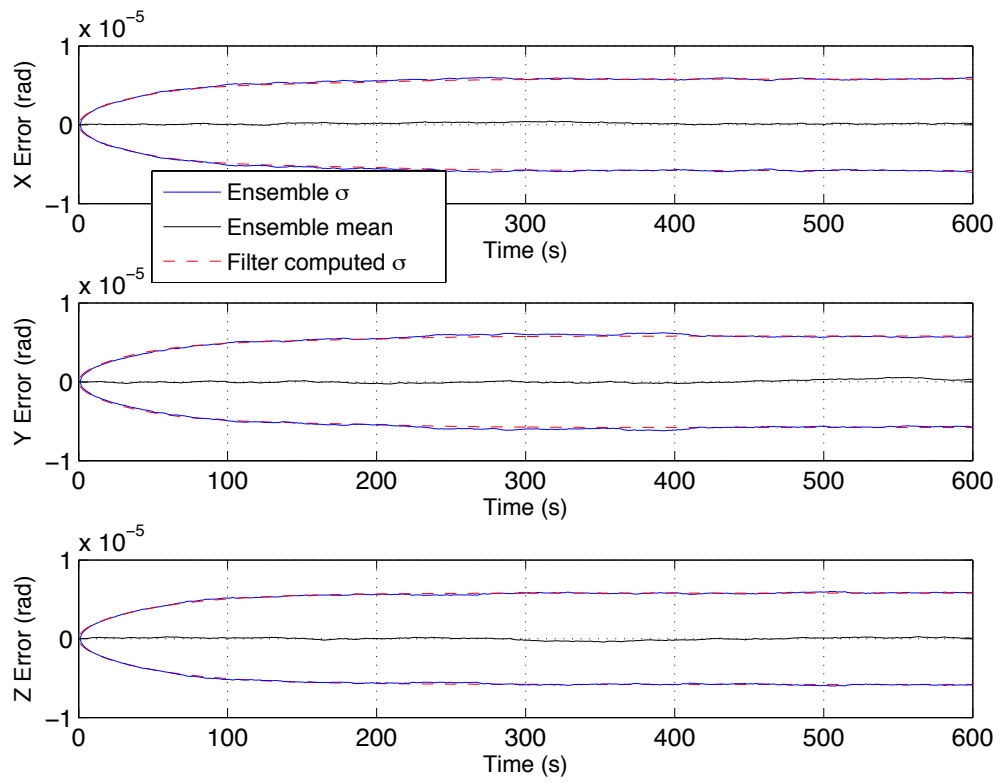


Figure 4.6: Tilt error for 1000 Monte Carlo runs of the first scenario for a navigation grade INS.

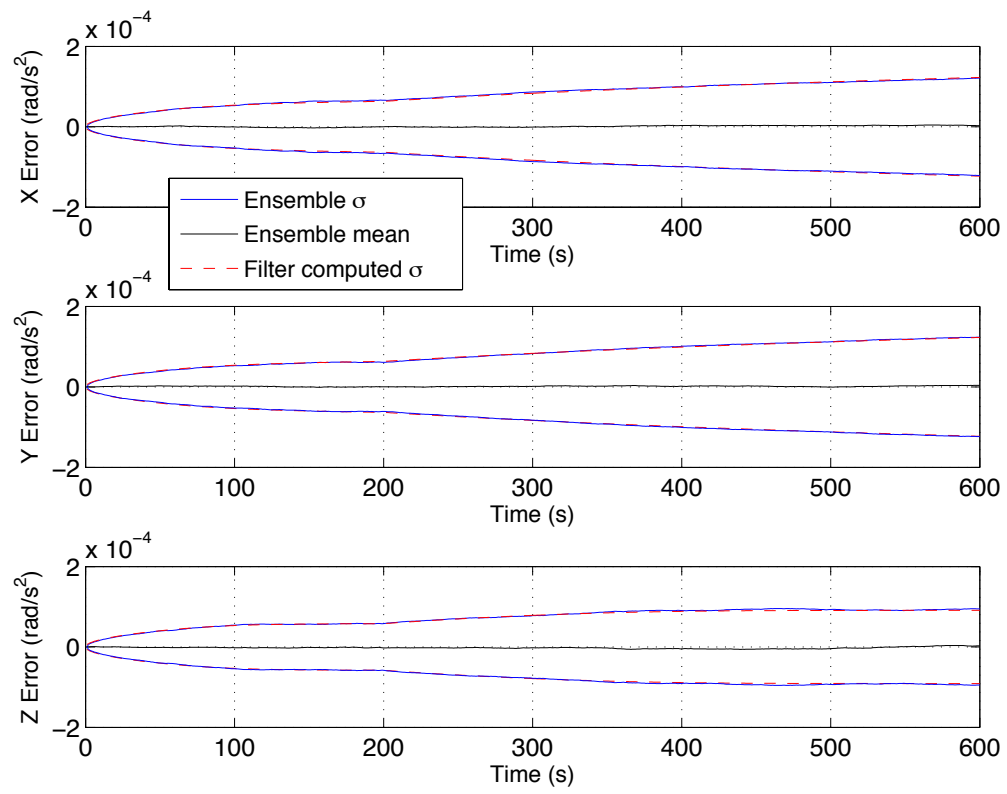


Figure 4.7: Accelerometer error for 1000 Monte Carlo runs of the first scenario for a navigation grade INS.

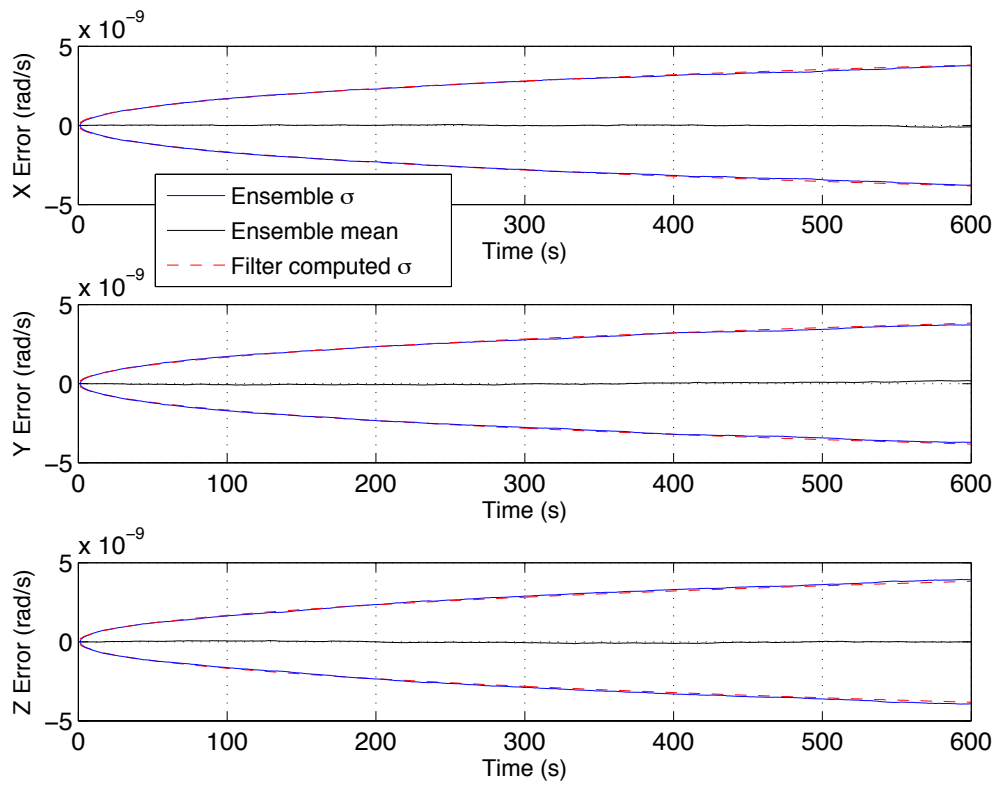


Figure 4.8: Gyroscope error for 1000 Monte Carlo runs of the first scenario for a navigation grade INS.

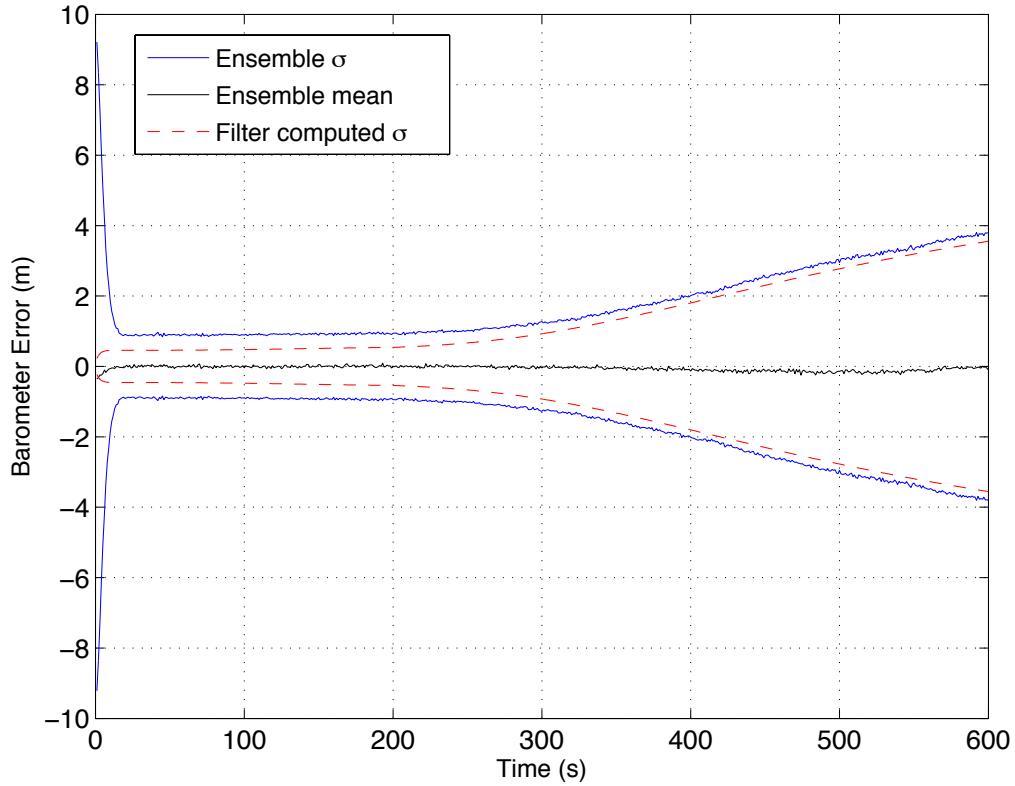


Figure 4.9: Barometer error for 1000 Monte Carlo runs of the first scenario for a navigation grade INS.

In order to measure the effects of INS grade on the results, tactical and commercial grade INS were simulated. Fig. 4.10 shows the position error for 1000 Monte Carlo runs for tactical grade INS with measurements from scenario one. We see improvement in the tactical grade when star tracker and barometer are used, compared to Fig. 4.2.

Fig 4.11 shows the position error for a commercial grade INS with measurements from scenario one. Also in the commercial grade, we see a good improvement when star tracker and barometer are used, compared to Fig. 4.1.

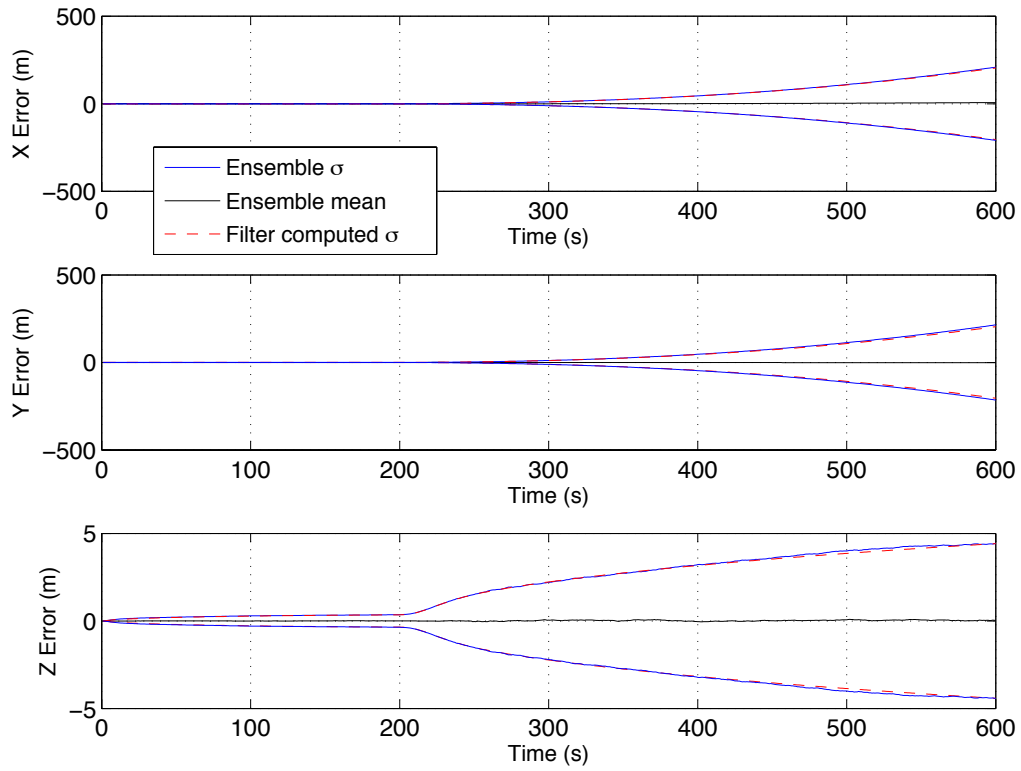


Figure 4.10: Position error for 1000 Monte Carlo runs of the first scenario (GPS outage at 200 sec.) for a tactical grade INS.

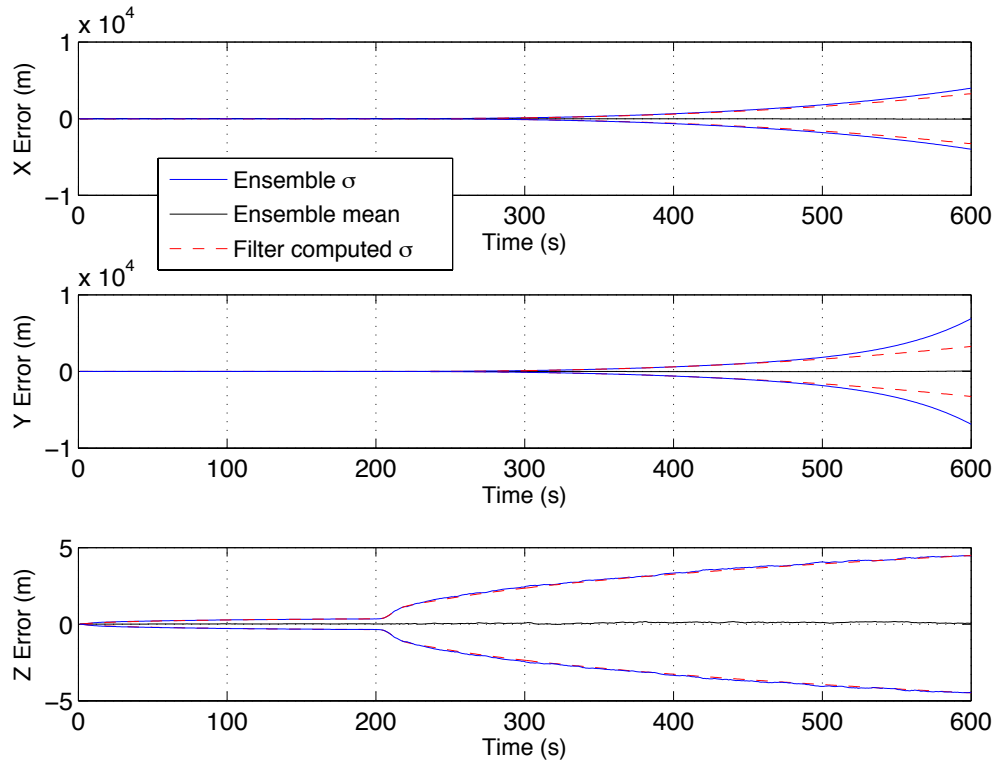


Figure 4.11: Position error for 1000 Monte Carlo runs of the first scenario for a commercial grade INS.

4.3 Star Tracker Performance Improvement on INS Grades

This section is to discuss the impact of both scenarios discussed in Section 4.1 on the different INS grades. Since the filter was validated in the previous section, performance analysis will be conducted based on a pure covariance analysis. The results in this section are generated in accordance with Tables 4.1, 4.2, and 4.3.

In this research we are primarily interested in the effect of using star tracker on two error states, position and tilt, and therefore the results in this section will show only

the error state covariance of the position and tilt. For convenience, the rest of the error states covariences will be included in Appendix A.

For the commercial grade INS, the estimated position error covariance for the two scenarios is simulated for 600 seconds and shown in Fig 4.12. We see from the figure how the star tracker (scenario one) has a significant improvement on the estimated position error covariance of the commercial grade INS, it decreased from $12 \times 10^4 \text{m}$ to 3600m in the x-axis and y-axis, where the z-axis remained at 6m for both scenarios because of the barometer aiding used in the two scenarios. Also, the estimated tilt covariance for the two scenarios is shown in Fig. 4.13. In the estimated tilts covariance we see a tremendous improvement when using star tracker as seen in scenario one. The commercial grade INS decreased to $5.8 \times 10^{-5} \text{rad}$ in the three axes when using the star tracker, and it increased to 0.9rad in the x-axis and y-axis when the star tracker is not used as seen in scenario two, and the z-axis increased to 1.7rad.

For the tactical grade INS, the estimated position error covariance for the two scenarios is simulated for 600 seconds and shown in Fig 4.14. We see from the figure how the star tracker (scenario one) has improved the estimated position error covariance of the tactical grade INS; it decreased from 1000m to 300m in the x-axis and y-axes. Also, the estimated tilt covariance for the two scenarios is shown in Fig. 4.15. In Fig 4.15 we see an improvement when using star tracker as seen in scenario one. The tactical grade INS decreased to $5.1 \times 10^{-5} \text{rad}$ in the three axes when using star tracker, while the estimated tilt covariance is $2 \times 10^{-3} \text{rad}$ in the three axes when star tracker is not used.

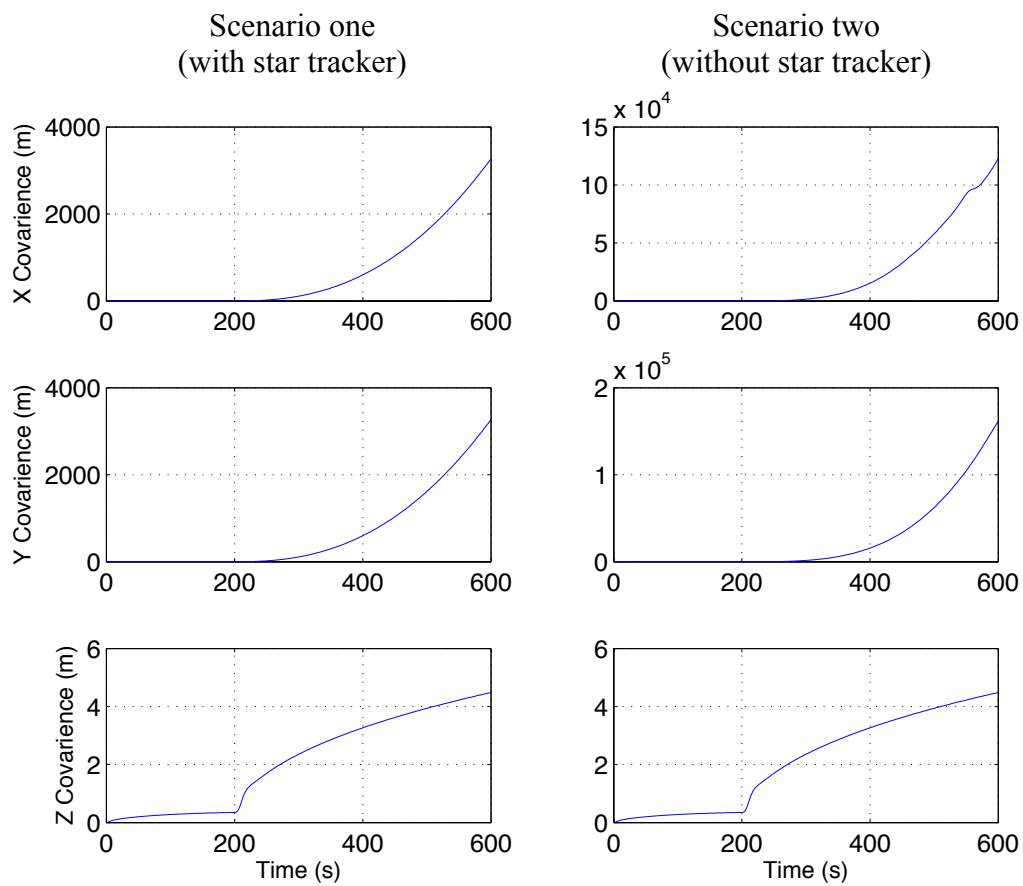


Figure 4.12: Estimated position error covariance for the two scenarios for commercial grade INS.

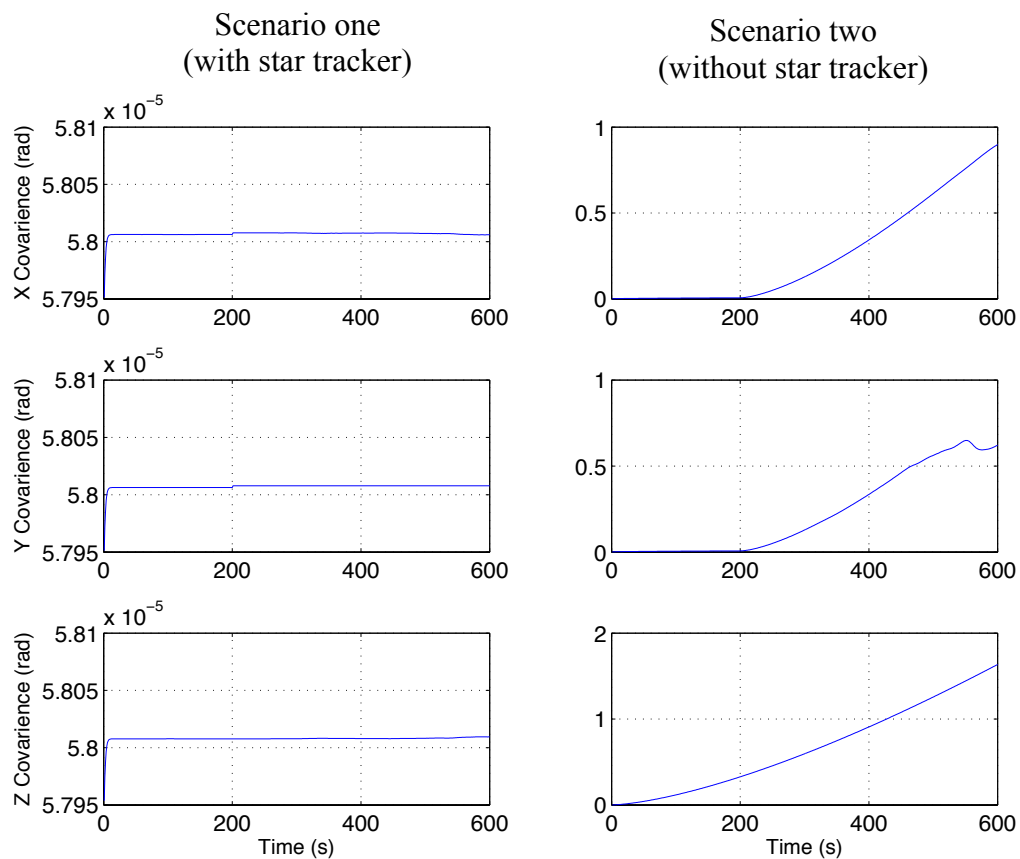


Figure 4.13: Estimated tilt covariance for the two scenarios for commercial grade INS.

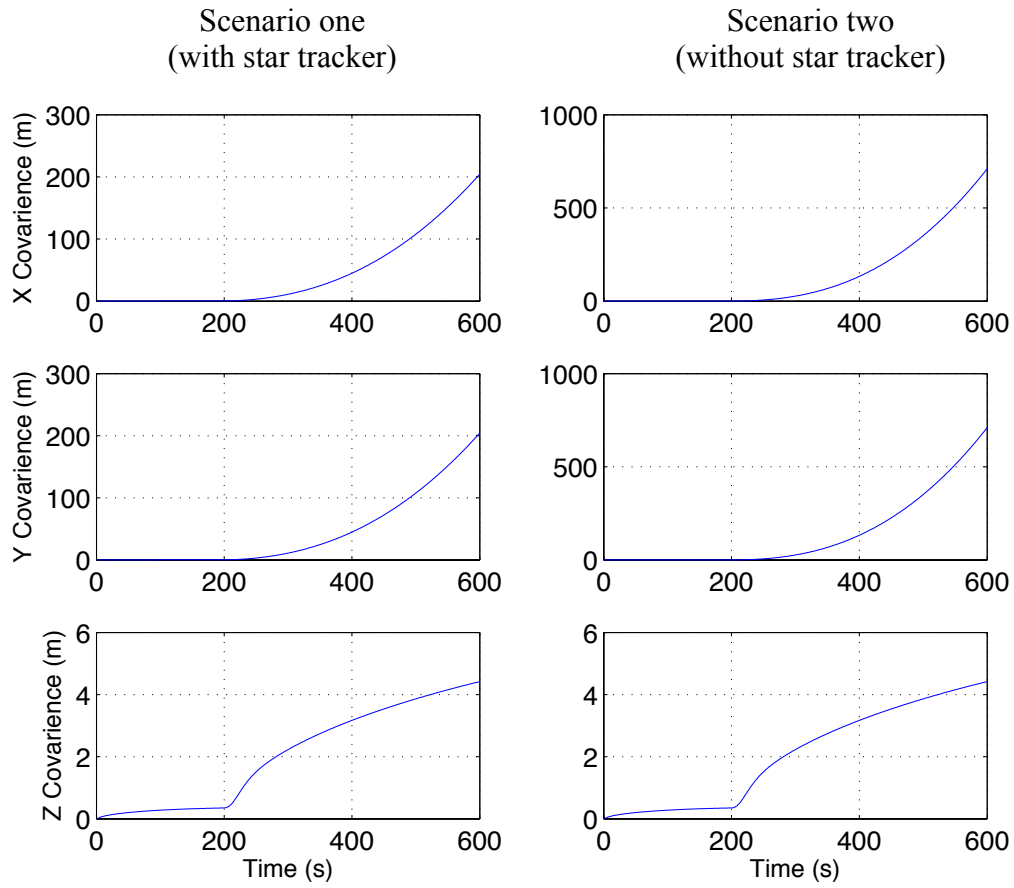


Figure 4.14: Estimated position error covariance for the two scenarios for tactical grade INS.

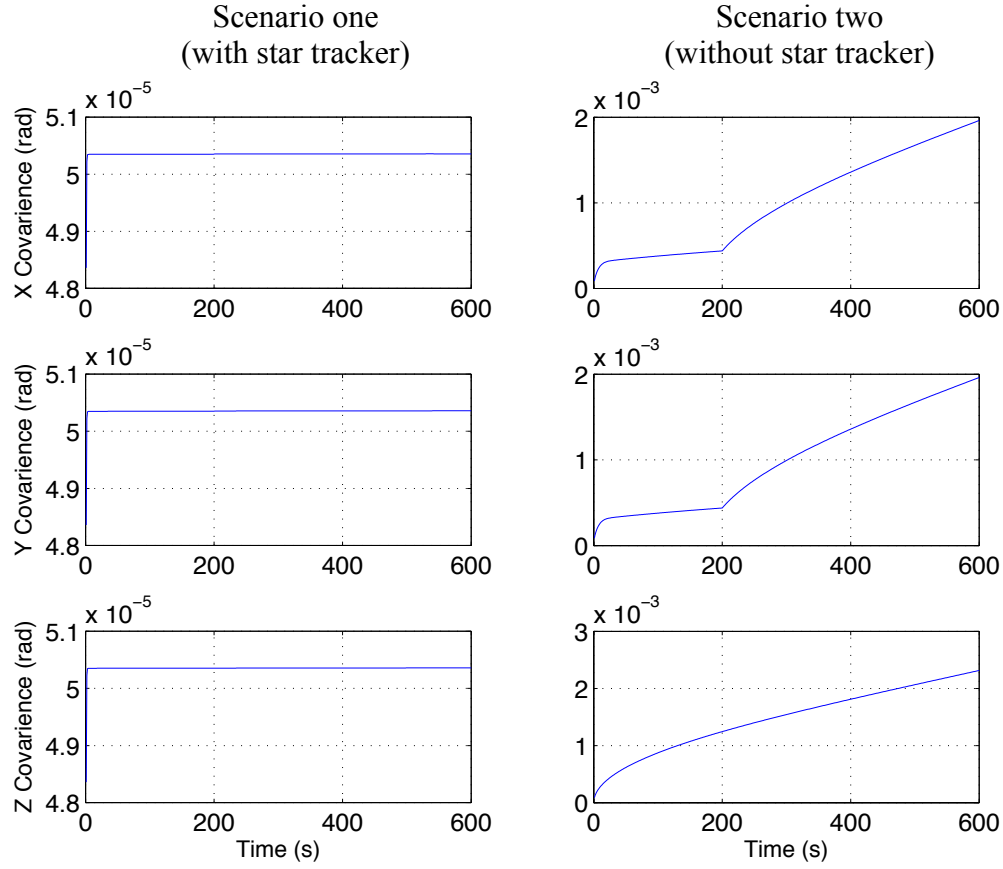


Figure 4.15: Estimated tilt covariance for the two scenarios for tactical grade INS.

The estimated position and tilt covariances for the two scenarios for the navigation grade INS are shown in Fig 4.16 and Fig. 4.17 respectively. In the two figures we notice there is very little improvement on the navigation grade INS when star tracker is used or not used, and that is because the navigation grade INS uses good quality of

gyroscopes and accelerometers which makes the position and tilts almost perfect for small flight durations (i.e. 600 seconds).

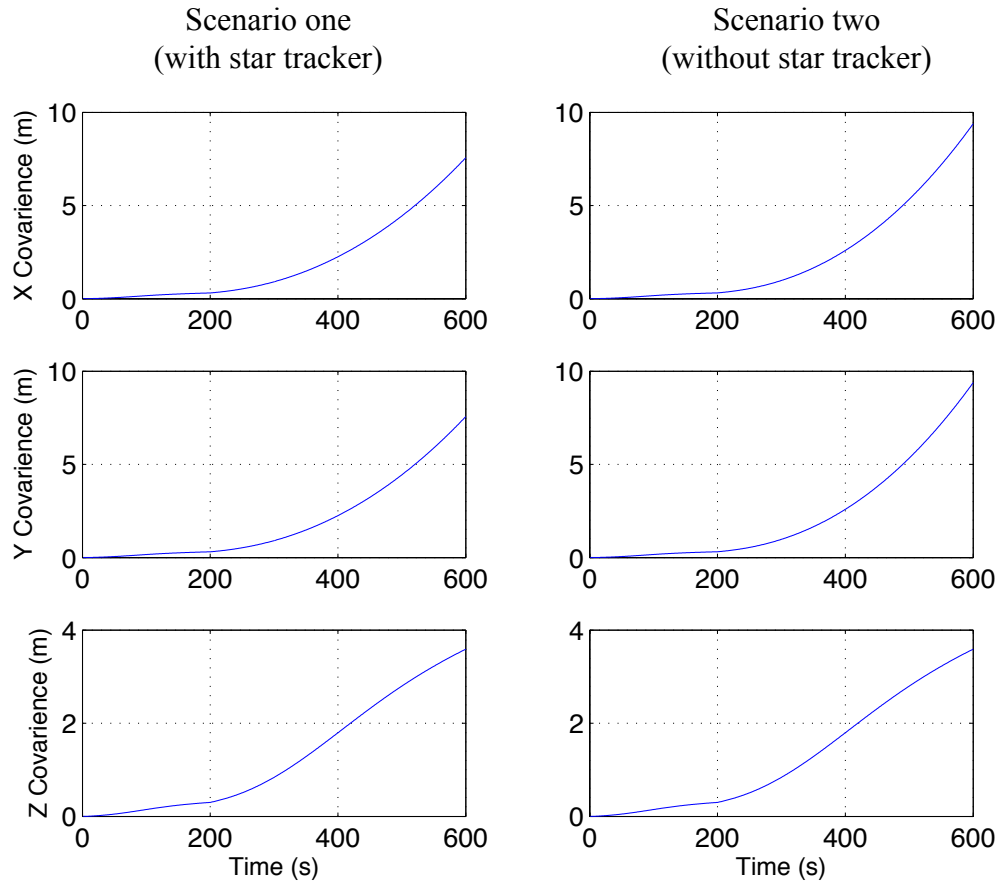


Figure 4.16: Estimated position error covariance for the two scenarios for navigation grade INS.

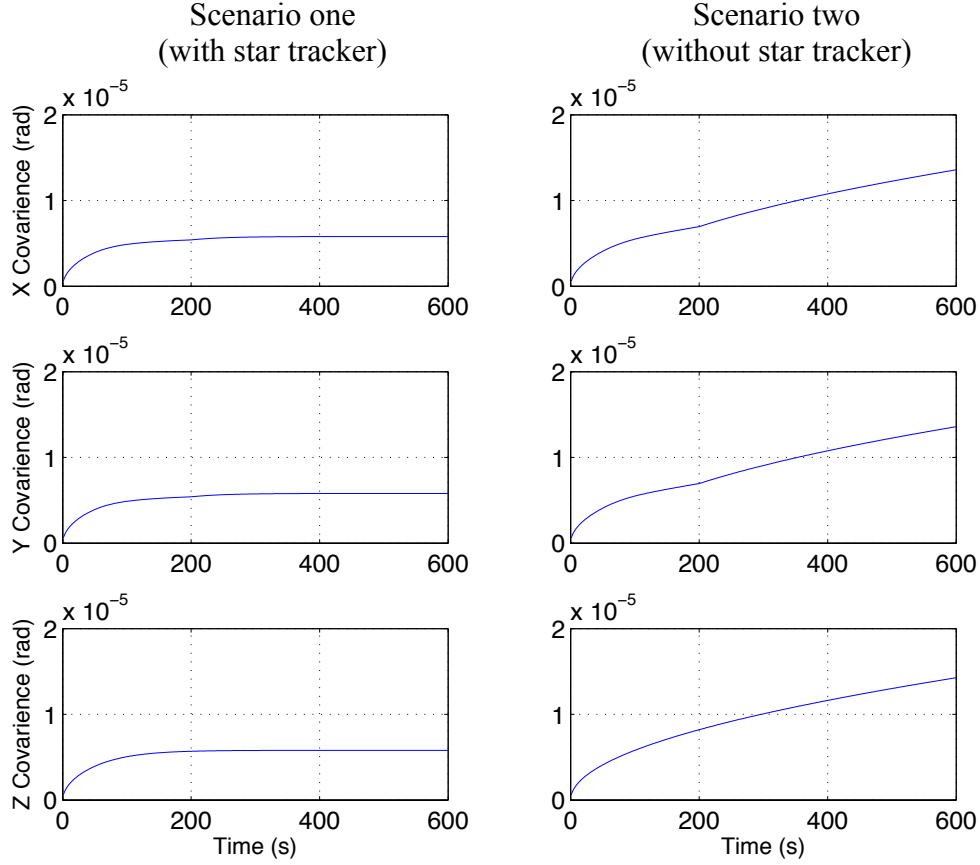


Figure 4.17: Estimated tilt covariance for the two scenarios for navigation grade INS.

Now, we increased the aircraft flight time from 600 seconds to 7200 seconds to see the effect of using star tracker on the navigation grade INS for long flight durations. Fig. 4.18 shows the estimated position error covariance for the two scenarios for the navigation grade INS. In Fig. 4.13 we see a very good improvement when the star tracker is used, as seen in scenario one. The estimated position error covariance decreased from

6603m to 3370m in the x-axis and y-axis when star tracker is used. Also, the estimated tilts covariance for the two scenarios is shown in Fig. 4.19. In Fig 4.19 we see an improvement when using the star tracker as seen in scenario one. The navigation grade INS decreased to 5.8×10^{-6} rad in the three axes when using the star tracker, while the estimated tilt covariance is 5.9×10^{-5} rad in the three axes when the star tracker is not used.

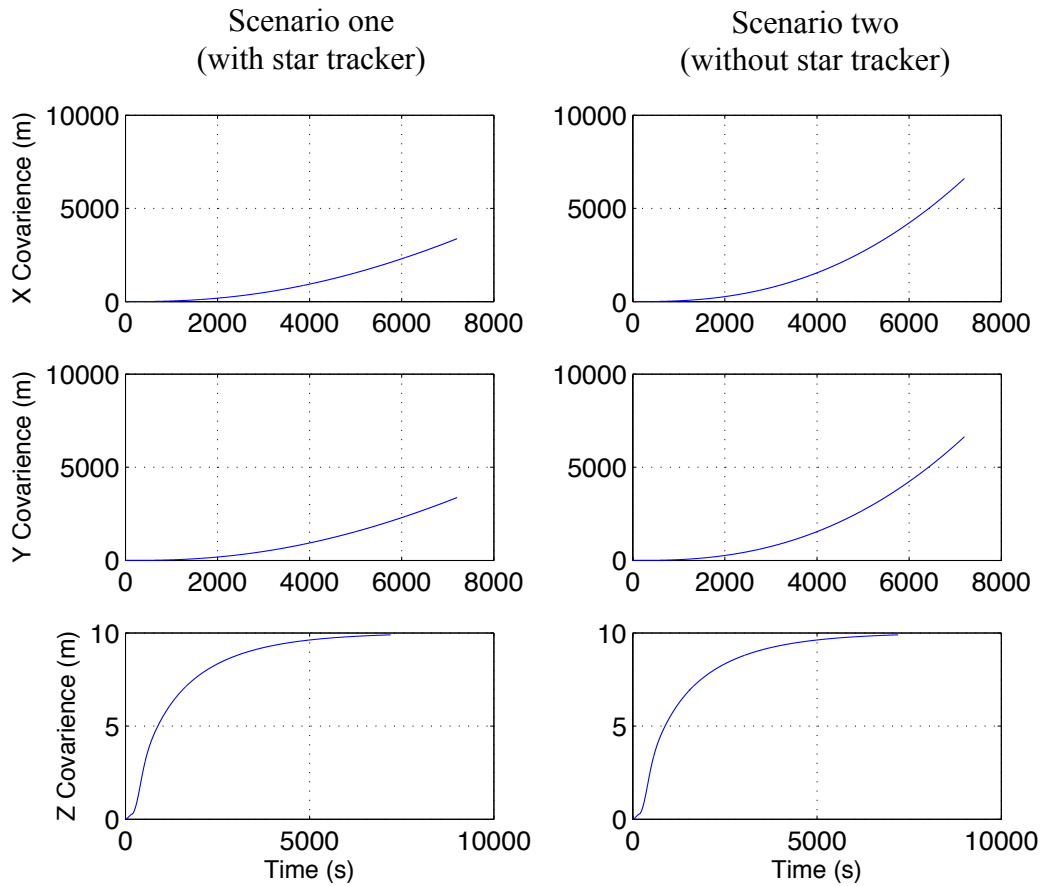


Figure 4.18: Estimated position error covariance for the two scenarios for navigation grade INS for 7200 seconds flight time.

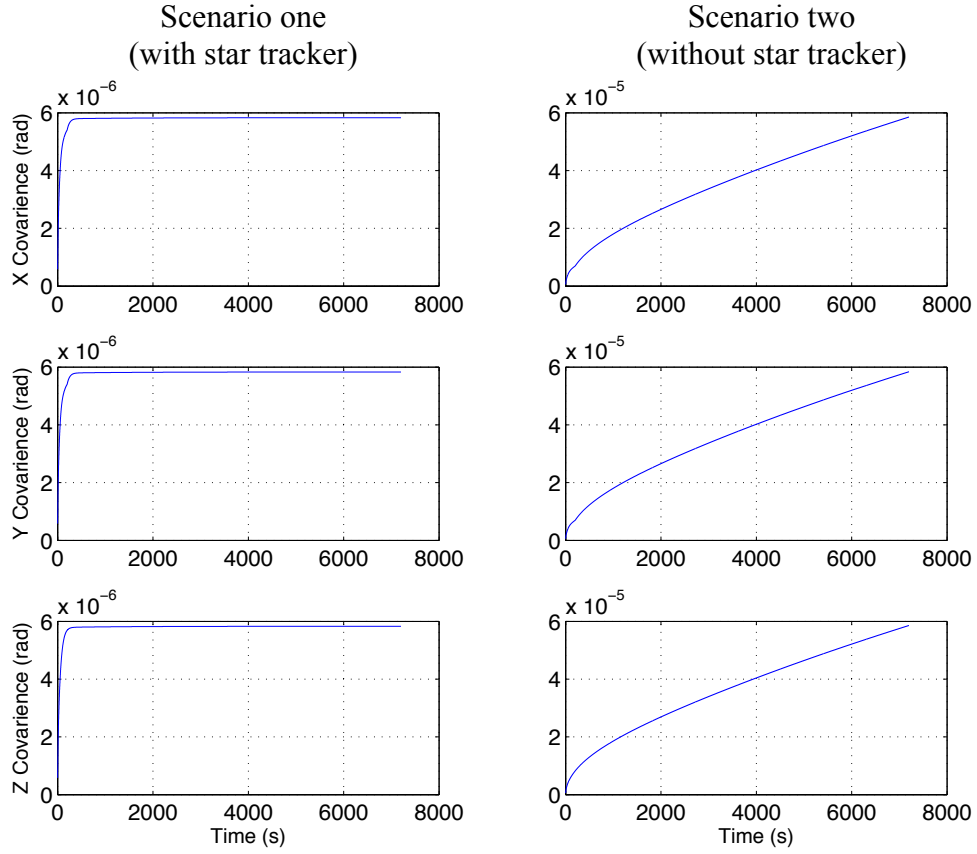


Figure 4.19: Estimated tilt covariance for the two scenarios for navigation grade INS.

In summary of this section, star trackers can enhance the performance of all the three INS grades to a significant improvement. Table 4.4 shows a summary of the results of this section.

Table 4.4: Summary of final error standard deviation for the three INS grades for both scenarios

Parameter (Units)	Commercial		Tactical		Navigation - 7200 sec.	
	Scenario 2	Scenario 1	Scenario 2	Scenario 1	Scenario 2	Scenario 1
Latitude (m)	12×10^4	3606	758	201	6603	3370
Longitude (m)	12×10^4	3606	758	201	6603	3370
Altitude (m)	4.2	4.2	4.2	4.2	10	10
ϵ_x (rad)	0.93	5.8×10^{-5}	2×10^{-3}	5×10^{-5}	5.9×10^{-5}	5.9×10^{-6}
ϵ_y (rad)	0.62	5.8×10^{-5}	2×10^{-3}	5×10^{-5}	5.9×10^{-5}	5.9×10^{-6}
ϵ_z (rad)	1.74	5.8×10^{-5}	2×10^{-3}	5×10^{-5}	5.9×10^{-5}	5.9×10^{-6}

4.4 Impact of Star Tracker Accuracy and INS Quality

This section is to illustrate the impact of star tracker accuracy on different INS grades. The Distance Root Mean Square (DRMS) value of the estimated horizontal position error covariance for a navigation grade INS after the GPS outage is simulated for both scenarios, scenario one is the blue line (with star tracker) and scenario two is the green line (without star tracker), and the results are shown in Fig. 4.20.

From Fig. 4.20, we notice there is no effect of star tracker accuracy on the second scenario since there is no star tracker measurement to update the Kalman filter. For the first scenario, the star tracker is continuously updating the Kalman filter and the DRMS value increases when the star tracker accuracy decreases. Table 4.5 shows the difference of the DRMS values of both scenarios for the navigation grade INS.

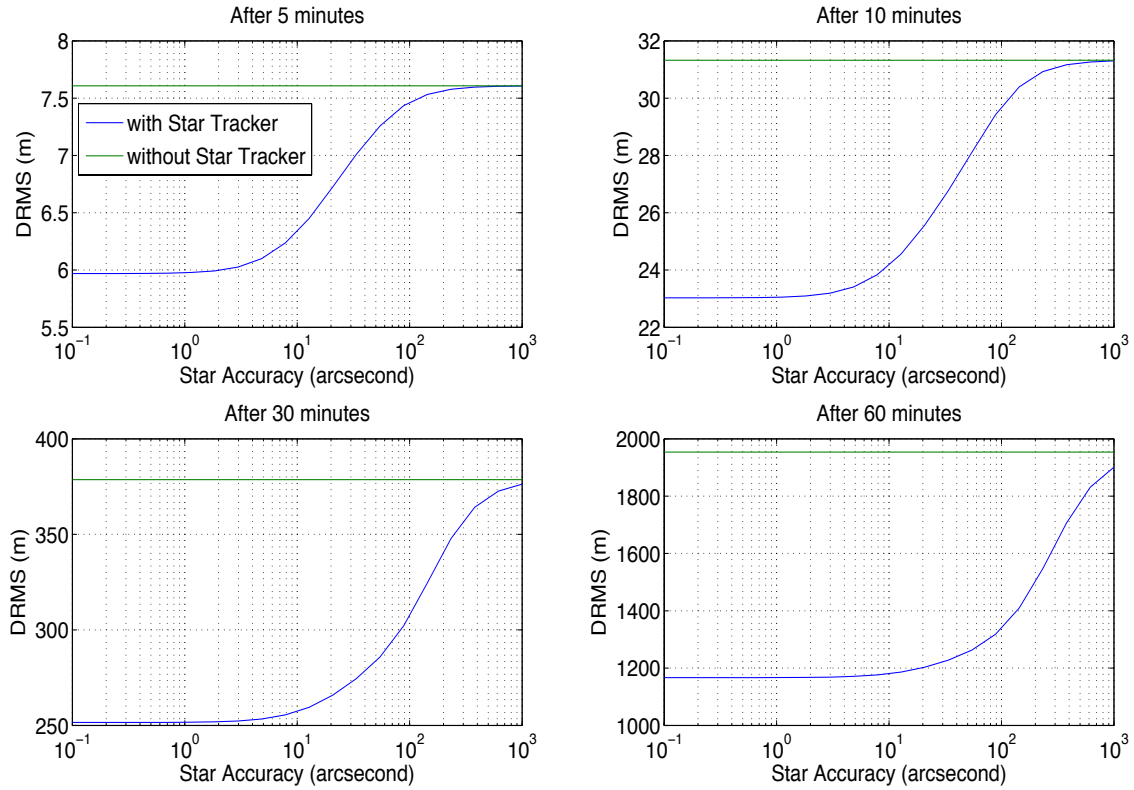


Figure 4.20: Star tracker accuracy effect after GPS outage for both scenarios for navigation grade INS. Scenario one is the blue line and scenario two is the green line.

Table 4.5: Improvement in DRMS values when using star tracker for the navigation grade INS.

Star tracker accuracy	DRMS Improvement			
	After 5 minutes	After 10 minutes	After 30 minutes	After 60 minutes
0.1 arcsecond	1.64 m	8.29 m	127.09 m	786.76 m
10 arcsecond	1.16 m	6.77 m	119.19 m	767.32 m
200 arcsecond	0.03 m	0.39 m	30.76 m	405.68 m
1000 arcsecond	0 m	0.02 m	2.38 m	52.48 m

In Table 4.5, we see the difference of the DRMS values of both scenarios. The difference increases when the GPS is not available, and that show how the star tracker improved the estimated position error covariance by 786.75m, when a 0.1 arcsecond star accuracy is used. Also, we notice that when 1000 arcsecond star tracker accuracy is used there is not much effect after the GPS outage occurred.

Fig. 4.21 and Fig. 4.22 show the DRMS value of the estimated position error covariance for scenario one for the tactical and commercial grades INS respectively. Scenario two was not plotted because there is no effect of the star tracker on it. In Fig. 4.21 and Fig. 4.22, we see how the star tracker accuracy effect both INS grades, and as expected when the star tracker accuracy decreases the DRMS value increases.

4.5 Chapter Summary

In this Chapter, the Kalman filter used was validated for all the three INS grades. Then, performance improvements to the different grades of INS when star tracker is used were shown and discussed. Also, the impact of star tracker accuracy on the INS grades was illustrated and discussed. The next Chapter will discuss the research conclusions and the future work recommendations for future improvement to the star tracker navigation technique.

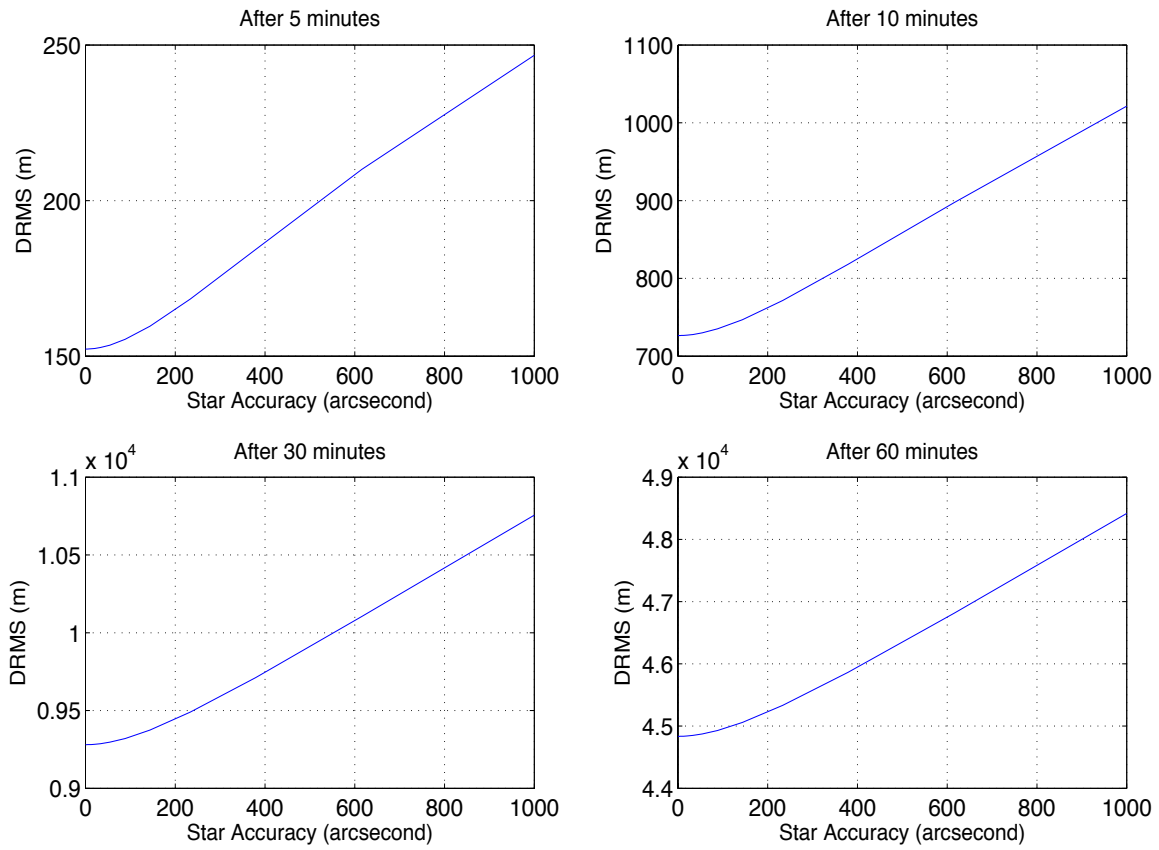


Figure 4.21: Star tracker accuracy effect after GPS outage for scenario one for tactical grade INS.

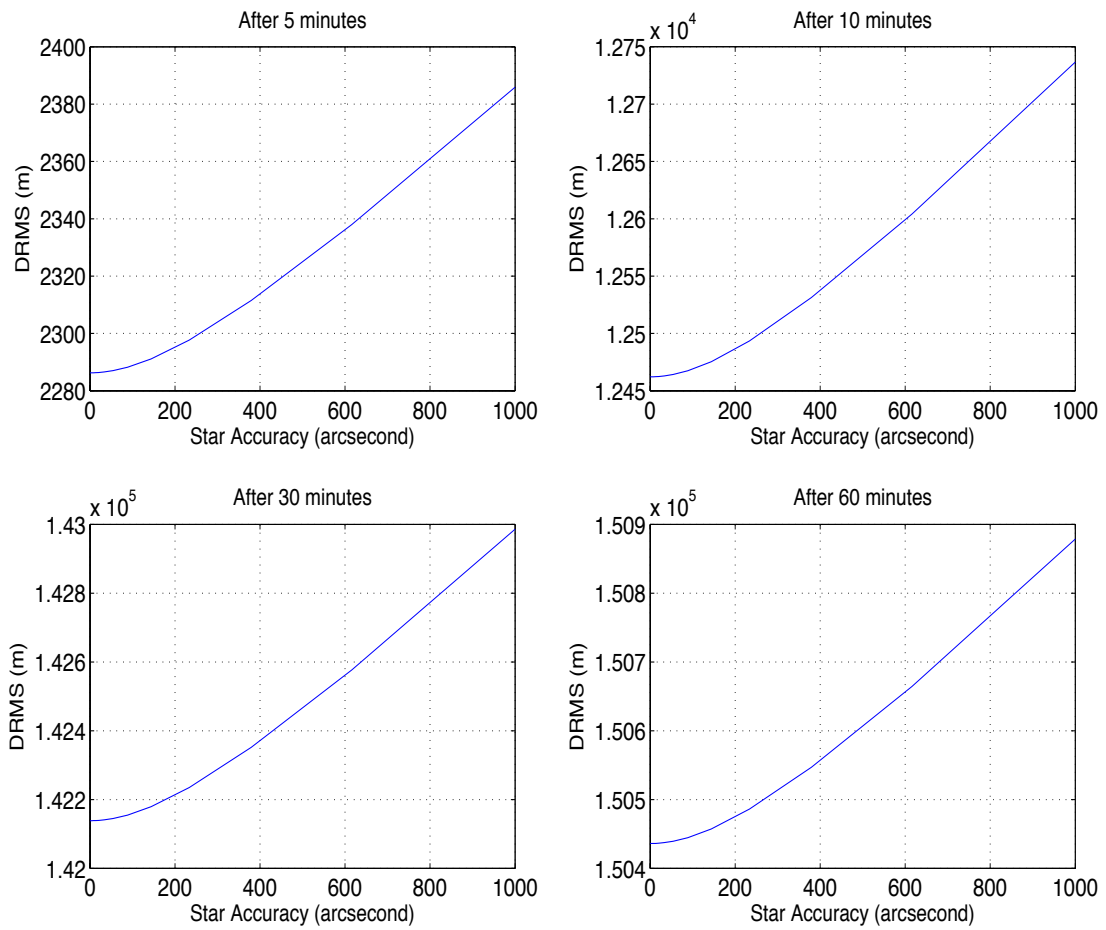


Figure 4.22: Star tracker accuracy effect after GPS outage for scenario one for commercial grade INS.

V. Conclusion

This thesis presents a simulation for integrated star tracker and inertial sensors for robust, self-contained, autonomous navigation. In this chapter, conclusions about the research effort are presented and discussed. Also, areas for future research work are addressed.

5.1 Conclusions

The goal of this research was to show the performance development in the different types of INS when using a star tracker. The star tracker was used as an aiding sensor to update and correct the orientation of the vehicle's INS, and subsequently to enhance the accuracy of position and velocity of the vehicle.

The research focused on two scenarios, these two scenarios were implemented with three grades of INS commercial, tactical, and navigation. The first scenario was about using the GPS for a small period in the beginning of the vehicle's flight time, and then it stops at a time where we assumed that the GPS is no longer available. In addition, the star tracker and barometer were available in the first scenario for the total vehicle's flight time. The second scenario was similar to the first scenario, but instead of using a star tracker, a barometer was used. These two scenarios were selected to show the advantages of using the star tracker over the three different grades of INS.

After simulating the two scenarios with the three grades of INS, we had good results that show the performance enhancement in the INS when a star tracker was used.

The star tracker was able to enhance the position, velocity, and tilts of all three grades of INS. The enhancement degree changes from one INS grade to another depending on the duration of the vehicle's flight time and the accuracy of the inertial sensors used in the three INS grades. The vehicle's flight time in the simulation was 600 seconds, and the GPS was used for the first 200 seconds.

For the commercial grade INS, the star tracker was able to correct the vehicle's position error covariance from $12 \times 10^4 \text{m}$ to 3600m, which is a tremendous improvement to the position. Also, it corrected the tilts covariance from 0.9rad to $5.8 \times 10^{-5} \text{rad}$. The star tracker showed a very good improvement to the commercial grade INS. Although the final accuracy of 3600m is not very good.

For the tactical grade INS, the star tracker was able to correct the vehicle's position error covariance from 1000m to 300m, and it corrected the tilt covariance from $2 \times 10^{-3} \text{rad}$ to $5.1 \times 10^{-5} \text{rad}$. The star tracker showed a very good improvement to the tactical grade INS, on the 600 seconds time interval.

For the navigation grade INS, the simulation was carried out for two different vehicle's flight time. The first vehicle's flight time was 600 seconds, and the star tracker when used showed very little improvement to the navigation grade INS, that is because the navigation grade INS uses a very good inertial sensors (i.e. gyroscopes and accelerometers), and the vehicle's flight time was small for the inertial sensors biases to increase to a limit where the star tracker can make a difference. So, we increased the vehicle's flight time to 7200 seconds and made the GPS available for the first 200 seconds. In this situation, the position error covariance of the navigation grade INS

decreased from 6603m to 3370m, and the tilts covariance decreased from 5.9×10^{-5} rad to 5.8×10^{-6} rad when the star tracker was used.

In conclusion, the star tracker was able to improve the performance of the commercial and tactical grades INS, for any duration of the vehicle's flight time. Also, the improvement in the performance of the navigation grade INS was not significant until the vehicle's flight time was more than approximately 1000 seconds.

5.2 Future Work Recommendations

This research has covered the basic simulation for using star tracker and the inertial sensors, and the following points can improve the technique

- Study the relationship between stars locations and the vehicle's location.
- Build a realistic star tracker measurement model.
- Test and analyze the star tracker measurement model by using different types of Kalman filter.

The first point in my recommendations for future work is to deeply study the relationship between the stars location and the navigating vehicle's location. It includes studying the stars locations in space and how can we benefit from knowing stars locations, and how can we transform the stars locations using certain reference frames.

The second recommendation is to build a realistic star tracker measurement model. This can be achieved if the first point is studied deeply. The measurement model will include the Euler angles (i.e. roll, pitch, and yaw) and using the Euler angles as an

update measurement to the Kalman filter can improve the vehicle's orientation and the INS navigating parameters.

Using a realistic star tracker measurement model will enhance the reality of the simulation results. Depending on the star tracker measurement model, different types of Kalman filter could be used, such as an Extended Kalman Filter (EKF) or an Unscented Kalman Filter (UKF). It would be useful to calculating the improvements to the simulation results when using three filters.

Appendix A

A1.1 1000 Monte Carlo Runs Simulation, Without Measurements

This section will show the rest of the INS states for the 1000 Monte Carlo runs simulation for INS-only.

A1.1.1 Navigation Grade INS

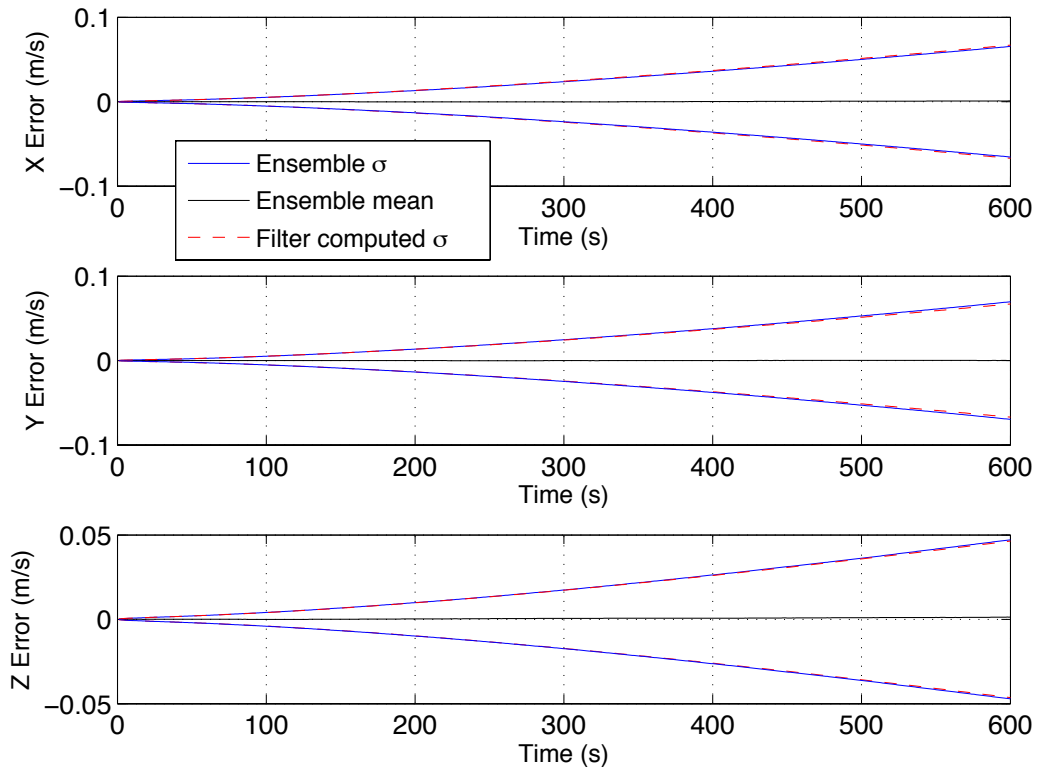


Figure A1.1: Velocity ensemble standard deviation and mean versus filter computed standard deviation for navigation grade INS, without measurements.

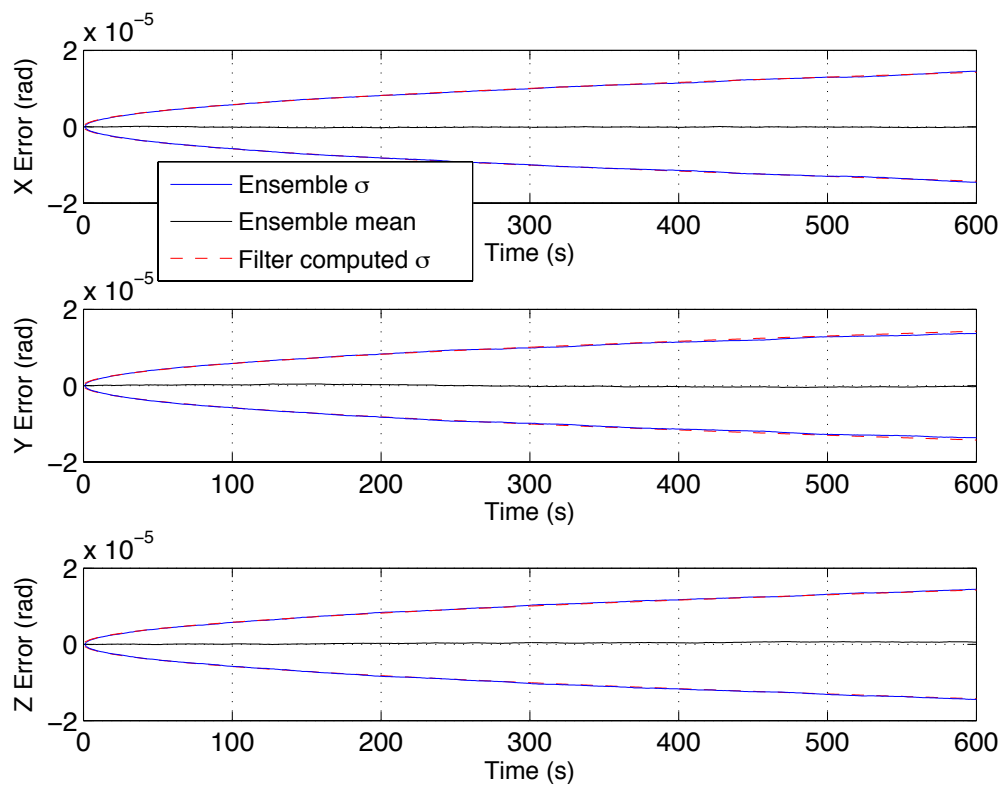


Figure A1.2: Tilt ensemble standard deviation and mean versus filter computed standard deviation for navigation grade INS, without measurements.

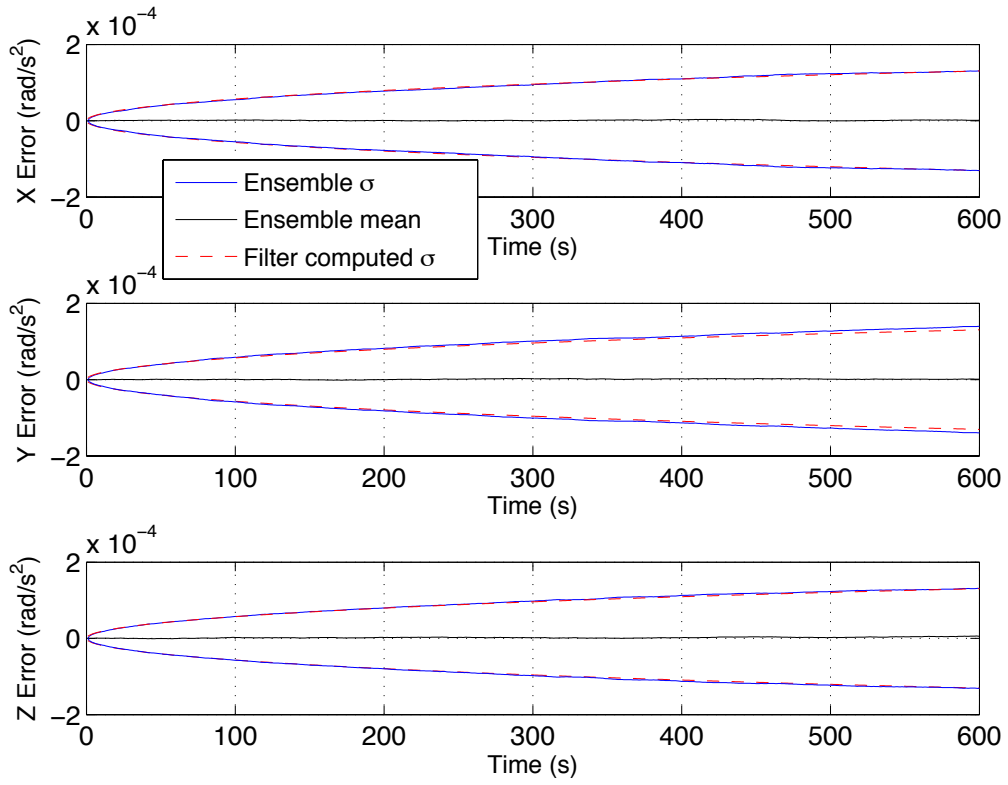


Figure A1.3: Accelerometer ensemble standard deviation and mean versus filter computed standard deviation for navigation grade INS, without measurements.

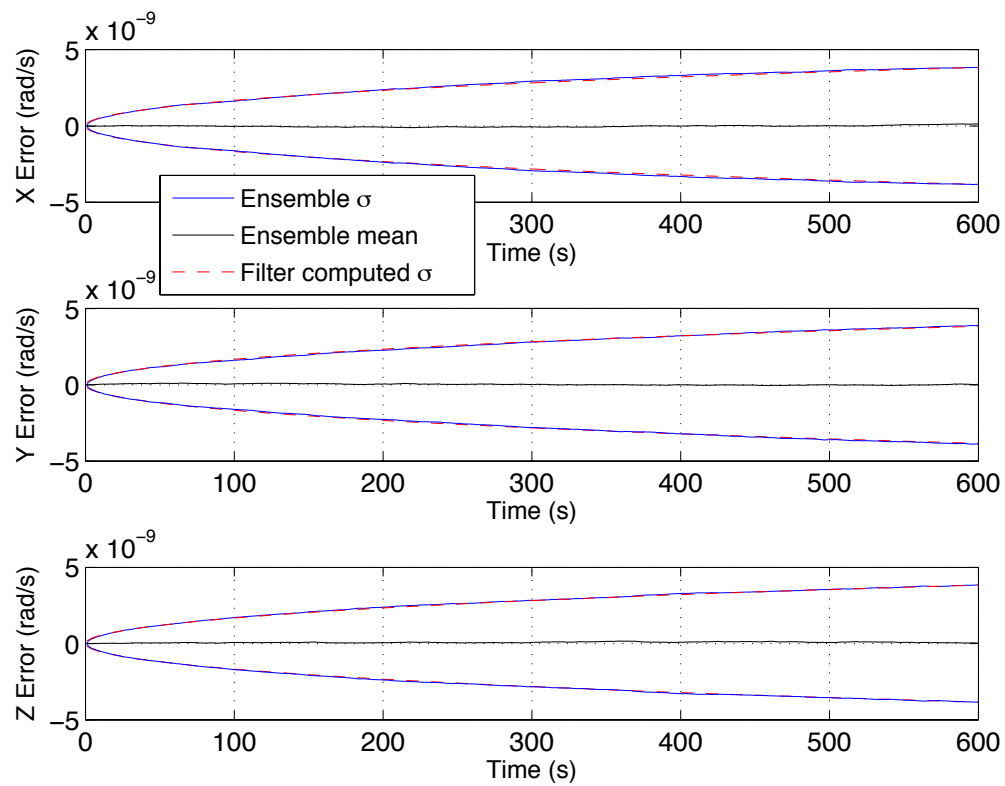


Figure A1.4: Gyroscope ensemble standard deviation and mean versus filter computed standard deviation for navigation grade INS, without measurements.

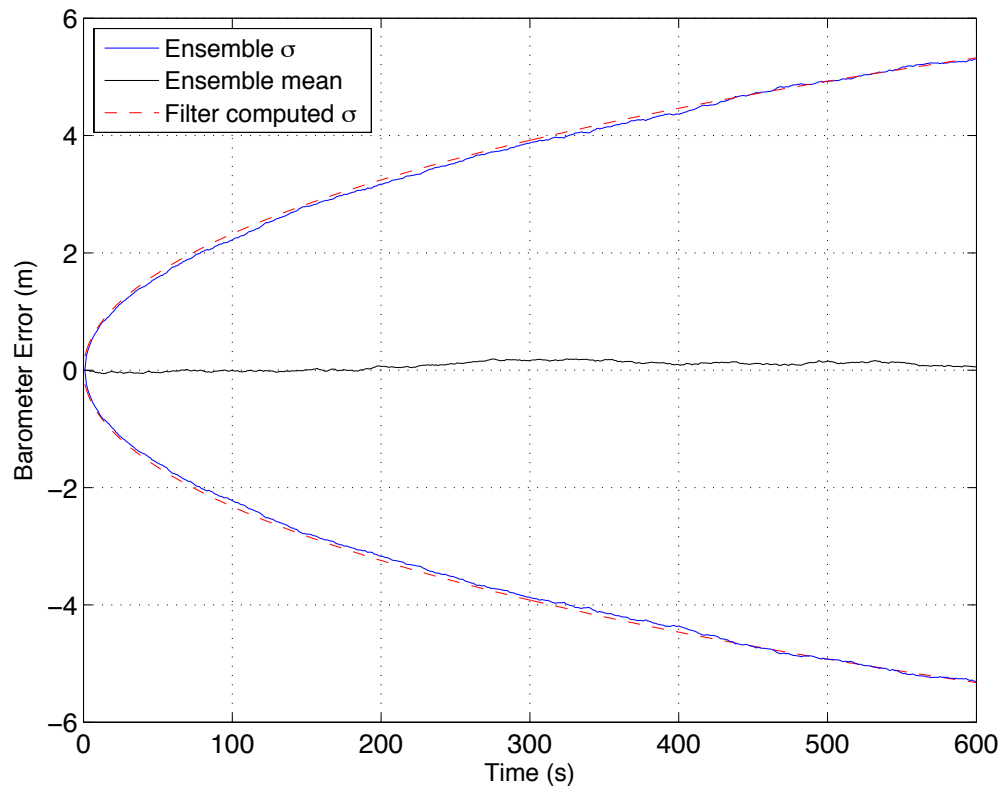


Figure A1.5: Barometer ensemble standard deviation and mean versus filter computed standard deviation for navigation grade INS, without measurements.

A1.1.2 Tactical Grade INS

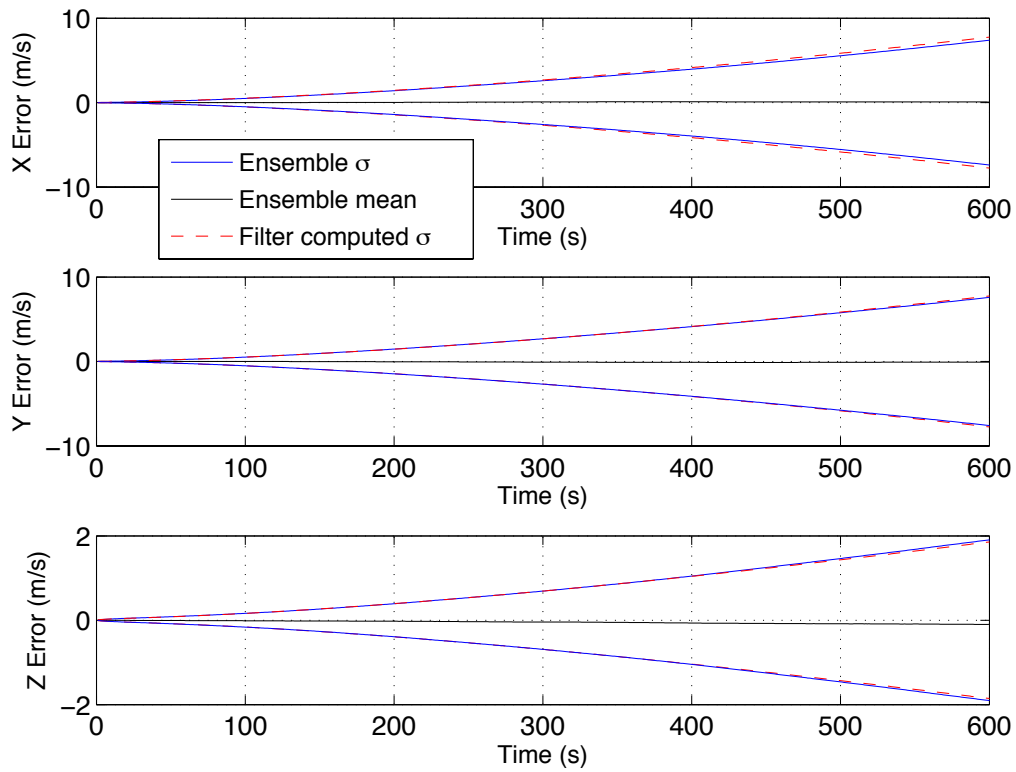


Figure A1.6: Velocity ensemble standard deviation and mean versus filter computed standard deviation for tactical grade INS, without measurements.

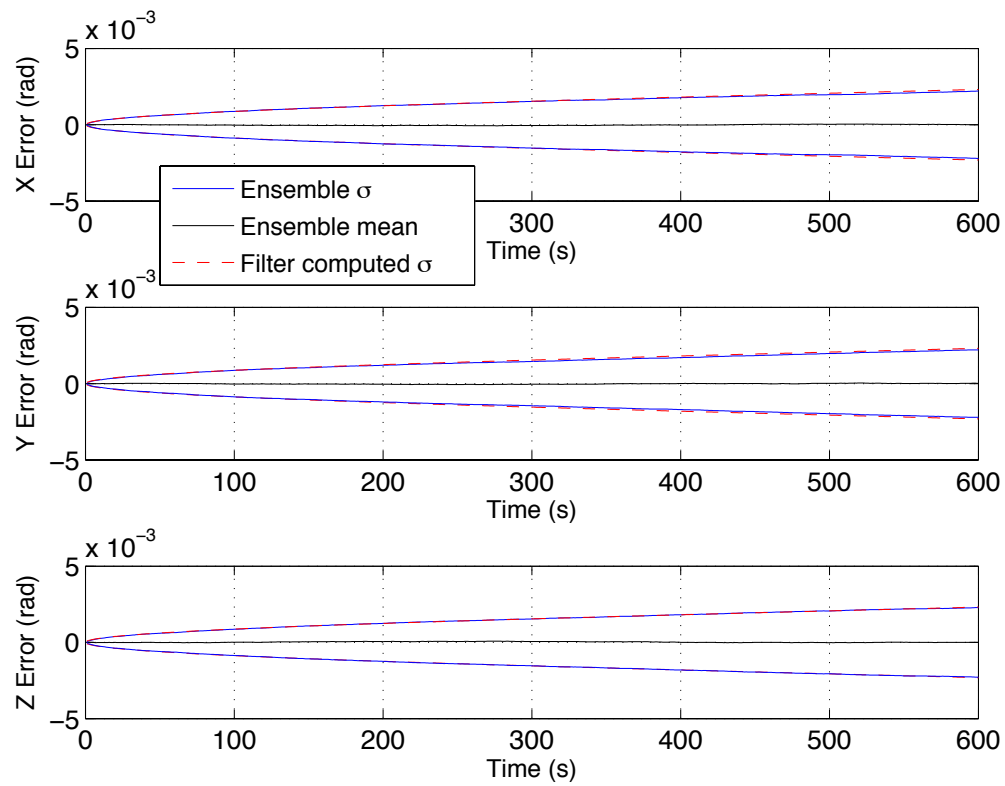


Figure A1.7: Tilt ensemble standard deviation and mean versus filter computed standard deviation for tactical grade INS, without measurements.

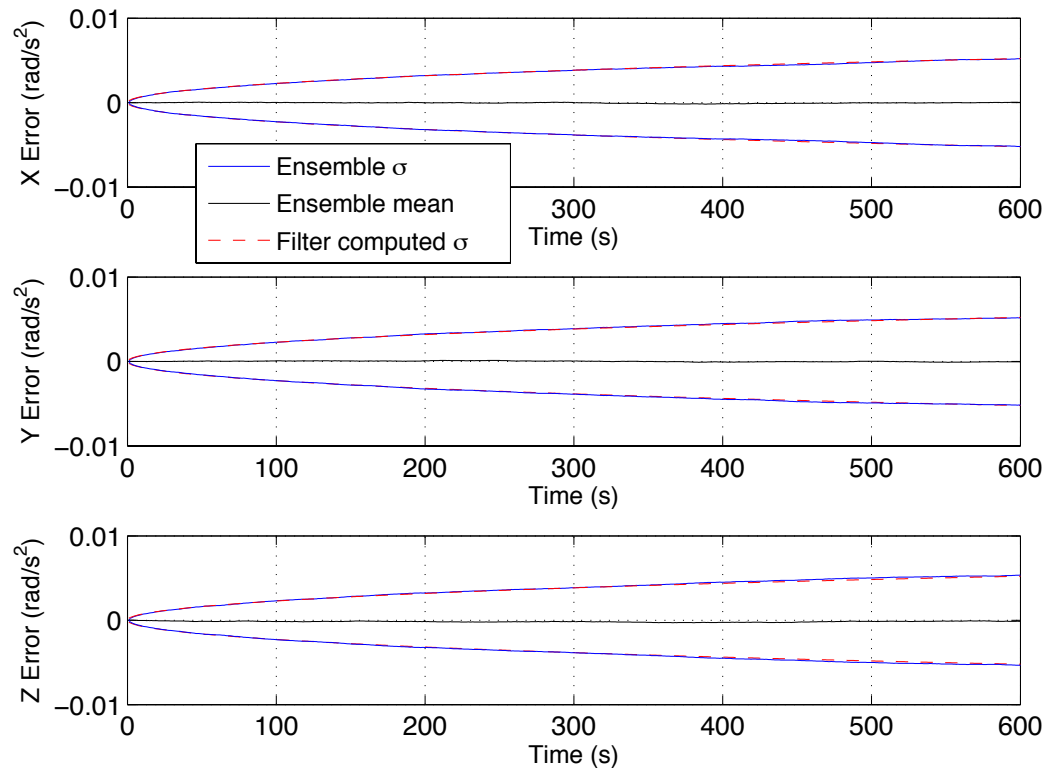


Figure A1.8: Accelerometer ensemble standard deviation and mean versus filter computed standard deviation for tactical grade INS, without measurements.

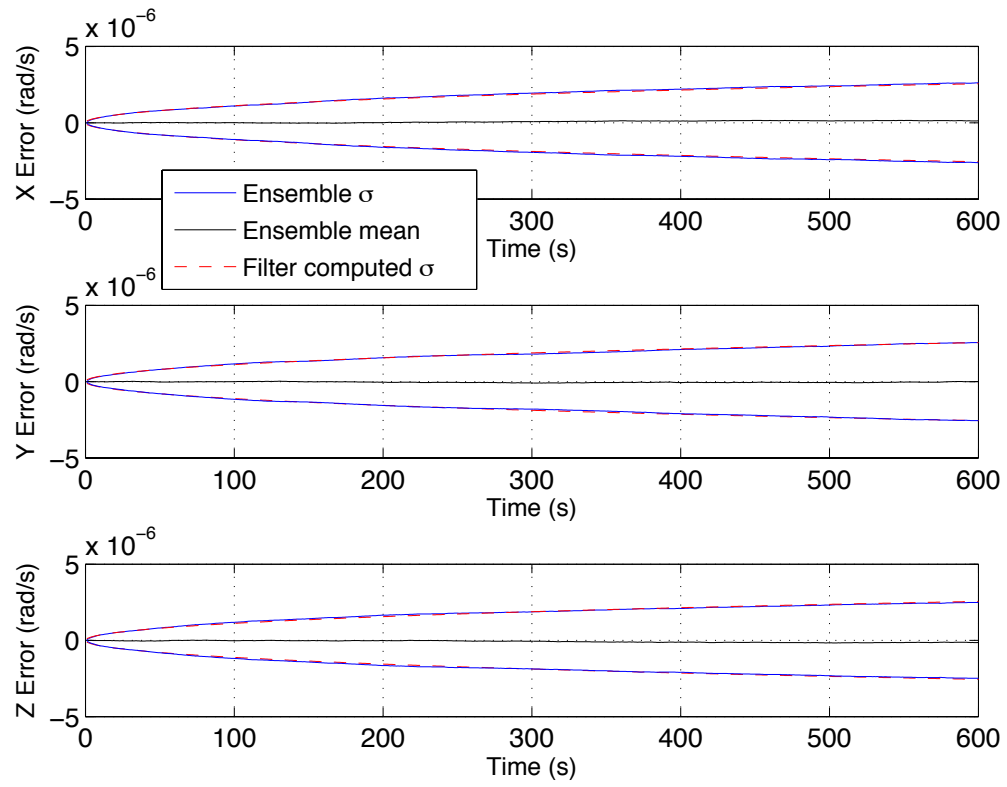


Figure A1.9: Gyroscope ensemble standard deviation and mean versus filter computed standard deviation for tactical grade INS, without measurements.

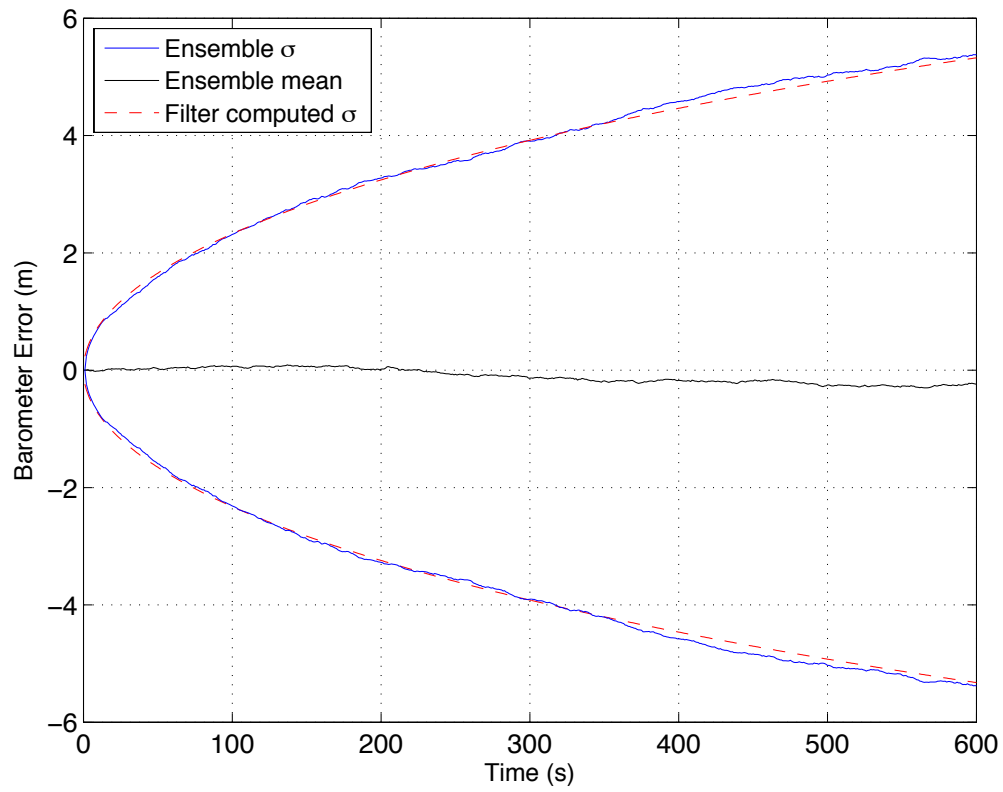


Figure A1.10: Barometer ensemble standard deviation and mean versus filter computed standard deviation for tactical grade INS, without measurements.

A1.1.3 Commercial Grade INS

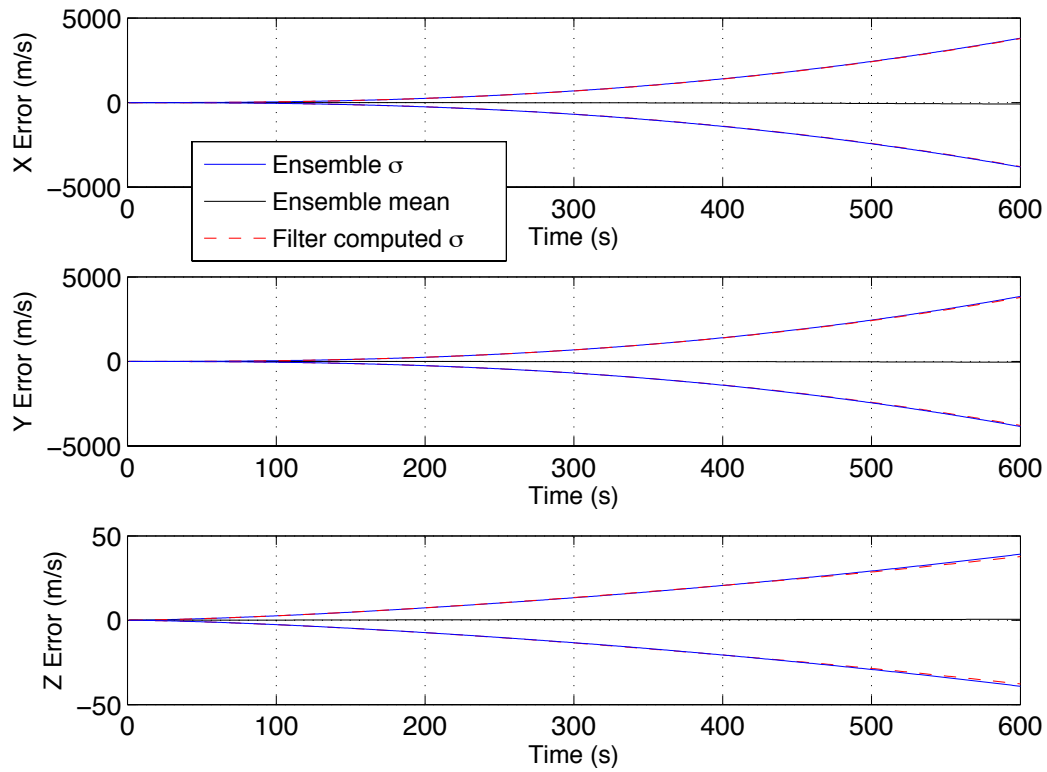


Figure A1.11: Velocity ensemble standard deviation and mean versus filter computed standard deviation for commercial grade INS, without measurements.

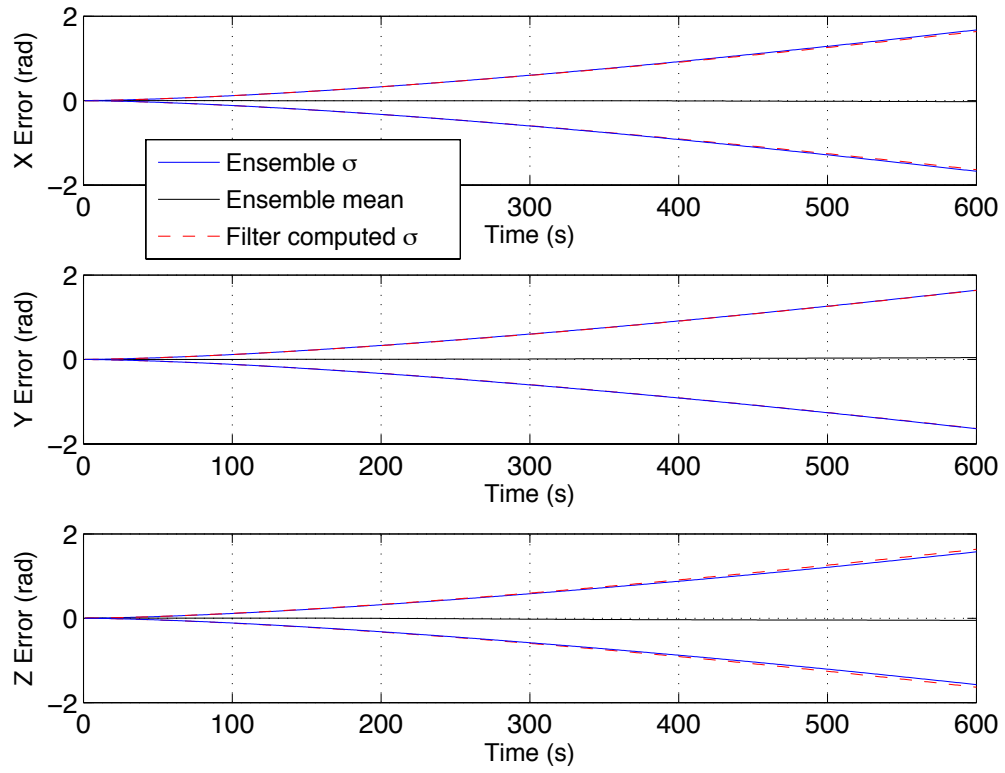


Figure A.12: Tilt ensemble standard deviation and mean versus filter computed standard deviation for commercial grade INS, without measurements.

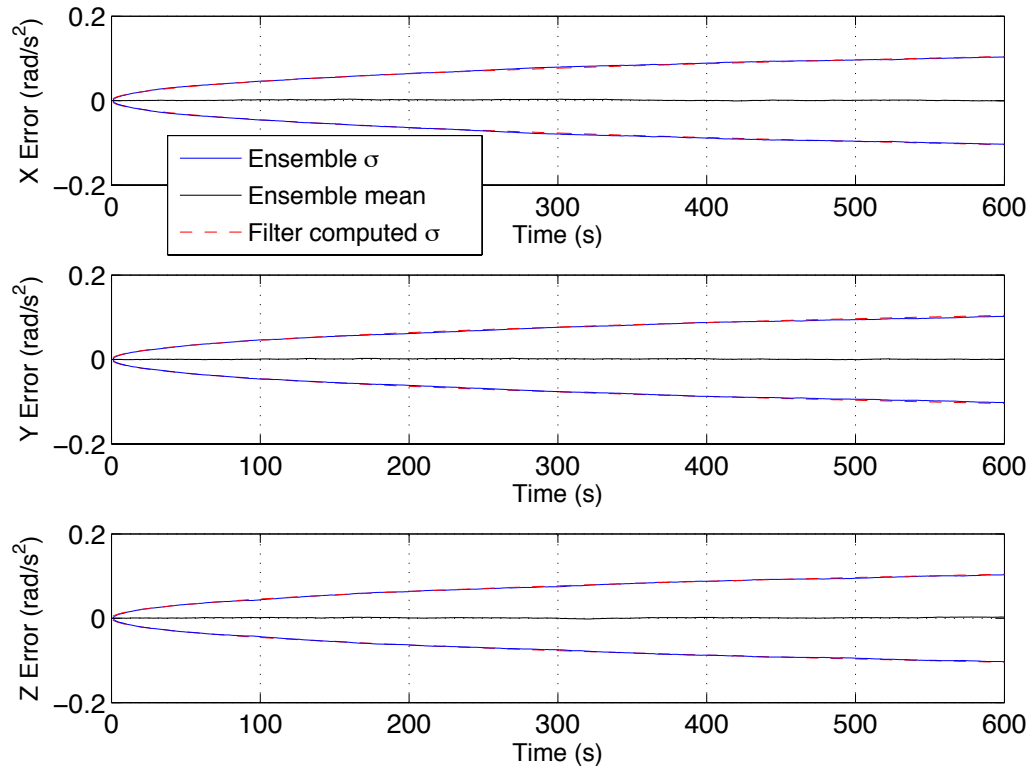


Figure A1.13: Accelerometer ensemble standard deviation and mean versus filter computed standard deviation for commercial grade INS, without measurements.

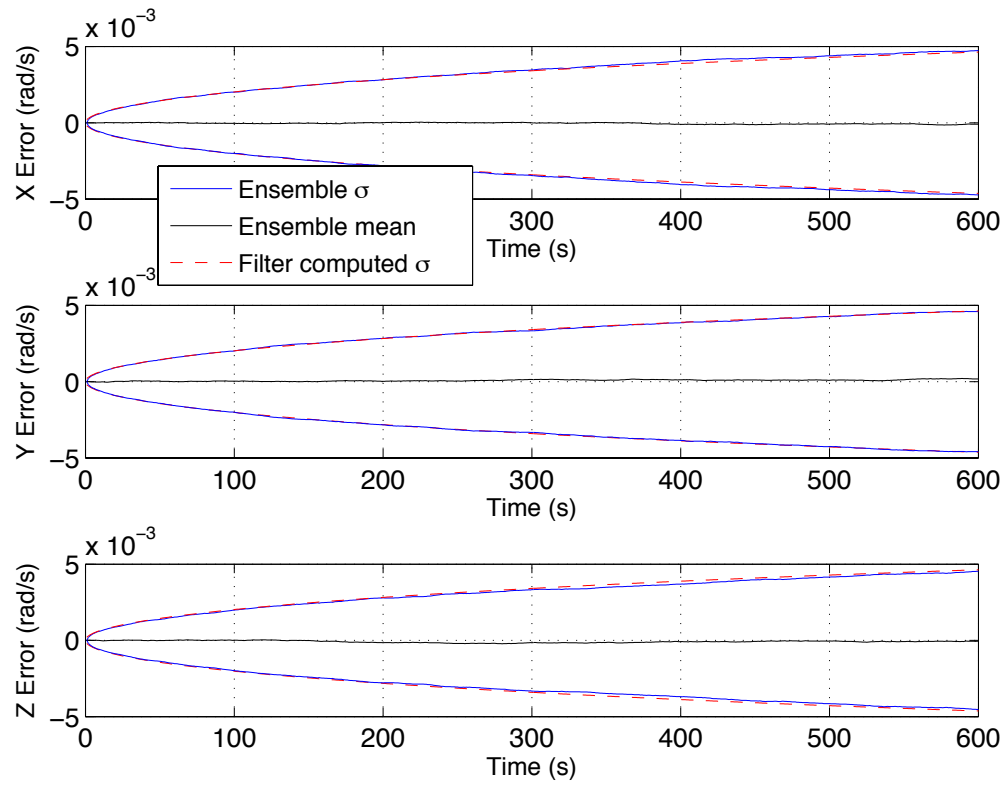


Figure A1.14: Gyroscope ensemble standard deviation and mean versus filter computed standard deviation for commercial grade INS, without measurements.

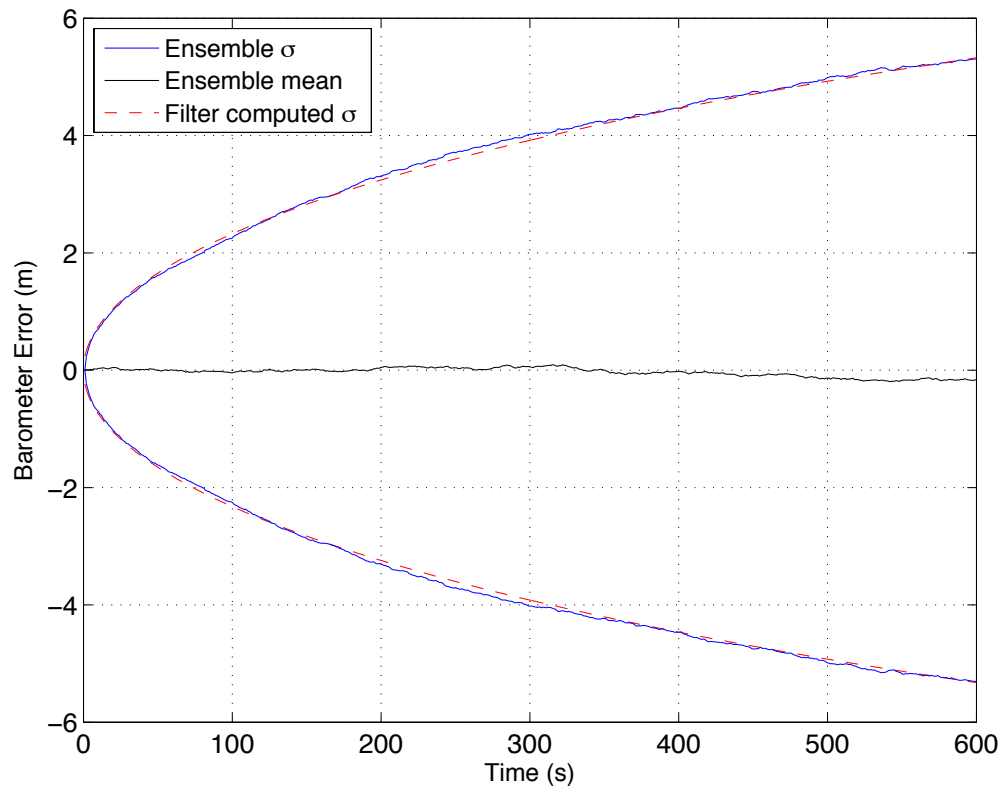


Figure A1.15: Barometer ensemble standard deviation and mean versus filter computed standard deviation for commercial grade INS, without measurements.

A1.2 Star Tracker Performance Improvement on INS Grades, with Measurements

This section will show the rest of the INS states when measurements are used for the two scenarios.

A1.2.1 Navigation Grade INS

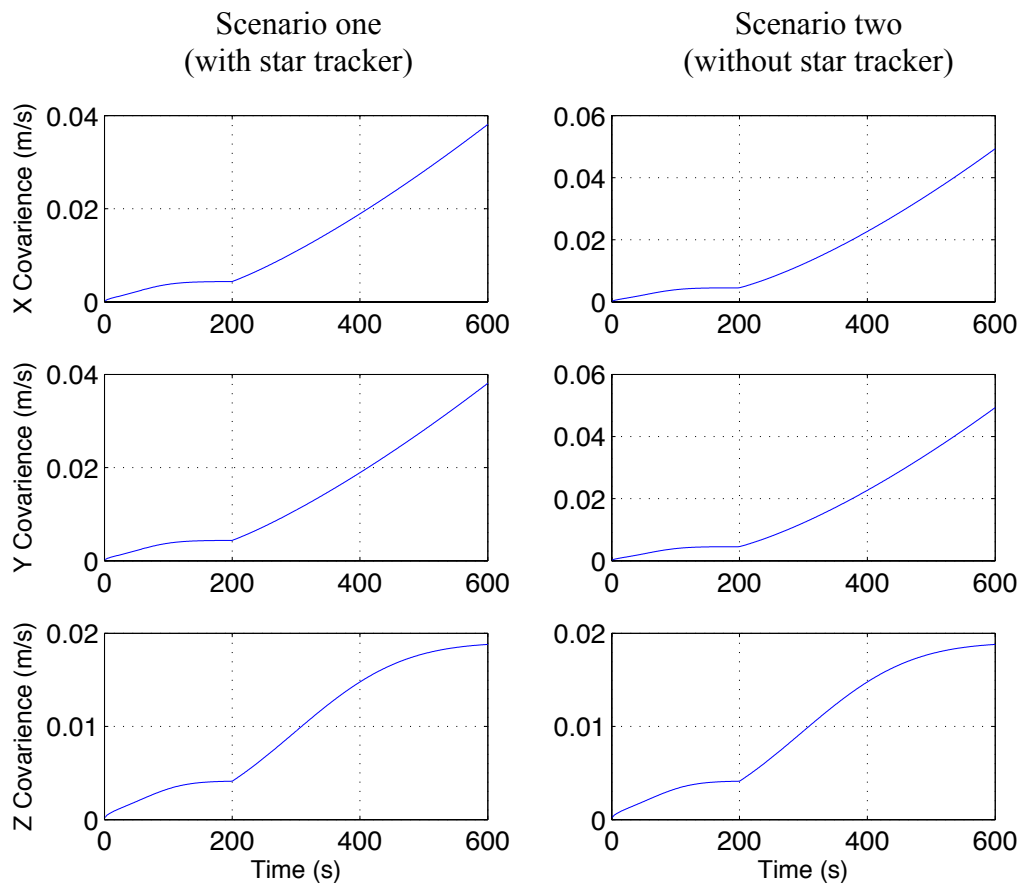


Figure A1.16: Estimated velocity error covariance for the two scenarios for navigation grade INS.

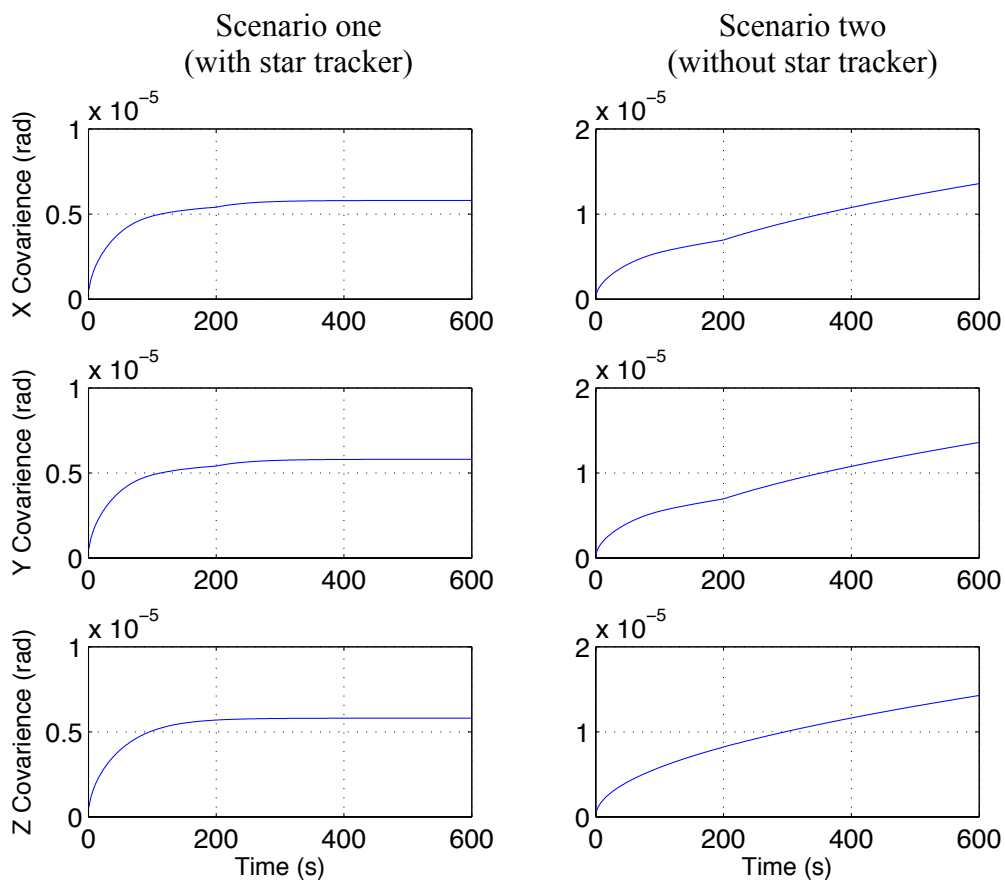


Figure A1.17: Estimated tilt error covariance for the two scenarios for navigation grade INS.

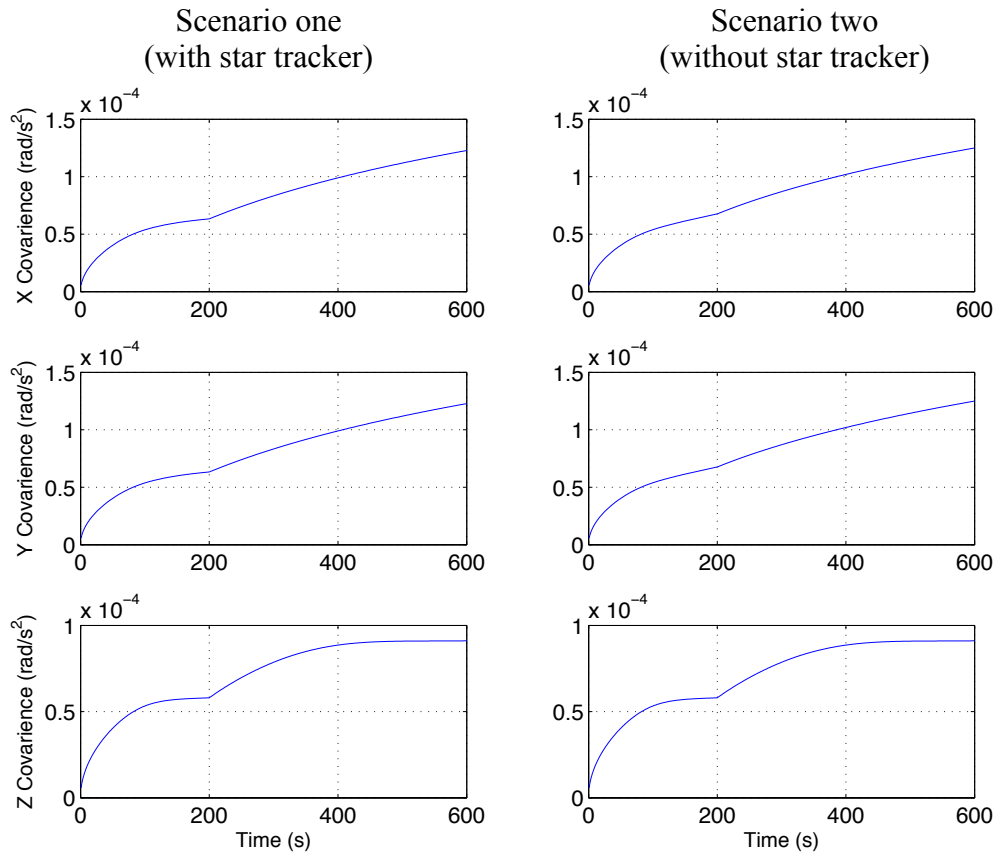


Figure A1.18: Estimated accelerometer error covariance for the two scenarios for navigation grade INS.

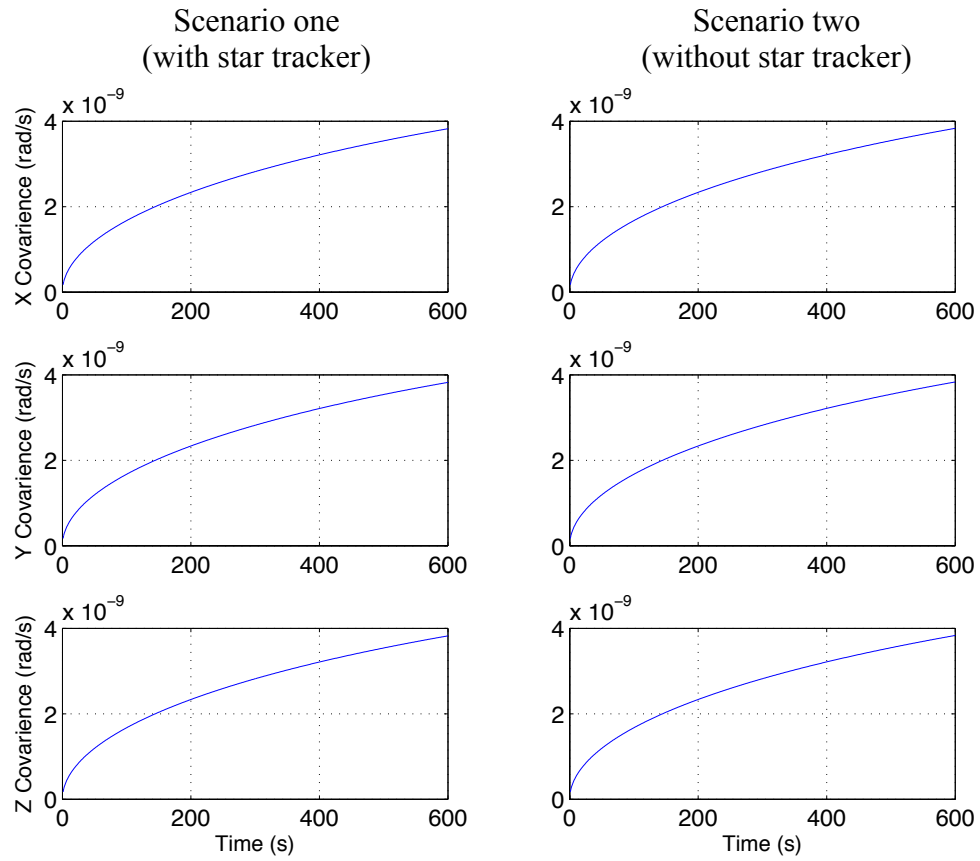


Figure A1.19: Estimated gyroscope error covariance for the two scenarios for navigation grade INS.

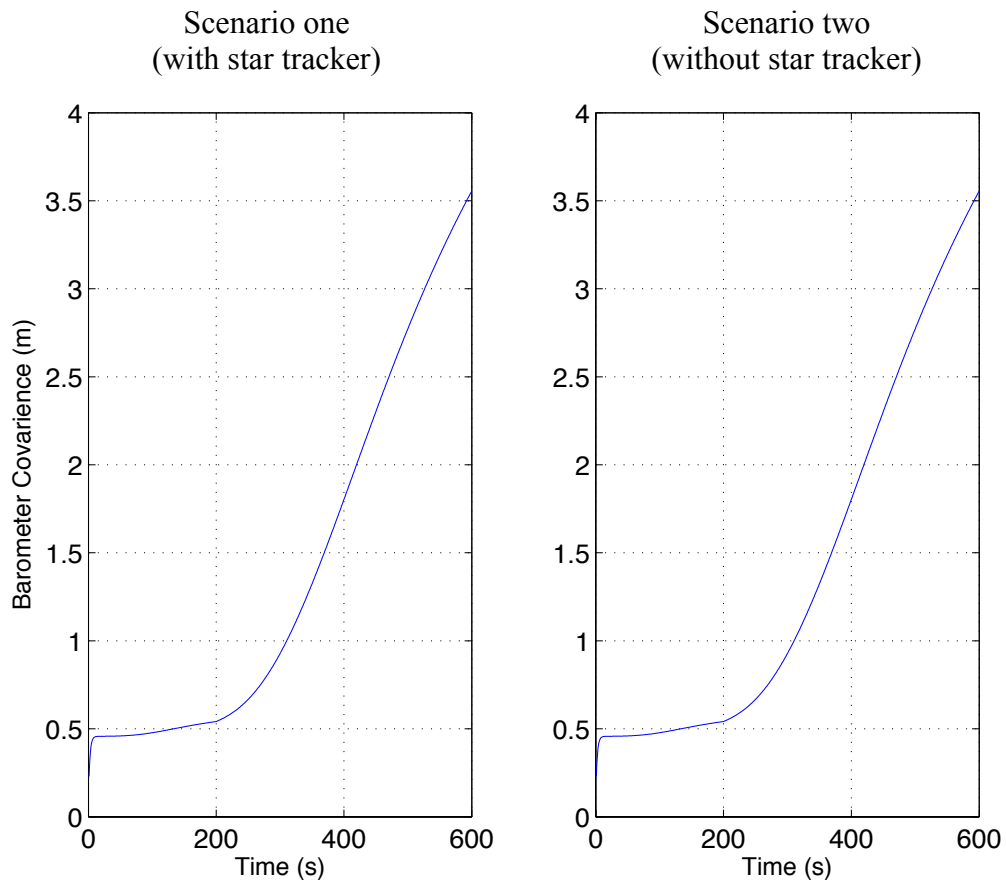


Figure A1.20: Estimated barometer error covariance for the two scenarios for navigation grade INS.

A1.2.2 Tactical Grade INS

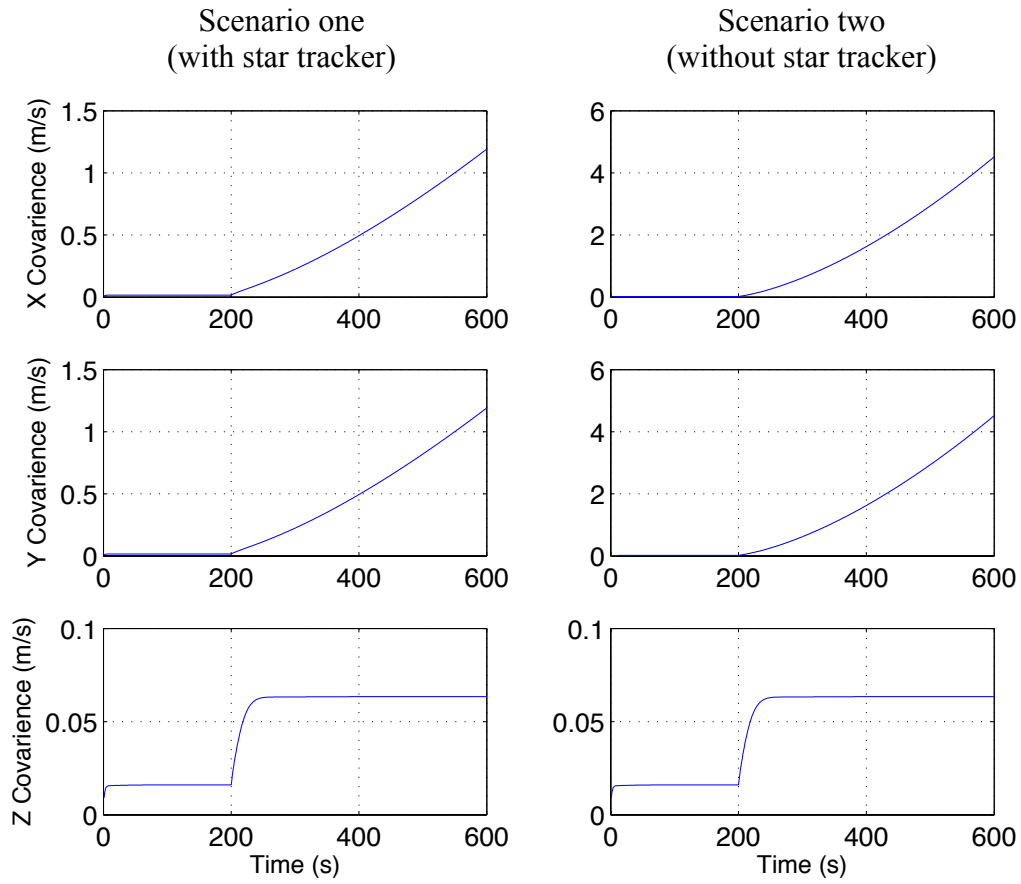


Figure A1.21: Estimated velocity error covariance for the two scenarios for tactical grade INS.

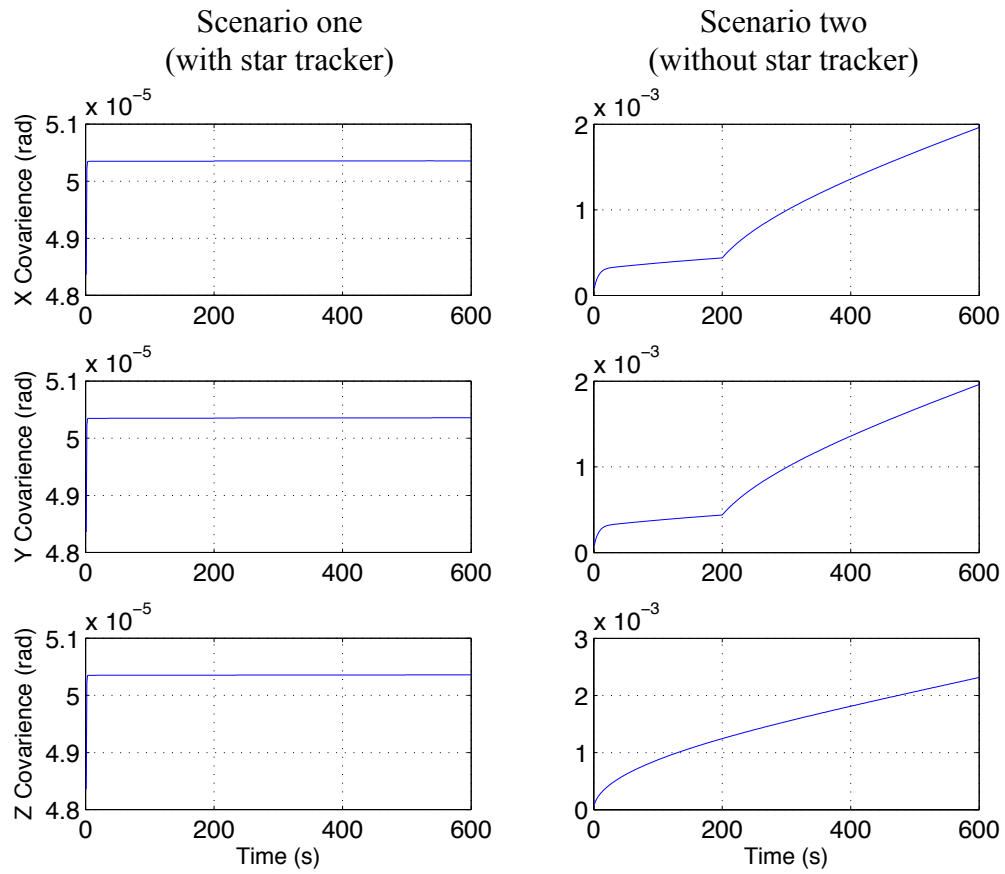


Figure A1.22: Estimated tilt error covariance for the two scenarios for tactical grade INS.

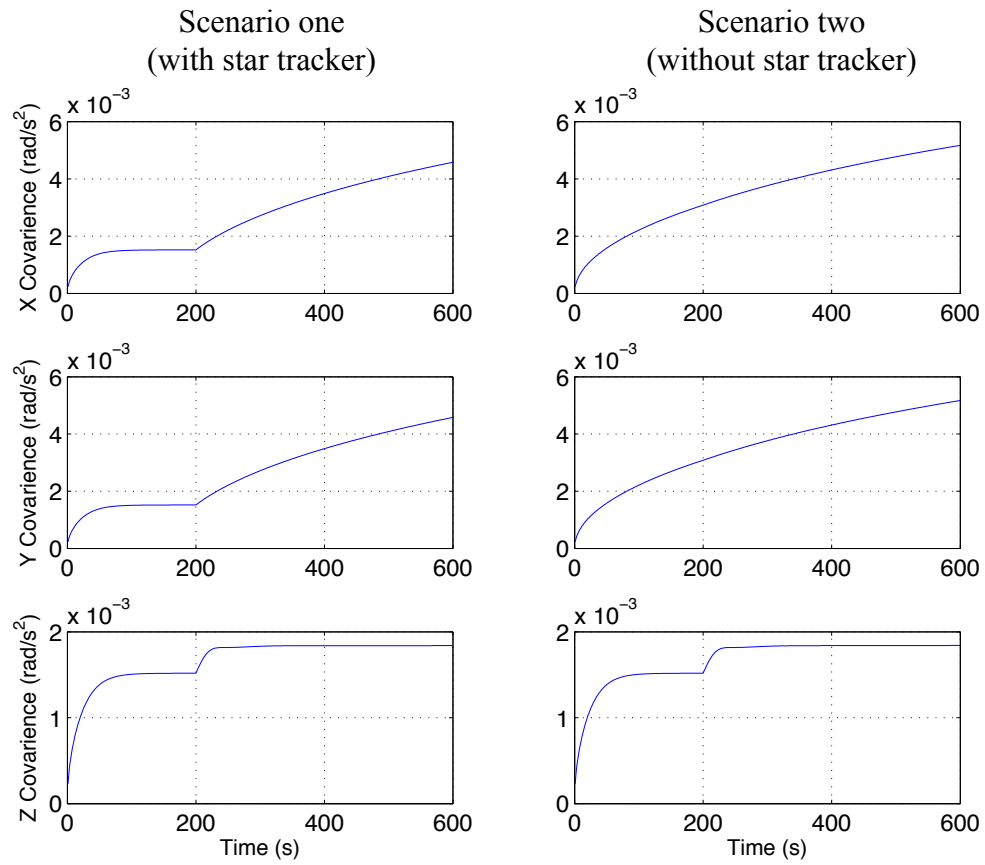


Figure A1.23: Estimated accelerometer error covariance for the two scenarios for tactical grade INS.

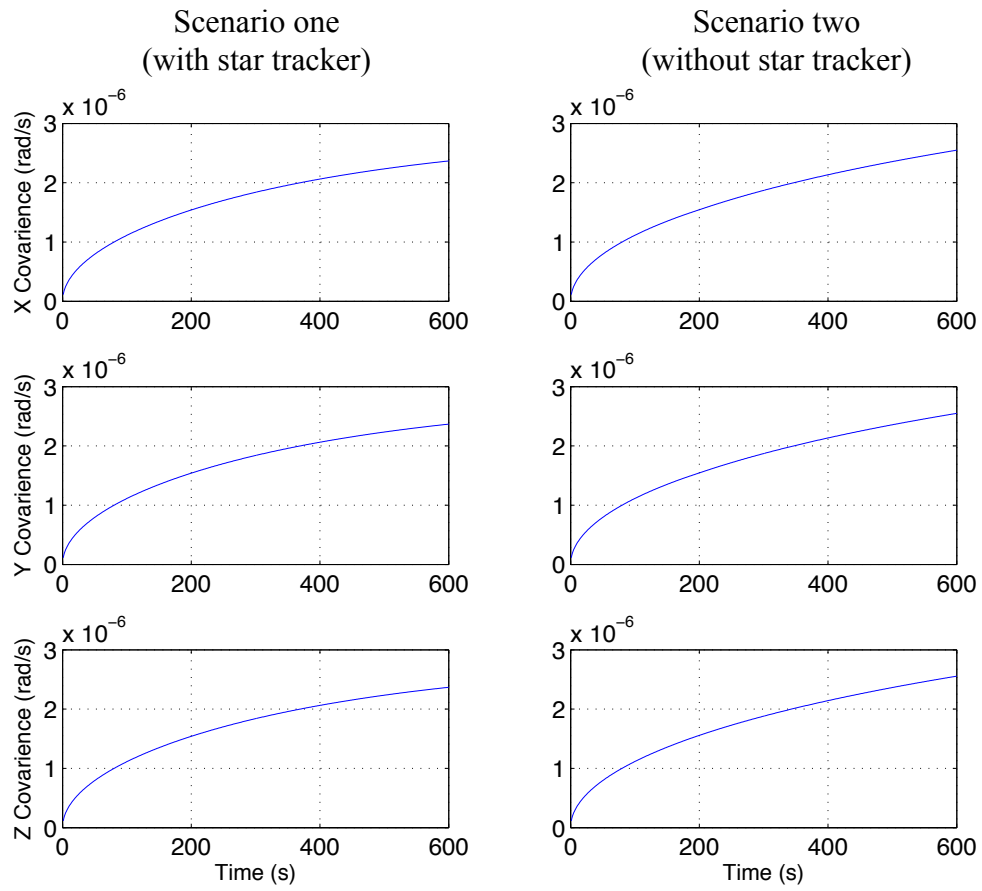


Figure A1.24: Estimated gyroscope error covariance for the two scenarios for tactical grade INS.

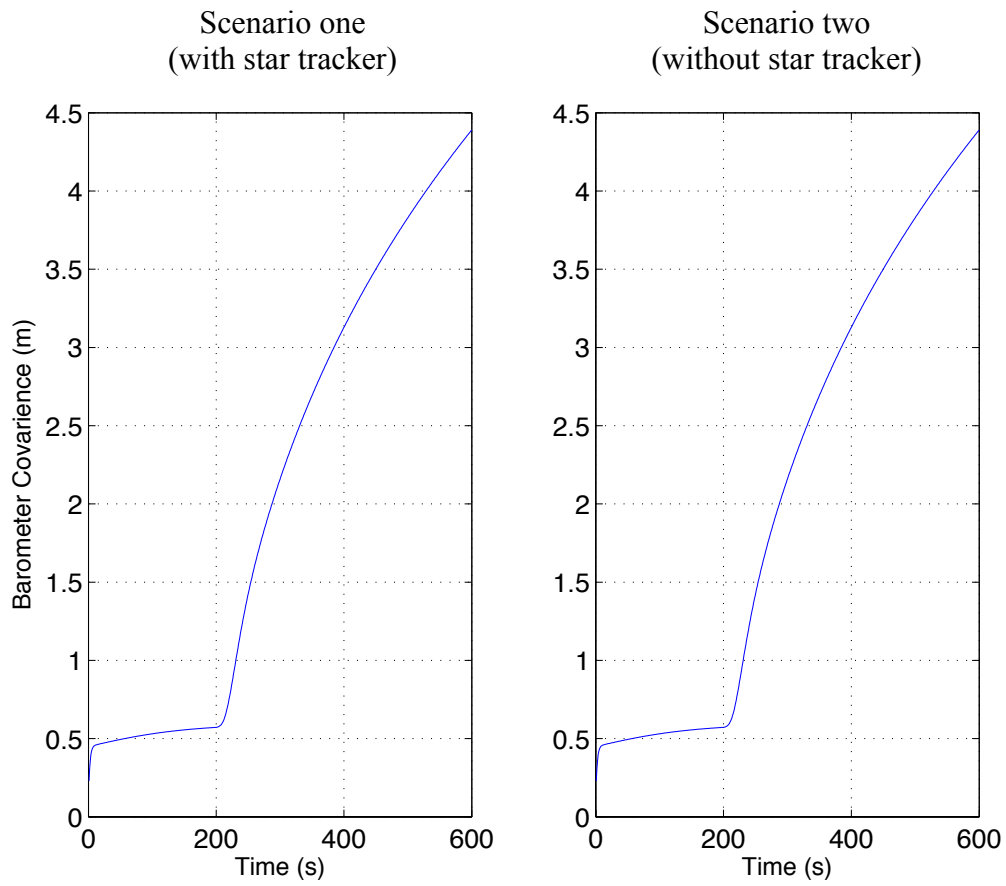


Figure A1.25: Estimated barometer error covariance for the two scenarios for tactical grade INS.

A1.2.3 Commercial Grade INS

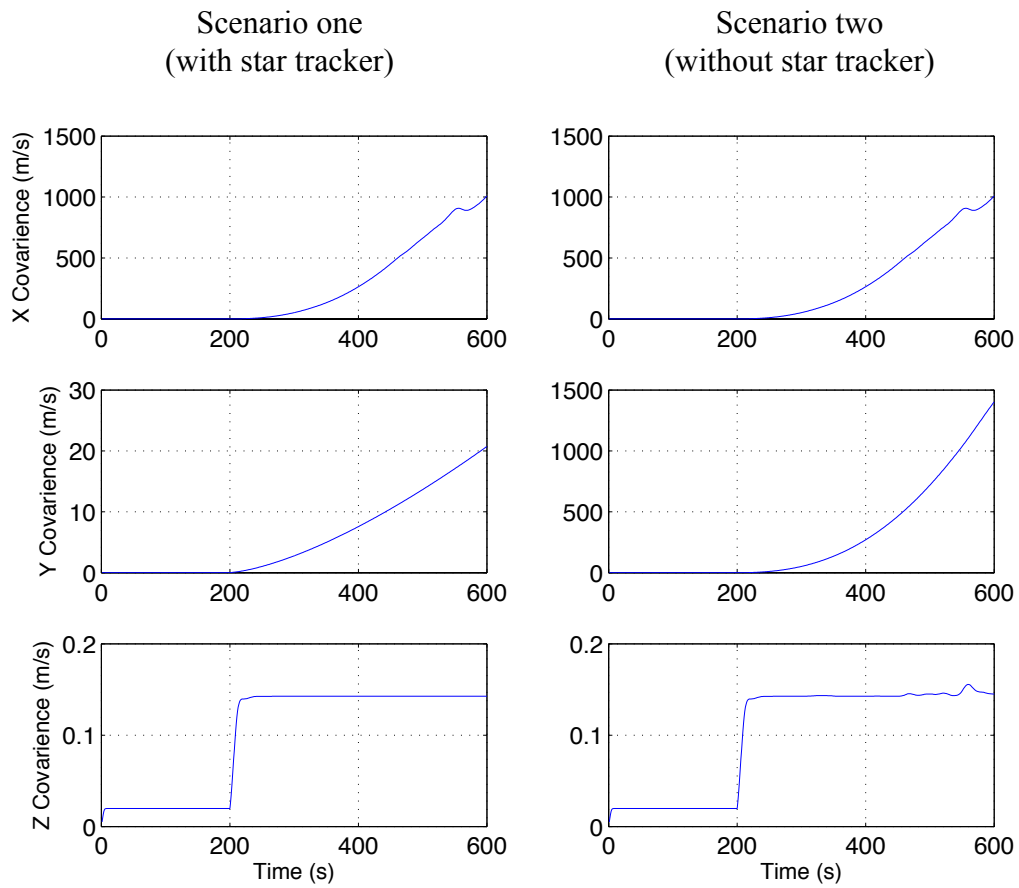


Figure A1.26: Estimated velocity error covariance for the two scenarios for commercial grade INS.

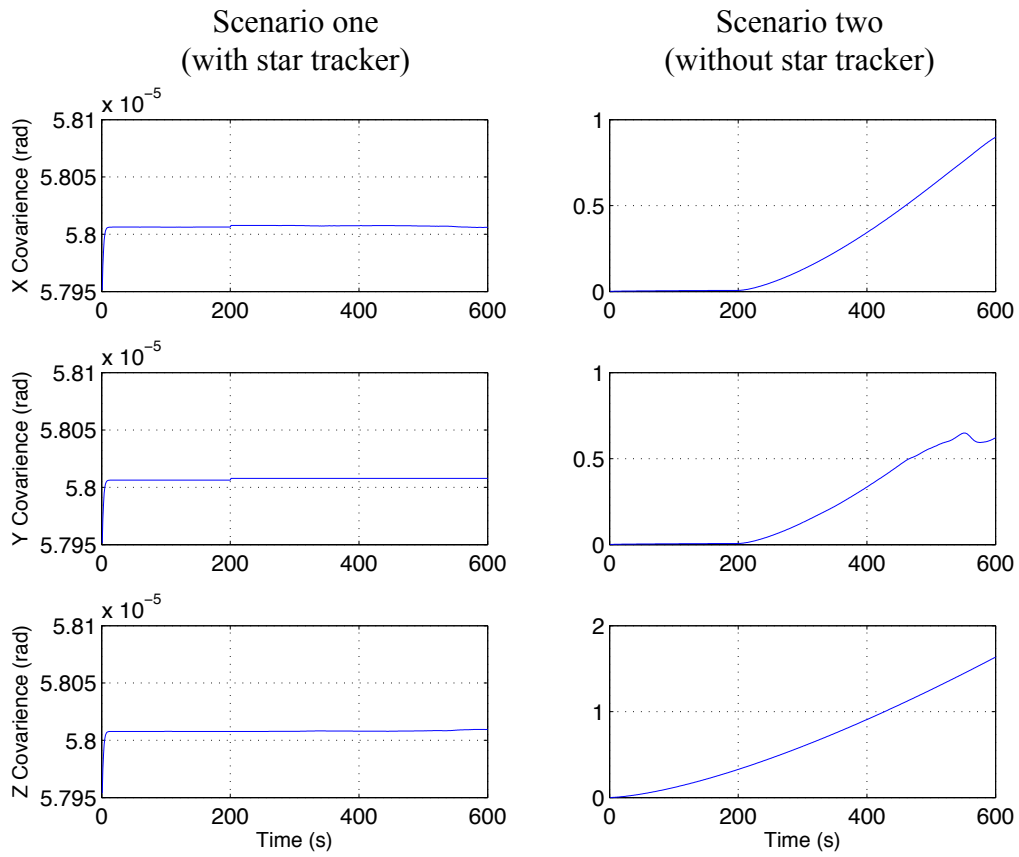


Figure A1.27: Estimated tilt error covariance for the two scenarios for commercial grade INS.

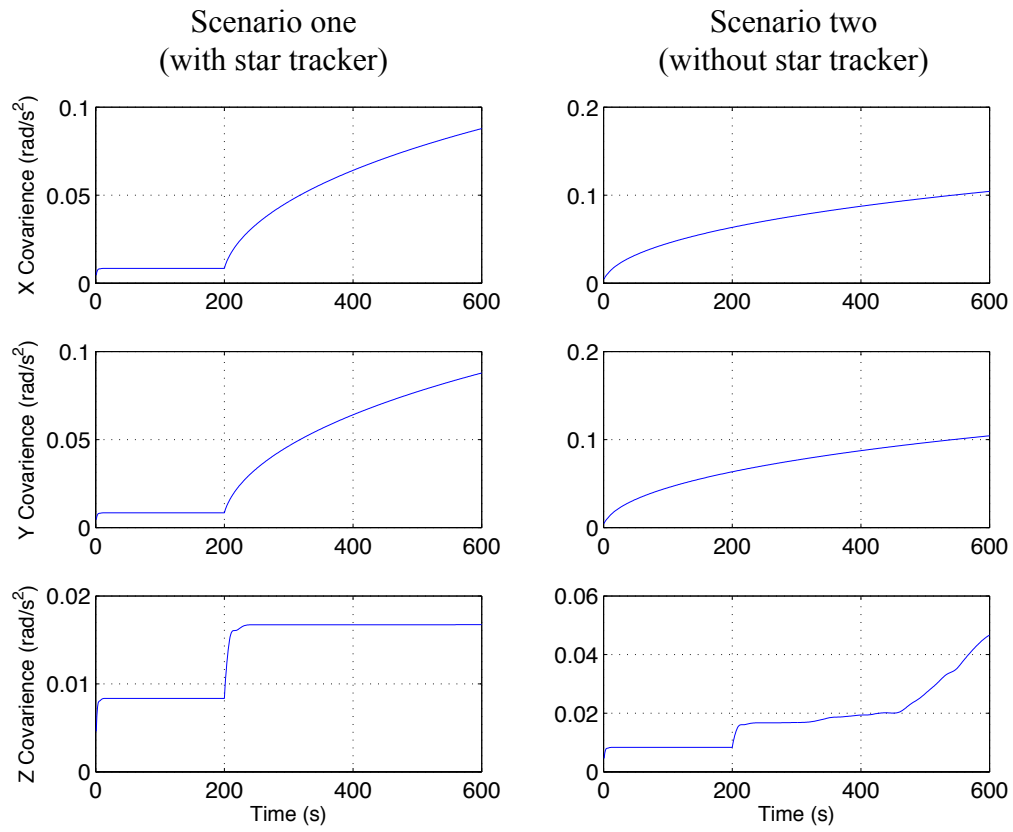


Figure A1.28: Estimated accelerometer error covariance for the two scenarios for commercial grade INS.

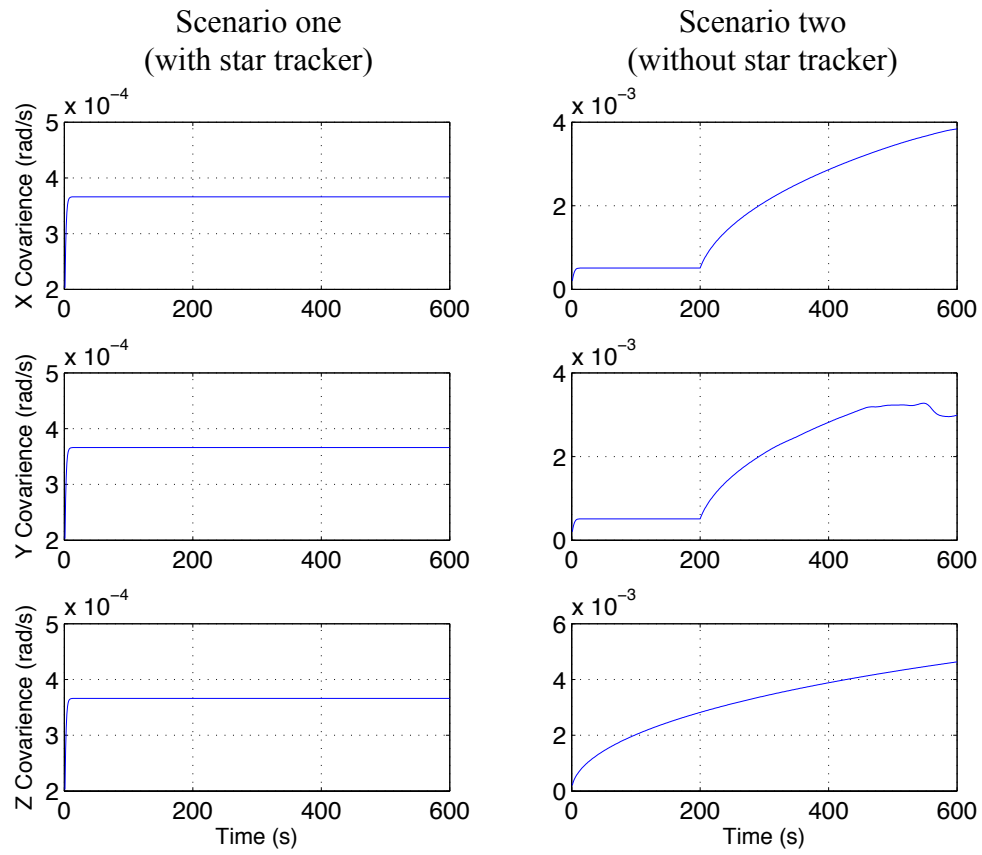


Figure A1.29: Estimated gyroscope error covariance for the two scenarios for commercial grade INS.

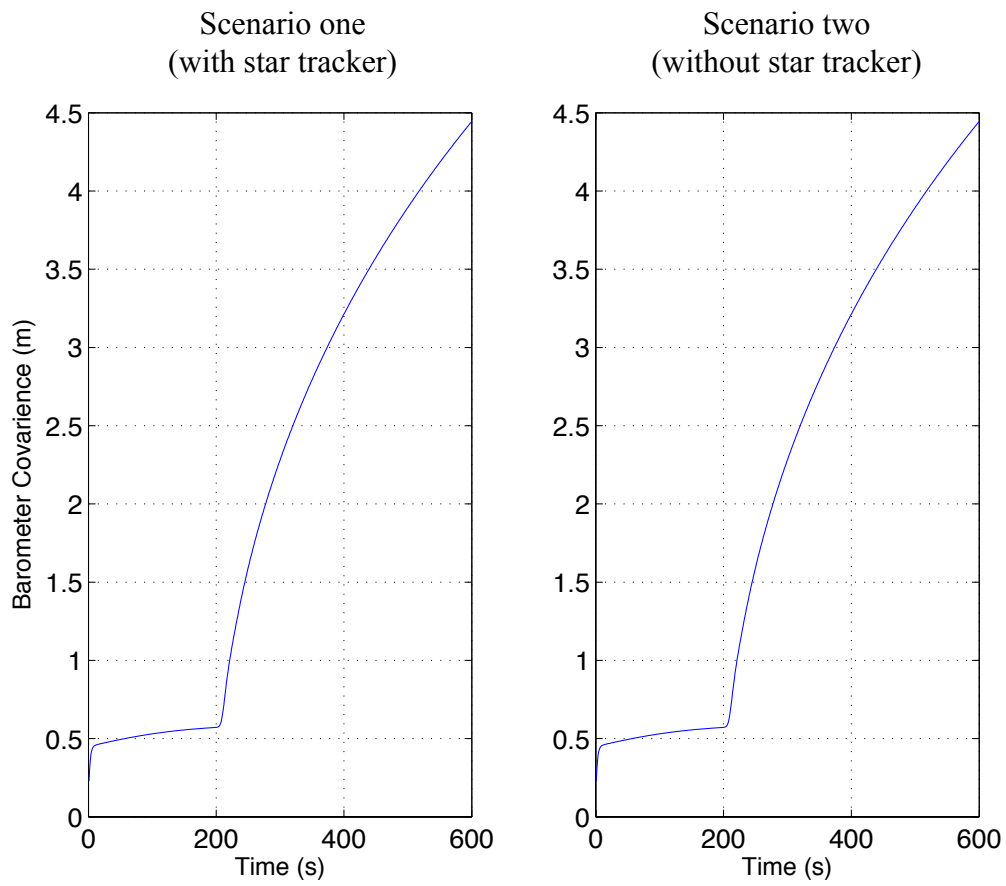


Figure A1.30: Estimated barometer error covariance for the two scenarios for commercial grade INS.

Bibliography

1. Britting, Kenneth R. *Inertial Navigation Systems Analysis*. Wiley-Interscience, 1971.
2. D. H. Titterton and J. L. Weston, “Strapdown Inertial Navigation Technology”, second Edition.
3. F. Gul and Fang Jiancheng “Correction Technique for Velocity and Position Errors of Inertial Navigation System by Celestial Observations”, *Emerging Technologies*, 2005. *Proceedings of the IEEE Symposium*, on page(s): 7 pp. – 12.
4. Farid Gul and Fang Jiancheng “Alternate of GPS for Ballistic Vehicle Navigation”, *Systems and Control in Aerospace and Astronautics*, 2006. *ISSCAA 2006. 1st International Symposium*, On Page(s): 6 pp. – 24.
5. Hofmann-Wellenhof, “Global Positioning System, Theory and Practice”, Springer-Verlag New York, Inc; 2nd edition (Aug 7 2002).
6. S. J. Julier and J. K. Uhlmann, “A new extension of the Kalman filter to nonlinear systems,” in *Proc. AeroSense: 11th Int. Symp. Aerospace/Defence Sensing, Simulation and Controls*, 1997, pp. 182-193.
7. Samaan, A. M., Mortari, D., & Junkins, L. J. (2008), “Compass Star Tracker for GPS-Like Applications”, *IEEE Transactions On Aerospace And Electronic Systems*. 44, 1629 – 1634.
8. National Imagery and Mapping Agency(NIMA) TR350.2,” World Geodetic System 198”, 3rd edition, Departement of Defence, 3 january 2000.
9. Huffman, Kara M. (2006, May 26). “Designing star trackers to meet micro satellite requirements”. Retrieved from <http://ssl.mit.edu/publications/theses/SM-2006-HuffmanKara.pdf>
10. Weston John. Retrieved from <http://www.globalspec.com/reference/26567/203279/chapter-11-strapdown-navigation-system-computation>
11. Maybeck, Peter S. “Stochastic Models Estimation and Control”, Vol I. *Academic Press, Inc.*, Orlando, Florida 32887, 1979.
12. M. Veth, “Fusion of imaging and inertial sensors for navigation,” Ph.D. dissertation, AFIT, Dayton, OH, 2006.

13. W.H. Steyn, M.J. Jacobs and P.J. Oosthuizen, “A High Performance Star Sensor System for Full Attitude Determination on a Microsatellite,” University of Stellenbosch, Stellenbosch 7600, South Africa.
14. Kyle Kauffman, “Radar based navigation in unknown terrain,” Ph.D. dissertation, AFIT, Dayton, OH, 2012.
15. Warden, John A., III. “Air Theory for the 21st Century”. Air and Space Expeditionary Operations, v4.0:108–119, 1994.
16. The Noble Qur'an, Translation by Sahih International, Surat Al-'An`ām, verse 97.
17. Michaels, D., “ Ball Aerospace Star Tracker Achieves High Tracking Accuracy for a Moving Stars Field,” *Aerospace Conference, 2005 IEEE* , vol., no., pp.1,7, 5-12 March 2005.

REPORT DOCUMENTATION PAGE				Form Approved OMB No. 074-0188	
<p>The public reporting burden for this collection of information is estimated to average 1 hour per response, including the time for reviewing instructions, searching existing data sources, gathering and maintaining the data needed, and completing and reviewing the collection of information. Send comments regarding this burden estimate or any other aspect of the collection of information, including suggestions for reducing this burden to Department of Defense, Washington Headquarters Services, Directorate for Information Operations and Reports (0704-0188), 1215 Jefferson Davis Highway, Suite 1204, Arlington, VA 22202-4302. Respondents should be aware that notwithstanding any other provision of law, no person shall be subject to a penalty for failing to comply with a collection of information if it does not display a currently valid OMB control number.</p> <p>PLEASE DO NOT RETURN YOUR FORM TO THE ABOVE ADDRESS.</p>					
1. REPORT DATE (DD-MM-YYYY) 18-09-2014		2. REPORT TYPE Master's Thesis		3. DATES COVERED (From – To) Mar 2012 – Sep 2014	
TITLE AND SUBTITLE Integration of a Star Tracker and Inertial Sensors Using an Attitude Update				5a. CONTRACT NUMBER	
				5b. GRANT NUMBER	
				5c. PROGRAM ELEMENT NUMBER	
6. AUTHOR(S) Humood Alkhaldi, Captain, RSAF				5d. PROJECT NUMBER	
				5e. TASK NUMBER	
				5f. WORK UNIT NUMBER	
7. PERFORMING ORGANIZATION NAMES(S) AND ADDRESS(S) Air Force Institute of Technology Graduate School of Engineering and Management (AFIT/EN) 2950 Hobson Way, Building 640 WPAFB OH 45433-8865				8. PERFORMING ORGANIZATION REPORT NUMBER AFIT-ENG-T-14-S-16	
9. SPONSORING/MONITORING AGENCY NAME(S) AND ADDRESS(ES) Intentionally left blank				10. SPONSOR/MONITOR'S ACRONYM(S)	
				11. SPONSOR/MONITOR'S REPORT NUMBER(S)	
12. DISTRIBUTION/AVAILABILITY STATEMENT DISTRIBUTION STATEMENT A. APPROVED FOR PUBLIC RELEASE; DISTRIBUTION UNLIMITED.					
13. SUPPLEMENTARY NOTES This material is declared a work of the U.S. Government and is not subject to copyright protection in the United States.					
14. ABSTRACT The Global Positioning System (GPS) is widely used in most of the military and civilian applications because of its precision navigation capability. Unfortunately, GPS is not available in all environments (e.g., indoors, under sea, under ground, or jamming environment). The motivation of this research is to address the limitations of GPS by using star trackers as an attitude update to an inertial navigation systems (INS). Commercial, tactical, and navigation grade INS are modeled and simulated with measurements from GPS, star tracker, and barometer. GPS measurements are used to update the INS position and velocity for a small duration in the beginning of the vehicle's flight time. Star tracker and barometer measurements are used to update the INS attitude and altitude, respectively. This research uses a Linear Kalman Filter as a recursive estimation system, to estimate the INS errors (i.e. position, velocity, tilts, accelerometer bias, gyroscope bias, and barometer bias) using the three types of measurement updates. The simulation results show that the star tracker was able to improve the performance of the commercial and tactical grades INS, for any duration of the vehicle's flight time. Also, the improvement in the performance of the navigation grade INS was not significant until the vehicle's flight time was more than approximately 1000 seconds. Also, the research shows the performance impact on the three INS grades when using different star tracker accuracies.					
15. SUBJECT TERMS navigation, image-aided navigation, inertial navigation, celestial navigation, autonomous navigation, global positioning, correspondence search, Kalman filter					
16. SECURITY CLASSIFICATION OF:			17. LIMITATION OF ABSTRACT	18. NUMBER OF PAGES	19a. NAME OF RESPONSIBLE PERSON
a. REPORT	b. ABSTRACT	c. THIS PAGE			Dr. John F Raquet, AFIT/ENG
U	U	U	UU	115	19b. TELEPHONE NUMBER (Include area code) (937) 255-6565, ext 7264 (john.raquet@afit.edu)

Standard Form 298 (Rev. 8-98)
Prescribed by ANSI Std. Z39-18